2013

Discrete phase simulations of drilled cuttings transport process in highly deviated wells

doguhan yilmaz
Louisiana State University and Agricultural and Mechanical College, doguhanyilmaz@gmail.com

DISCRETE PHASE SIMULATIONS OF DRILLED CUTTINGS TRANSPORT PROCESS IN HIGHLY DEVIATED WELLS

A Thesis

Submitted to the Graduate Faculty of the
Louisiana State University and
Agricultural and Mechanical College
in partial fulfillment of the
requirements for the degree of
Master of Science in Petroleum Engineering.

in

The Craft and Hawkins Department of Petroleum Engineering

by
Doguhan Yilmaz
B.S., Istanbul Technical University, Turkey, 2007
May 2012

ACKNOWLEDGEMENTS

I wish to thank to my advisor, Dr. Mayank Tyagi for his excellent guidance, friendly attitude and his contributions to my skills through his deep scientific knowledge and professional stance. His encouragement and trust in my abilities were also a vital support for me to complete this study.

Appreciation is extended to my committee members Dr. Andrew K. Wojtanowcitz, Dr. John Rodger Smith and all faculty members of the Craft & Hawkins Petroleum Engineering Department for their efforts and contributions to my personal and professional development during the time I spent in LSU.

I would like to thank to Turkish Petroleum Corporation for their financial support in my Masters education.

I also specially thank to my family for their lifetime support and encouragement.

TABLE OF CONTENTS

LIST OF TABLES

LIST OF FIGURES

NOMENCLATURE

F_D	Drag Force
u	Fluid Velocity
u_p	Particle Velocity
g_x	Gravitational Force
ρ	Fluid Density
ρ_p	Particle Density
F_x	Additional Force
t	Time
$\overline{u}$	Average Component of the Particle Velocity
u′	Fluctuating Component of the Particle Velocity
v	Particle Velocity in the y Direction
w	Particle Velocity in the z Direction
ζ	Random Number between 1 and 0
k	Turbulence Kinetic Energy
ω	Specific Dissipation Rate
Γ	Effective Viscosity
μ_t	Turbulent Viscosity
σ_k	Prandtl number for k
σ_ω	Prandtl numbers for ω
τ_0	Yield Point
G,Y, D	Generation, Dissipation, and Cross-Diffusion terms of Turbulence Kinetic Energy transport

ABBREVIATIONS

CFD Computational Fluid Dynamics

DPM Discrete Phase Model

SST Shear Stress Transport

ABH Actual Stationary Bed Height obtained from measurements in the experiments

ABSTRACT

Transporting drilled cuttings from the bottomhole to the surface becomes more difficult and problematic in highly deviated wells than in vertical wells. Cuttings tend to settle down on the low side of the annulus typically in the form of a bed which can cause further problems. The height of this bed depends on many parameters such as annular domain geometry, drilling fluid density and rheology, annular flow rate, drill pipe rotation speed, cuttings size, shape, and their density. Prediction of the stationary cuttings bed height with respect to these aforementioned parameters is thus necessary to optimize the range of the controllable parameters for a desired level of wellbore cleaning.

A computational setup that represents the spatial geometry of the cuttings transport domain, and utilizes discrete phase model coupled with numerical solution of the Navier-Stokes equations augmented by a turbulence closure model – SST version of k-ω is used for predicting the bed height of the stationary cuttings bed and moving cuttings velocities. Discrete phase model is a mathematical tool to navigate large number of particles in a flow field by calculating the particle paths in a Lagrangian frame by the time integration of force balance on each individual particle. Turbulence effects on the particle motion are also incorporated through a random walk model. The drag force on non-spherical particles is incorporated using a sphericity based correlation. Roughness of stationary bed surface is also incorporated through the modified law-of-the wall model. A snapshot technique is applied here in these simulations by computing flow solutions in the geometric domains with pre-defined stationary bed heights. The statistics of particle - wall collisions are analyzed over these geometrically pre-defined stationary bed surfaces to predict which domain would represent the equilibrium cuttings bed height.

A systematic validation study is presented by comparing the simulation results against published experimental datasets for velocity profile estimation of non-Newtonian fluids flowing in turbulent regime, stationary bed heights, and moving bed velocities. Further, a parametric study is presented for the effects of wellbore inclination, fluid density and rheology, particle size and sphericity, inner pipe rotation and the inner pipe rotation speed.

1. INTRODUCTION

Transportation of drilled cuttings to the surface during drilling operations in horizontal and highly deviated wellbores is more complex and problematic than in vertical and near vertical wellbores. In vertical and near vertical wells, the cuttings are transported when the axial component of fluid velocity exceeds the particle settling velocity. The difference between the average particle velocity and the average fluid velocity is called transport velocity and their ratio is called transport ratio. These two parameters are commonly used to define the transport efficiency (Sample and Bourgoyne, 1978). However, the transport mechanisms are quite different in highly deviated wellbores. For higher wellbore inclinations, fluid drag force on a particle and the gravitational force are nearly perpendicular to each other, in other words, gravitational settling has little compensation from the fluid drag. Cuttings tend to concentrate on the low side of the wellbore and form a stationary bed (Brown et al. 1989). Moreover, these cuttings are transported in a variety of flow patterns such as homogenous/heterogeneous suspension, moving clusters, moving bed in which cuttings are transported by rolling/sliding action just over the bed formed by accumulated particles (Ford et al. 1990). Considering the flow physics, making predictions for bed heights and velocities solely based on particle settling velocities is not appropriate and therefore, physics-based models are required to address the cuttings transport process in highly deviated wellbores.

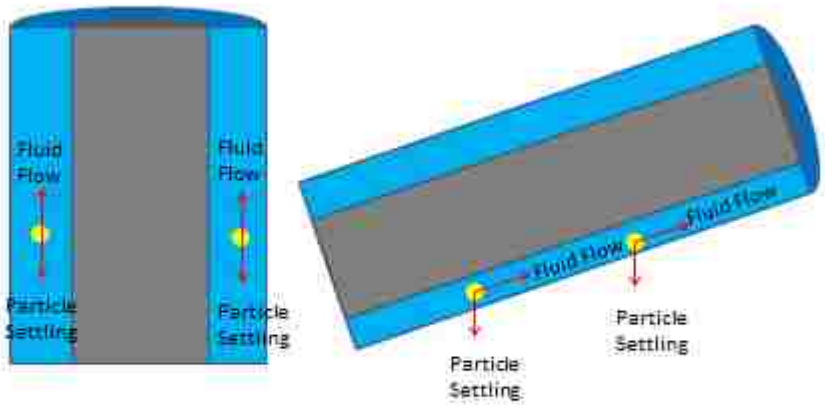

Figure 1.1 Schematic of the cuttings transport processes in vertical wells vs. horizontal/deviated wells

To better understand the cuttings transport process in highly deviated wellbores, the borehole annulus is divided into layers based on particle concentration motion patterns. The first layer is the stationary cuttings bed where the motionless cuttings are accumulated on the low side of the annulus. The area open to flow decreases as the cuttings accumulate on the bed. Subsequently, the bulk flow velocity increases and the flow also becomes more turbulent provided that the carrier fluid flow rate is maintained constant.

At a later time in the accumulation process, the particle carrying capacity of the flow reaches a state where all particles are in motion as well as the accumulation/erosion processes on the bed reach equilibrium. Although the accumulation and erosion on the bed remain dynamic, their net balance results in the stationary bed height. The stationary bed height is measured from the lowest side of the annulus to the bed surface. When the stationary bed reaches equilibrium, particles are transported in a narrow layer just above the stationary bed surface by rolling and sliding action. This layer is called as the "moving bed layer" (Kelessidis and Mpandelis, 2004). At further higher mass flow rates, a small portion of sparsely populated cuttings may be seen to travel away from the bed surface and in the open flow area (Tomren et al, 1983). This layer is called as "the suspension layer". A schematic illustration of these aforementioned cuttings transport patterns is shown in figure 1.2.

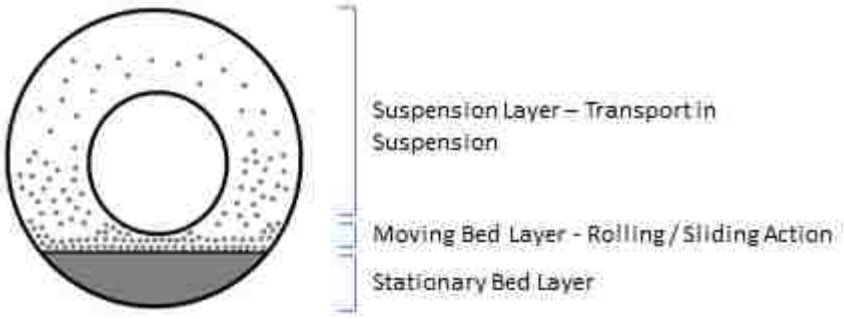

Figure 1.2 Cross-sectional view of flow in highly deviated wellbores to show main cuttings transport patterns in different layers

A variety of problems are encountered for efficient cuttings transport dependent upon wellbore inclination. Wellbore inclinations are divided into three categories dependent upon cuttings transport mechanisms and problems are encountered. The first category is the near vertical inclinations which are generally between 0 to 45 degrees from the vertical. The only cuttings transport pattern here is suspension and no particle accumulation in the form of bed is seen in this category. The main problem for this case is the downwards particle settling due to inadequate upwards fluid velocity. The second category is the critical inclinations which are generallly between 45 to 60 degrees from the vertical. Particles are transported in suspension as well as rolling and sliding action over the low side of the annulus. These particles tend to settle down and form an unstable, thin stationary bed on the low side of the annulus. The main problem in this category is the downwards sliding of the unstable stationary cuttings bed and formation of very high cuttings concentrations instantaneously as a result. The third category is the near horizontal inclinations which are typically 60 to 90 degrees. Majority of these particles are transported in a moving bed pattern while a small portion of these particles moves in a suspension pattern. The main problem in this category is the formation of thick and stable stationary beds by downwards particle

settling that is difficult to remove (Tomren et al, 1983). The cuttings transport mechanisms and problems encountered at different inclinations are depicted in figure 1.3. The focus in this study is given to cuttings transport process in highly deviated wellbores.

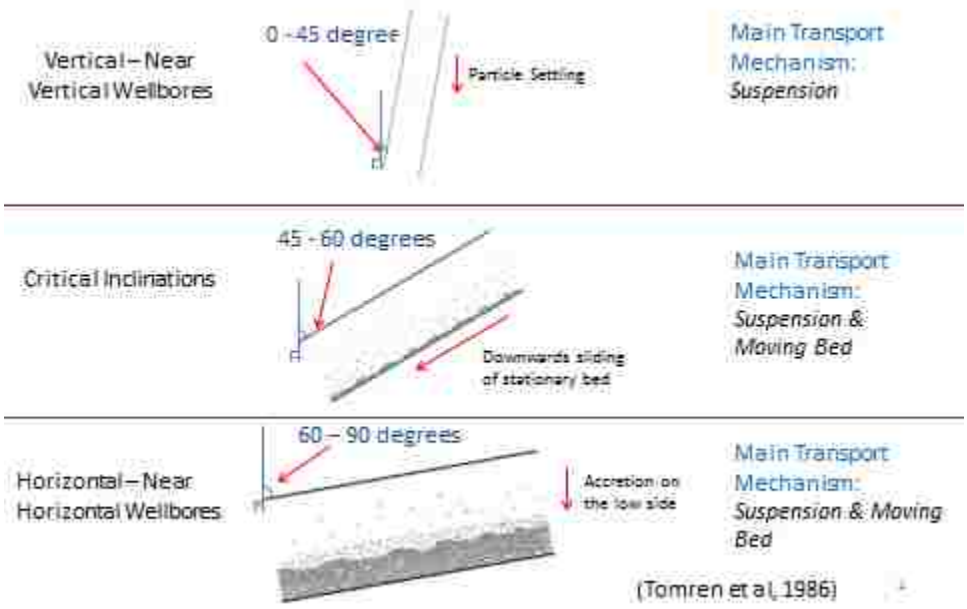

Figure 1.3 Various cuttings transport mechanisms and problems encountered at different wellbore inclinations (Adapted from Tomren et al. 1986)

Many experimental studies have been carried out by using flow loops for investigating the cuttings transport process in highly deviated and horizontal wellbores (Garcia-Hernandez et al. 2007). Different parameters such as the minimum fluid velocity to keep all cuttings moving (Minimum Transport Velocity), height of the stationary cuttings bed, accumulation and erosion rates, and the volumetric cuttings concentration were used to evaluate the cuttings transport efficiency in deviated wellbores. Several factors affecting the transport efficiency were investigated using flow loop experiments for example; fluid velocity, rate of penetration, fluid properties, flow regime, wellbore geometry and drill pipe eccentricity, cuttings size and shape. Based on such experimental parametric studies, correlations were derived for predicting cuttings transport performance. Nguyen et al. (1996) pointed out that these empirical correlations were valid only in a limited range of operating conditions. Apart from such empirical correlations, many mathematical, numerical and semi-empirical models have been proposed for cuttings transport processes. Kelessidis and Bandelis (2004) highlighted issues pertaining to the validation studies for such models using inappropriate data or at times not even using any data for validation as well as comparison studies with other model results instead of relevant experimental data. Cho et al. (2000) showed that the several earlier models gave inaccurate predictions when compared to experimental data,

were unable to provide credible predictions when modeling the process over a wide range of conditions, and had discrepancies with other models. Mendoza and Gutierrez (2008) criticized previous modeling efforts for being constructed using an intuitive process with hidden assumptions and unsupported simplifications. Some examples of such models are presented in the literature review section.

1.1 Cuttings Transport Physics Description and Proposed Simulation Methodology

Particle transport in directional oil well drilling is much more complicated than particle transport in other areas such as chemical engineering, civil engineering, mining industry or oceanography. Particles heavier than carrier fluids need to be carried in great distances beneath the earth inside an annular hole geometry with large range of wellbore inclinations. If the drilling parameters are not well optimized for efficient transport of drilled cuttings, it could result in problems such as stuck pipe, poor hole conditioning, and difficulty in landing and cementing the casing leading to tremendous financial losses (Brown et al. 1989).

Modeling of the cuttings transport process in highly deviated wells is complex in nature due to large amount of parameters and processes involved. Some easily measurable parameters are: annular geometry, drilling fluid density and rheological parameters describing Newtonian and non-Newtonian drilling fluids, annular flow rate, drill pipe rotation speed and cuttings density. Other hard to measure parameters include: particle size, shape, and drill pipe eccentricity during the process. To make matter worse, calculated second order parameters such as lift and drag forces on particles, turbulence effects both on fluid and particles, inter-particle and particle wall adhesive forces, momentum loss of particles upon wall impact, particle settling in different kinds of fluids are also needed to describe the underlying flow physics. It is important to make appropriate simplifications and assumptions in the modeling of cuttings transport process to retain the correct physics.

Computational Fluid Dynamics (CFD) methods are considered to be physics-based and more appropriate in complex flow problems such as cuttings transport process in highly deviated flow channels. As a general definition, Computational Fluid Dynamics (CFD) methods involve a numerical solution of the Navier – Stokes equations in a discretized spatial domain. A commercial CFD software, Fluent™ ver. 12.1 is used for simulations of cuttings transport process in this research study. Discrete phase model (DPM) is used in a coupled fashion with the Navier-Stokes equations augmented with the SST version of k-ω turbulence closure model. SST version of k-ω turbulence model is found to be more stable computationally and compatible with discrete phase model in this study when compared to other two equation turbulence models such as different versions of k-ε turbulence model, although it is reported in earlier studies to have similar performances with other two equation turbulence models for annular flows (Vieira et al, 2011). Modified law of the wall model is also used to include wall roughness effects on fluid

flow. Discrete phase model (DPM) is a mathematical tool for calculating particle- paths, and velocities in a flow field. It can handle a large number of particles due to its simplicity. DPM calculates particle trajectories in a Lagrangian frame and it is partially coupled with the Navier-Stokes equations closed with k-ω turbulence model that solves the flow field in an Eulerian frame. DPM calculates force balance on a particle at the discritized time steps in order to calculate the instantaneous particle velocity. The particle paths are obtained by the time integration of instantaneous particle velocities. Dispersion of particles due to turbulence eddies is also incorporated using a random walk model. DPM is also capable of incorporating size distributions as well as particle shape factors in the form of non-spherical drag force. DPM also has a significant advantage over granular fluid – multiphase models by allowing the analysis of particle wall collisions and turbulence effects.

The main goal of this study is to understand the cuttings transport process in highly deviated wellbores using CFD simulation methodology with representative computational geometry and flow physics. The setup is designed to predict the stationary cuttings bed height, velocities of moving particles, and to handle all the parameters involved in the process mentioned in earlier sections. Accurate prediction of stationary bed height is necessary to optimize controllable drilling parameters for desired amount of wellbore cleaning. Accurate prediction of moving particle (on the bed) velocities is required to estimate the circulation time and particle concentrations. Estimation of the effect of moving particles on frictional pressure losses is possible via two – way coupling, but it is deemed outside the scope of this study.

Numerical study includes a systematic validation of the computational setup with a variety of relevant experimental datasets. Since accurate representation of particle behavior is dependent on accurate solution of the flow field, first, the capability of CFD in predicting the velocity profiles of non-Newtonian fluids in turbulent flow regime is compared against experimental datasets of Pinho and Whitelaw (1990) and Pereira and Pinho (1994). Next, the model prediction accuracy at different flow rates is validated with the experimental datasets of Garcia-Hernandez et al. (2007). Average moving bed velocities are also compared against these experimental measurements. Lastly, a parametric study is performed to understand the effects of wellbore inclination, inner pipe rotation, inner pipe rotation speed, fluid rheology and density, particle size distribution and particle shape. Effects of wellbore inclination and the inner pipe rotation are validated for model predictions with experimental data while the effects of remaining parameters are evaluated qualitatively (Tables 1.1 and 1.2).

Table 1.1 Summary of simulations conducted for model validation.

#	Bulk Velocity, ft/sec	Inclination	Rotation	Carrier Fluid	Geometry	Experimental Data for Validation	Particle Tracking
1	16	90	No	water with 4% CMC	25.4 mm pipe	Pinho and Whitelaw (1990)	N/A
2	18		No	water with 4% Tylose	26 mm pipe	Pereira and Pinho (1994)	N/A
3	3.4	90	No	Water	8" × 4.5" Annulus	Garcia - Hernandez et al. (2007)	Steady
4	4.2		No	Water			Steady
5	4.8		No	Water			Steady
6	4.2	70	No	Water			Steady
7	4.2	90	Yes	Water			Steady
9	3.4	90	No	Water	8" × 4.5" Annulus	Garcia - Hernandez et al. (2007)	Unsteady
10	4.2	90	No	Water			Unsteady
11	4.8	90	No	Water			Unsteady

Table 1.2 Summary of simulations in the parametric study section. All simulations are performed in 8" × 4.5" annulus, 300 gpm flow rate, 70 degree wellbore inclination.

	Density	Rheology	Particle Size Distribution	Particle Sphericity	Rotation Speed
Simulated Values	8.33 ppg	Water	4 mm Uniform	Spherical	0
	10 ppg	Medium Effective Viscosity Yield Power Law - high n	4 - 6 mm Rosin-Rammler	0.1	40
	11 ppg	Medium Effective Viscosity Yield Power Law - low n	4 - 6 mm Rosin-Rammler	0.1	80
	11 ppg	High Effective Viscosity Yield Power Law - High n	4 - 6 mm Rosin-Rammler	0.1	120
	11 ppg	High Effective Viscosity Yield Power Law - Low n	4 - 6 mm Rosin-Rammler	0.1	120

2. LITERATURE REVIEW

In this chapter, a brief review of some representative research works is presented and is organized in the sections for the overview of mathematical modeling of cuttings transport, earlier CFD simulation attempts, and the studies of various influencing factors.

2.1 Review of Numerical and Mathematical Models for Cuttings Transport Process

Luo et al. (1992) proposed a model for predicting the minimum flow rate needed to prevent stationary bed remove accumulated particles. Dimension analysis technique is used by using Rayleigh method where various parameters affecting cuttings transport are arranged into dimensionless groups in order to derive equations for minimum flow rate. The model results are compared to experiments conducted by the same group and good performance in estimating the effects of parameters affecting cuttings transport is reported. Rubiandini (1999) presented a model for estimating minimum transport velocity to keep all particles moving by modifying a particle slip velocity calculation method developed for vertical wells. Correction factors are obtained by dimensionless plotting of slip velocities in vertical wells versus empirical correlations from various studies that include effects of wellbore inclination, rotation speed and fluid density. Model results are compared to correlations output which are also used in developing the model for validation.

Clark and Bickham (1994) presented a mechanistic model for analyzing cuttings transport. The model combines equations developed for fluid-mechanical relationships for describing modes of cuttings transport: Rolling, Lifting and settling. Four equations are utilized for the description of the cuttings transport. The first two equations are to calculate the critical velocity in order to mobilize a single cutting by either rolling or lifting. The third equation is based on Kelvin-Helmholtz stability theory for determining the velocity of the mud that enables the destabilization of the low side cuttings bed and the dispersion of the cuttings over the wellbore cross section. The fourth equation describes the mixture velocity in the flowing layer to ensure that the suspended cuttings volumetric concentration is not exceeding five percent. The largest annular velocity obtained from these four equations is regarded as the critical velocity for efficient cuttings transport. High difference between model prediction and experimental data for critical transport rate is reported. Ramadan et al. (2001) introduced a mechanistic model where balance of extensive range of forces acting on a single particle is calculated. Drag force calculation includes the average pressure and shear stress, wall effects and inter - particle cohesion. Lift force is obtained by Saffman's lift force equation corrected for particles moving in the turbulent boundary layer and also the forces resulting from cohesion between particles in the bed is included. The particle

acceleration later related to bed erosion rate. Comparison of model output to experimental data confirmed that there is a correlation between particle acceleration and bed erosion.

Martins et al. (1992) presented a two layer model based mass and linear momentum conservation laws as well as constitutive relationships. Top layer consists of drilling fluid with a cuttings concentration in it and the lower layer is the stationary bed. The shear stress on the interface of two layers is computed based on an experimental correlation and a force due to contact between the particle and stationary bed is also defined. A diffusion equation gives the particle concentration profile in the upper layer. A three layer model was proposed by Nguyen and Rahman (1996) for representing the sedimentation and transport processes in the horizontal and highly deviated annuli. In this theoretical model, the annulus consists of three zones (Layers) based on their particle concentration and the state of mobility of the particles. The top layer is the fluid flow layer in which the particles are in a fluid suspension or there is no solid phase at all. The middle layer is the dispersed layer with a variable cuttings concentration and the bottom layer is a bed with uniform cuttings concentration. The transport process is described by 3 momentum equations for each layer and 2 continuity equations for each phase (Solid and Liquid). The thickness of the layers is defined by the shear stress interactions between the layers. Although there is no numerical comparison with the experimental data, the qualitative effects of drilling fluid rheology, mud weight, cuttings density, coefficients of dry friction, and eccentricity in the annulus are investigated through the model are compared to findings in experimental studies.

Ford et al. (1996) developed a semi-empirical model based on experimental and theoretical research. The model is calculating minimum transport velocities for cuttings rolling and suspension to ensure efficient hole cleaning. It is assumed that one single spherical particle is transported in the wellbore and particle does not interact with the fluid. Then the balance of gravitational, frictional, fluid lift and drag forces acting on the particle are calculated and the mean velocity and effective viscosity that will ensure sufficient force to initiate transport is determined. The model prediction of minimum transport velocity and experimental results are reported as 20% difference for rolling cuttings and 10% difference for cuttings in suspension.

In another similar study by Cho et al. (2000), three layer model has been utilized for describing cuttings build up and erosion processes in the annulus. Different physical models are presented for near horizontal, transient and vertical segments of the wellbore. The cross sectional areas of each layer, the cuttings concentration in the suspension layer and moving bed velocity is computed through continuity and momentum equations based on forces acting on each layer. Published results for particle concentration and stationary bed area are in good agreement with experimental data at near horizontal sections.

A two layer model is developed by Parades et al. (2007) with volume averaging method. One equation model is obtained by volume averaged transport equations derived for porous medium (Stationary cuttings bed) and the fluid section. After the coupling conditions are identified between two layers, average pressure and average velocity can be calculated for fully suspended flow and flow with a stationary bed. The dimensionless pressure data vs. bulk fluid velocity data generated by the model is compared to experimental data. The predicted data for flow with a stationary bed is in good agreement with the experimental data, however the flow with a fully suspended flow is not adequate according to comparison with the experimental data. To this end, we propose to use the Reynolds-averaged Navier-Stokes equations to model the momentum transport of the carrier fluid and the integration of individual particle trajectories for the cuttings transport modeling. The forcing between the carrier fluid and cutting is closed using empirical drag laws as well as through incorporation of turbulence effects as random walk model.

2.2 Review of CFD Applications Related to Cuttings Transport

The study of cuttings transport efficiency by a fluid mechanics tool is proposed by King and Trenty in 2000. ESTET (by EDF and Simulog) is the fluid mechanics tool used in the research which utilizes finite volumes and finite elements meshes in solution of the Navier - Stokes Equations for Newtonian fluids. Modifications have been made for the non-Newtonian behavior of the drilling fluids. Various cases including the effects of drill pipe eccentricity, drill pipe rotation, cuttings bed accumulation inclination has been investigated by the study of the velocity, shear stress and pressure profiles on the cross-section of the wellbore.

A study with computational fluid dynamics is presented by Bilgesu et al (2002) with three dimensional steady state flow. Solid-liquid multiphase flow model is used with power law viscosity and Newtonian viscosity models used for fluid phase. The investigations are based on determining cuttings transport efficiency defined as percentage of solid cuttings in a defined volume. No statements are made on segmented flow phenomena. Predicted results were in good agreement with laboratory data.

Vieira Neto et al (2011) simulated the flow of Newtonian fluids by a Computational Fluid Dynamics Software in eccentric annuli and with inner shaft rotation and obtained velocity profiles for various cases. Five turbulence models are tested and results are reported to be close for all models. Obtained velocity profiles are compared to experimental ones and computed errors reported as 5.5% for non-rotating flows and less than 5% for rotating flows.

Eesa and Bargou simulated the laminar pipe flow of nearly buoyant particles in non-Newtonian fluids utilizing a CFD software. The published results for the velocity profiles particles in suspension were in matched the experimental results with good accuracy (2008).

In our CFD simulations, the care has been taken to represent various physically coupled effects in a systematic fashion: the turbulent flow is represented using two-equation k-omega model, non-Newtonian fluid rheology using various generalized constitutive relations, boundary layer effects on cuttings bed using "modified" law-of-the-wall accounting for roughness, and a random walk model is used in the force balance on particle trajectories for turbulent flow effects.

2.3 Review of Parameters Influencing the Cuttings Transport Process

2.3.1 Annular Bulk Fluid Velocity

Ozbayoglu et al. (2004) investigated the effects of various on cuttings bed height buildup through dimensionless cross sectional bed area concept. They asserted that the annular bulk fluid velocity is the most important parameter on cuttings bed accumulation. Similar views are also expressed by Adari et al. (2000).

2.3.2 Fluid Density

Gao and Young (1995) highlighted that fluid density resist the gravitational settling of cuttings through increased buoyancy, so any increase in fluid density would help cleaning efficiency. Becker and Azar (1985) conducted flow loop experiments with various mud weights at different inclinations. They asserted that cuttings concentration increased dramatically with increasing wellbore inclination for unweighted mud, however, the cuttings concentration decreased and became a linear function of wellbore inclination as the mud weight is increased. Ozbayoglu et al. (2004) also stated that increase in mud weight would also lead to increase in Reynolds number, so the flow can reach turbulent state more easily.

2.3.3 Flow Regime and Fluid Rheology

An extensive study based on flow loop experiments was published by Tomren et al (1983). Cuttings concentrations, stationary bed thicknesses and bed build up times, average particle velocities of particles in suspension are measured at tests with different values of parameters such as flow rate, wellbore inclination and pipe/hole eccentricity with various mud types. At laminar flow regime, bed build up was faster with low viscosity fluid; however, the rate of bed build-up was equal for both high viscosity and low viscosity fluids at turbulent flow regime.

Adari et al. (2000) experimentally investigated cuttings bed accumulation and erosion for highly inclined and horizontal wellbores. They concluded that high k/n ratio enables lower cuttings bed and also reported that turbulent flow regime provides better particle cleaning. Okrajni and Azar (1985) conducted experiments for understanding the effects of mud rheology on cleaning performance based on annular cuttings concentration measurements. They stated that changing rheological parameters did not make any significant difference at turbulent flow regimes in high inclination. Similar results were also reported by Peden et al. (1990). However, for laminar flow, increase in yield point also increases the cleaning performance only at inclinations close to vertical, because the axial components of particle slip velocities are still effective at low inclination angles. In the same inclination range, a higher YP/PV ratio (or lower values of n) provides a flatter velocity profile which helps in eroding the stationary bed. For the laminar flow regime at high inclination angles, improvement was observed with increasing the yield point and YP/PV ratio, because the flatter velocity profile creates higher velocity point values at the region near cuttings bed. Peden et al. (1990) investigated the cuttings transport based on Minimum Transport Velocity (MTV) concept through flow loop experiments. MTV is defined as the minimum fluid velocity in order to keep all particles moving either by suspension or sliding/rolling action. They stated that the mud rheology has minor impact on initiating suspension than rolling action. Increasing the mud viscosity did not always decrease the required MTV. In terms of transporting by rolling mechanism, water reported to display the best cleaning performance. The performance of the low viscosity fluid was second to water and the medium viscosity fluid showed the poorest performance among the test fluids. This behavior is explained as the water and the low viscosity fluid have more tendencies to turbulence. Similar conclusions are also stated by Ozbayoglu et al. (2004). Kelessidis and Mpandelis (2004) conducted experiments with different parameters and in a transparent pipe and observed the particle behavior. They stated that in laminar flow at low flow rates, particles fall to the bottom and start building up a stationary bed as soon as they enter the loop. At turbulence flows particles fell to the bottom, however not deposited. Particles are reported to be moving right above the low side surface and in the viscous sublayer.

2.3.4 Wellbore Inclination

In the study of Tomren et al. (1983), inclined wellbore is classified into three sections. At low inclination angles (10 – 30 degrees from vertical), a generally small and unstable cuttings bed starts to form with increasing inclination angle and decreasing mean annular velocity. At low mean annular velocities, particles on the low side tend to slide downwards and again rise in the annulus after re-entering high velocity region. Significant changes on particle behavior were observed in the transition or critical angles (30 – 60 degrees). It is reported that very few particles reach to the outlet of the test tube before the formation of a cuttings bed. Cuttings bed is higher than low inclination case and usually slides

downwards resulting in very high cuttings concentrations. At high angles of inclination (60 – 90 degrees), cuttings bed instantly formed and there were no downwards sliding movement. A thin moving bed over the stationary bed was also reported. Adari et al. (2000) stated that the rate of bed accumulation and time required to erode the bed increases with increasing hole inclination. Gao and Young (1995) addressed that MTV required for transporting cuttings in suspension increases with increasing hole inclination. However, MTV required for cuttings by rolling mechanism increases with increasing hole inclination and reaches a maximum between 50 to 60 degrees. After that point, required MTV decreases for rolling mechanism. Sifferman et al. (1990) also observed similar bed behavior with Tomren et al. (1983) in their flow loop experiments. They stated that bed height should be higher at high inclination angles than medium and low inclinations, however a higher cuttings bed was observed at 45 degrees of inclination. They observed an unstable stationary cuttings bed between 45 and 60 degrees which has a variable bed thickness and tendency to slide downwards. Okranji and Azar (1985) highlighted that the annular fluid velocity for efficient cleaning in inclined wellbores should be higher than vertical wellbores, because the radial component of particle velocity which pushes the particle to the low side of the annulus becomes more dominant with increasing inclination.

2.3.5 Drill Pipe Rotation

Sanchez et al. (1997) investigated the effect of rotation on cuttings transport along with various parameters. They reported that rotation provided improvement at all speeds. At low flow rates, increasing rotation from 25 to 75 did not make a significant effect; on the other hand, increasing rotary speed from 100 to 150 rpm provided much more improvement than the latter. It is also mentioned that this trend is reversed at high flow rates. In their review paper, Nazari and Azar (2010) asserted that rotation is more effective in smaller annular dimensions. They also stated that rotation helps removing particles in the narrow side of an eccentric well. Tomren et al. (1983) observed that particles are swayed tangentially with inner pipe rotation, resulting in a higher buildup of cuttings on one side.

2.3.6 Cuttings Size

Martins et al. (1996) observed that larger particles are more difficult to transport, based on their flow loop experiments. In similar experiments, Duan et al. (2006) observed a different behavior. In the experiments with water, smaller particles were harder to transport. In the experiments with a non-Newtonian fluid however, the opposite behavior is reported.

3. DESCRIPTION OF COMPUTATIONAL SETUP FOR CUTTINGS TRANSPORT

Computational Fluid Dynamics (CFD) methods are utilized for simulating the cuttings transport process. The Reynolds-averaged Navier – Stokes equations are numerically solved in a discretized domain. An Eulerian – Lagrangian approach is used for simulating particle laden flow. In this approach, Eularian and Lagrangian phases are solved simultaneously in a partially coupled fashion for the carrier fluid and the cuttings respectively. Shear stress transport (SST) version of k- ω turbulence model is used for solving the carrier phase and the discrete phase model (DPM) is used for obtaining the particle paths in the moving fluid phase. All the models described in sections 3.1 and 3.2 are summarized from the Fluent™ User Guide (2009) and Fluent™ Theory Guide (2009).

3.1 Tracking Individual Cutting: The Lagrangian Phase

In the numerical setup, particle paths in the flow field are obtained by the Discrete Phase Model (DPM). DPM is a mathematical model that calculates the tracks of large number of particles in the flow field and allows including body forces and defining particle – wall interactions. The effect of particle shape on particle motion can also be incorporated to the model by the non-spherical drag law. DPM uses an Eulerian – Lagrangian approach. The continuous phase and discrete phase equations are solved together in a partially coupled fashion where the continuous phase calculations are performed in an Eulerian reference frame (fixed) and the discrete phase calculations are performed in a Lagrangian reference frame (moving). Trajectory of a particle is obtained by integrating the force balance (in fact accelaration) twice on each particle. The effect of turbulence is also included as the fluctuations in particle velocities due to turbulence eddies by the "Discrete Random Walk Model".

The force balance on a particle at a particular time step is given as:

$$\frac{\partial u_p}{\partial t} = F_D\left(u - u_p\right) + \frac{g_x(\rho_p - \rho)}{\rho_p} + F_x \qquad 3.1$$

The first term is the drag force per unit mass, the second term is the gravitational force, and F_x is any additional force that can be incorporated. In this study, the force resulting from the pressure gradient, and the "virtual mass" force which is the force needed to accelerate the fluid surrounding the particle are also included in the governing equation.

The effect of the particle shape on the drag force is incorporated in form of drag coefficient calculated by the non-spherical drag law. A shape factor is needed to be set, which is defined as the ratio of the surface

area of a spherical particle having the same volume as the non-spherical particle, to the actual surface area of the particle. Since drilled cuttings are expected to have irregular shapes, and determining the actual shape factor is very difficult, the cuttings are assumed to have a very low shape factor.

The effect of turbulence on particle motion is reflected by the "Discrete Random Walk Model". In this method, the instantaneous velocity is the sum of the averaged component ($\overline{u}$), which is calculated on the basis of force balance acting on a particle as mentioned above and the random component (u'), that is based on the use of Monte Carlo method:

$$u = \overline{u} + u' \tag{3.2}$$

When a particle is moves into an eddy, the particle retards the eddy due to friction between the fluid and the particle, and it gets accelerated. An eddy is characterized by a lifetime and fluctuating component of velocity (u'). Discrete Random Walk model assumes that the fluctuating component of velocity remains constant through characteristic eddy lifetime. The quadratic means of fluctuating components of velocity related to local turbulence kinetic energy are defined as:

$$\sqrt{\overline{u^2}} = \sqrt{\overline{v^2}} = \sqrt{\overline{w^2}} = \sqrt{2k/3} \tag{3.3}$$

The fluctuating components of the velocity that is sampled based on the assumption that they are compliant to a normal probability distribution:

$$u' = \zeta\sqrt{\overline{u^2}} \tag{3.4}$$

Here, ζ is a random number from a distribution having a mean of 0 and variance of 1. When the eddy lifetime is through, a new instantaneous velocity is calculated with a new random ζ value. A full complement of equations can be found in the appendix that also includes the time integration of trajectories.

Inclusion of turbulent dispersion of particles to the model provides more realistic estimations of particle tracks. Moreover, large amount of information can be extracted from a single particle since the fluctuating components of velocity are discrete piecewise constant functions of time in which instantaneous velocities are calculated independently from the previous ones.

3.2 Flow of Carrier Fluid on Cuttings Bed: The Eulerian Phase

The Navier-Stokes equations (NSE) for turbulent flows are closed with two-equations Reynolds Averaged Navier-Stokes (RANS) turbulence model, in particular; the Shear Stress Transport (SST) version of k-ω is used for solving the continuous fluid flow field. In this section, only the details of turbulence model, rheology, and wall layer are discussed. The k-ω turbulence model, developed by Wilcox, is applicable to wall bounded flows and free shear flows, which is an empirical model based on equations for turbulent kinetic energy (k), and specific dissipation rate (ω). SST version of the k-ω combines the strengths of both k-ε and k-ω models by a blending function. This function is activated in the near wall region and turned off away from the wall boundary. It also includes modifications such as a damped cross-diffusion term in the specific dissipation rate (ω) equation. In the SST version, the turbulent viscosity also accounts for the transport of the turbulent shear stress and it has improved model constants. The modifications made the model accurate for a variety of flow types and recommended for boundary layer simulations which requires high accuracy.

The governing equation for turbulence kinetic energy (k):

$$\frac{\partial}{\partial t}(\rho k) + \frac{\partial}{\partial x_i}(\rho k u_i) = \frac{\partial}{\partial x_j}\left(\Gamma_k \frac{\partial \omega}{\partial x_j}\right) + G_k - Y_k \qquad 3.5$$

Specific dissipation rate (ω) which is defined as the ratio of dissipation rate (ε), to the turbulence kinetic energy (k):

$$\frac{\partial}{\partial t}(\rho \omega) + \frac{\partial}{\partial x_i}(\rho \omega u_i) = \frac{\partial}{\partial x_j}\left(\Gamma_\omega \frac{\partial \omega}{\partial x_j}\right) + G_\omega - Y_\omega + D_\omega \qquad 3.6$$

Here, G terms represent generation of turbulence kinetic energy and generation, and Y terms represent the dissipation of those terms. D is the cross – diffusion term unique to the SST k – ω model, which is used to incorporate k – ε model into k – ω, in order to use the best parts of each model.

The equations defining the effective viscosities for k and ω:

$$\Gamma_k = \mu + \frac{\mu_t}{\sigma_k} \qquad 3.7$$

$$\Gamma_\omega = \mu + \frac{\mu_t}{\rho \sigma_\omega} \qquad 3.8$$

Here, σ are the turbulent Prandtl numbers for k and ω, μ_t is the turbulent viscosity (Alternatively kinematic eddy viscosity), which is defined as:

$$\mu_t = \frac{\rho k}{\omega} \frac{1}{\max\left[\frac{1}{\alpha^* \alpha_1 \omega}, \frac{SF_2}{}\right]} \quad 3.9$$

All other closure coefficients, constants and auxiliary relations can be found in related literature.

Since the particle transport mostly takes place in the boundary layer right above the stationary bed, accurate solution of the boundary layer is crucial in this study. SST k-ω model provided reasonable accuracy for pipe flow and requires a modest computational expense. However, the full advantage of this model can be exploited by using Low-Reynolds Corrections as the near wall treatment in the boundary layer, which requires very high mesh resolution in the boundary layer. The discrete phase model gave unphysical results in the high resolution area of the simulation domain, so wall functions had to be used instead of low Reynolds number corrections which require lower mesh resolution.

The stationary bed surface should be expected to be very rough and irregular, since it consists of faces of accumulated crushed particles. The roughness effects are incorporated to the turbulence model by the modified law of the wall model. The observations in experiments suggest that the near – wall region can be divided into subsequent layers; the viscous sub layer is the closest region to the wall where viscosity is dominant and flow is nearly laminar. In the buffer layer, both turbulence and viscosity are equally important, and in the log – law region, or the fully turbulent region, the effects of turbulence are dominant.

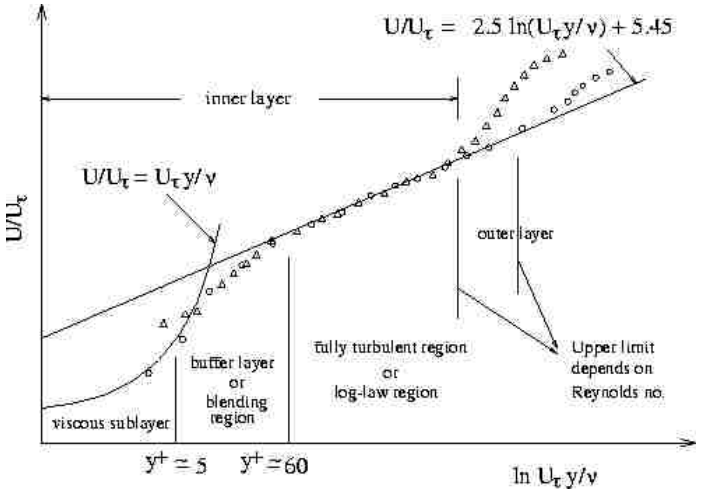

Figure 3.1 Sub-layers of near wall region (ANSYS Fluent Theory Guide, 2009)

In figure 3.1, y^+ is the dimensionless distance from the wall where y is distance from the closest wall and defined as $y^+ = \rho \frac{y u_\tau}{\mu}$ as where u_τ is the friction velocity at the closest wall and is μ the fluid kinematic viscosity.

The mean velocity in log region can be represented by the following the standard wall function for smooth walls:

$$\frac{uu^*}{\tau_w/\rho} = \frac{1}{\kappa}\ln(Ey^*) + \Delta B \qquad 3.10$$

Here, $y^*$is used instead of y^+ for mean velocity. Variables are defined as:

$$y^+ = \rho y u^* / \mu \qquad 3.11$$

$$u^* = C_\mu^{1/4} k^{1/2} \qquad 3.12$$

where C_μ, κ are constants and k and u are the turbulent kinetic energy and mean velocity at point locations. For incorporating roughness, the log region has the same slope, $\frac{1}{\kappa}$, however it has a difference in the intercept, ΔB. It is defined as:

$$\Delta B = \frac{1}{\kappa} \ln fr \qquad 3.13$$

fr is the roughness function defined by roughness constant and roughness height. A roughness constant, 0.75 is used for defining an irregular surface, and a roughness height value of 2 mm is used, which is the half of the average cuttings size. The roughness is only active for the Eulerian phase and indirectly affects the discrete phase; however, it is not involved in the particle – wall interactions.

The inner pipe rotation is included by simply defining a velocity component on the inner pipe wall tangential to the wall.

Non – Newtonian rheology is used various cases, since most drilling fluids have non-Newtonian character. The shear stress (η) – shear rate ($\dot{\gamma}$) relation in power law model is given by:

$$\eta = k\dot{\gamma}^{n-1} \qquad 3.14$$

here, k is the consistency index and n is the power law index obtained from viscometer readings. The yield power law model is defined as:

$$\eta = \tau_0 + k\dot{\gamma}^{n-1} \quad 3.15$$

where the only difference from the power law is the inclusion of yield point. The material remains rigid if the yield stress is under the yield point and starts flowing if the yield stress exceeds the yield point.

The shear stress (η) – shear rate relation in Carreau model is defined as:

$$\eta = (\eta_\infty + (\eta_0 - \eta_\infty)[1 + \dot{\gamma}^2\lambda^2]^{(n-1)/2} \quad 3.16$$

where η_∞, η_0, λ, and n are model parameters. These two models are used in the validation of the numerical model for the turbulent flow of non-Newtonian fluids with experimental data.

4. VERIFICATION STUDY: VELOCITY PROFILES OF NON-NEWTONIAN FLOWS IN TURBULENT REGIME

The first step in the systematic validation process is to test the capability of the numerical setup in predicting the local velocities of non-Newtonian fluids flowing in turbulent regime. The accuracy of discrete phase model computations is primarily dependent upon the accurate solution of the Eulerian phase. The SST k-ω turbulence model is used for closing the Navier-Stokes equations in order to incorporate the effects of turbulence regime on the flow characteristics. Another reason for performing this set of validation is that the water is used as the carrier fluid in the experiments of Garcia-Hernandez et al. (2007) where data from these experiments are used for validating the capability of the present numerical setup in predicting the equilibrium stationary bed height and the average cuttings transport velocities. Since the setup is expected to work for a wide range of drilling fluids, the capability of predicting pipe flows of non-Newtonian fluids should also be demonstrated. In the similar experiments of Pinho and Whitelaw (1990) and Pereira and Pinho (1994), the velocity profiles of turbulent pipe flow of non-Newtonian fluids are obtained from the fluid velocity measurements in pipe flow by using the laser velocimetry method.

Table 4.1 Parameters of the two experiments on turbulent pipe flow of non-Newtonian fluids

	Pinho and Whitelaw	**Pereira and Pinho**
Pipe Radius, mm:	25.4	26
Fluid:	Water with 0.4% CMC	Water with 0.4% Tylose
Rheology Model:	Power Law	Carreau
Model Parameters:	k = 0.447, n = 0.56	λ (s) = 0.0208, μ_o = 0.00407, n = 0.725
Mean Velocity, m/s:	4.8	5.59
Reynolds Number:		

Pinho and Whitelaw (1990) used a Power Law fluid while Pereira and Pinho (1994) used a Carreau fluid in their experiments. The test matrix of those experiments is given in table 4.1. The same parameters are replicated in the pipe flow simulations where Navier-Stokes equations with the SST k-ω turbulence model closure model are solved. Simulations are performed by using wall functions first, and repeated by using Low Reynolds corrections in solution of near – wall region for performance comparison of two approaches. The velocity profiles obtained through simulations with two different near – wall modeling approaches together with experimental local velocity measurements are shown in figures 4.1 and 4.2.

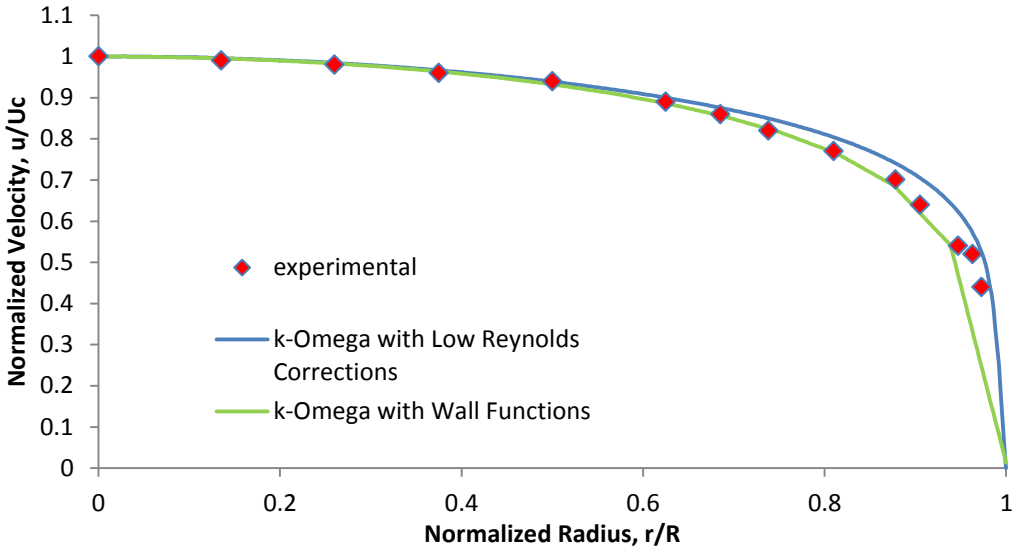

Figure 4.1 Comparison of simulation results with experimental measurements from Pinho and Whitelaw (1990)

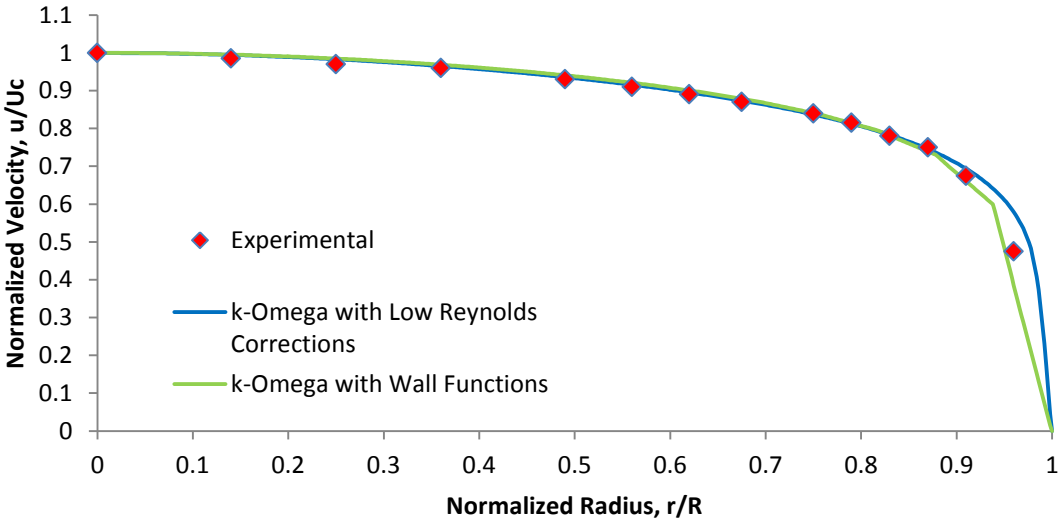

Figure 4.2 Comparison of simulation results with experimental measurements from Pereira and Pinho (1994)

Comparisons show good agreement between the CFD model predictions for the velocity profiles of non – Newtonian fluids flowing in turbulent regime. Both near-wall modeling approaches performed similarly. However, wall function approach is preferred for the simulations performed in the rest of the study due to far less near-wall mesh resolution requirement and better compatibility with discrete phase model. It is seen that the discrete phase model produced unphysical results due to numerical instability when used in the same computational setup with low Reynolds number corrections.

5. VALIDATION STUDY: PREDICTION OF THE STATIONARY CUTTINGS BED HEIGHT AND ANALYSIS PROCEDURE

As stated before, having a stationary bed in the annulus creates undesirable situations during drilling such as high torque and drag, poor hole condition, stuck pipe and difficulty in running and cementing casing (Brown et al., 1989). In order to decide on what measurements to take for preventing the formation of a stationary bed, or for reducing it down to a tolerable level, a model that is capable of predicting the equilibrium height of the stationary cuttings bed as a function of present drilling parameters is necessary. The most decent way of achieving this goal with the current configuration is to incorporate a particle accumulation model which defines the termination of particle motion and the packing of particles to form a bed. This approach is found to be unfeasible for the present study where the reasons are to be explained further in this section. An indigenously developed alternate method of predicting the equilibrium stationary bed height by analyzing the particle tracks generated by the discrete phase model is to be presented.

5.1 Particle – Wall Interactions

Particles start accumulating when the fluid drag is not adequate to enable further motion of the particles. In vertical and near vertical flow channels, drag force should surpass gravitational force which is almost in the opposite direction of the drag force. Otherwise, upwards particle motion will terminate and particle settling will occur. On the other hand, gravitational force is almost perpendicular to the drag force in highly deviated and horizontal channels. The gravitational force immediately settles down particles, however, particle motion continues very close to the low side surface of the channel in form of bouncing, rolling and sliding action, provided that the flow rate is adequate. In this case, particle – wall interactions controls the termination of motion. This pattern of motion is referred as the "moving bed".

Particles lose a portion of its momentum upon contact with the flow channel surface, where it is the lowest side of the channel for the vast majority of particles in highly deviated channels. This contact referred as particle – wall impact (Sommerfeld and Huber, 1999). The magnitude of momentum loss of a particle upon wall impact under certain conditions is expressed by the restitution coefficient, which can simply be defined as the ratio of particle velocity immediately before wall impact to the particle velocity immediately after wall impact:

$$u_r = e \cdot u_i \qquad 5.1$$

Here, u_i and u_r are the normal components of the particle velocity before (Initial) and after (Rebound) the impact in the first equation. The restitution coefficient is dependent on particle material properties,

particle shape and size, as well as the impact surface material properties and the impact surface roughness (Sommerfeld and Huber, 1999). Also the restitution coefficient is affected by the carrier phase fluid properties (Joseph, et al, 2000) and also is a function of impact velocity which is the particle velocity immediately before wall impact (Wall et al, 2012).

Particle will recover from the impact provided that the drag force is large enough to compensate the particle momentum loss resulting from wall impact and continue moving forward. If the drag force is insufficient in compensating the momentum loss resulting from wall impact, particle motion will terminate after successive wall impacts. Since the flow conditions will be similar for the vast majority of particles, poor fluid phase support will result in large amount of particles terminating their motion, in other words, particle accumulation will occur.

Impact angle is the angle between the assumedly linear path that the particle follows just prior to the impact and the impact surface. Sommerfeld and Huber (1999) conducted experiments with particle loaded air flow in a horizontal channel. They tracked particles with particle tracking velocimetry method in order to obtain particle velocities and to calculate the restitution coefficients. Figure 5.1 displays some of their experimental results which tell that the particles lose more momentum in collisions with larger impact angles, especially the non-spherical quartz particles. It can be concluded that the likelihood of terminating motion is greater for particles making wall impacts with larger angles.

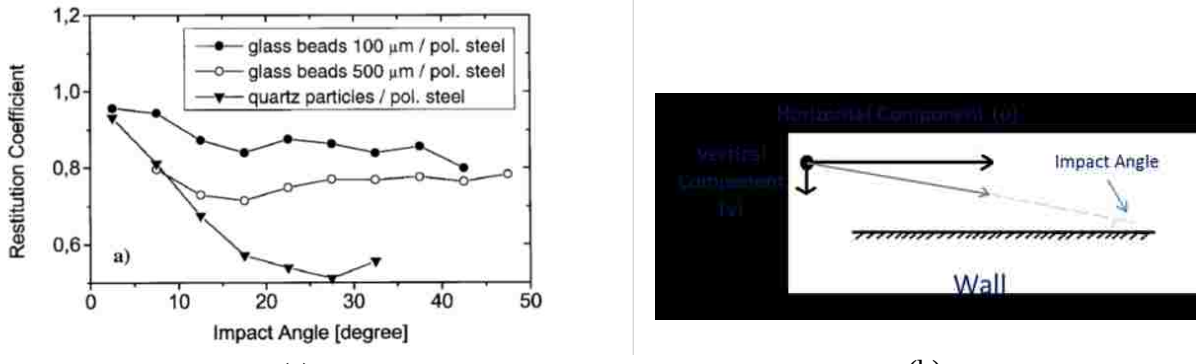

(a) (b)

Figure 5.1 a) Dependence of restitution coefficient on impact angle with particles having different size and sphericity. (Sommerfeld and Huber, 1999) b) Schematic for the definition of the impact angle

Impact velocity is the particles velocity immediately before the impact. Wall et al. (2007) measured the particle velocities before and after the vertical wall impacts with Doppler velocimetry method in their controlled experiments in order to relate restitution coefficient with impact velocity. Some results from their study are shown in figure 5.2. It can be seen that momentum loss is diminished with increasing impact velocity.

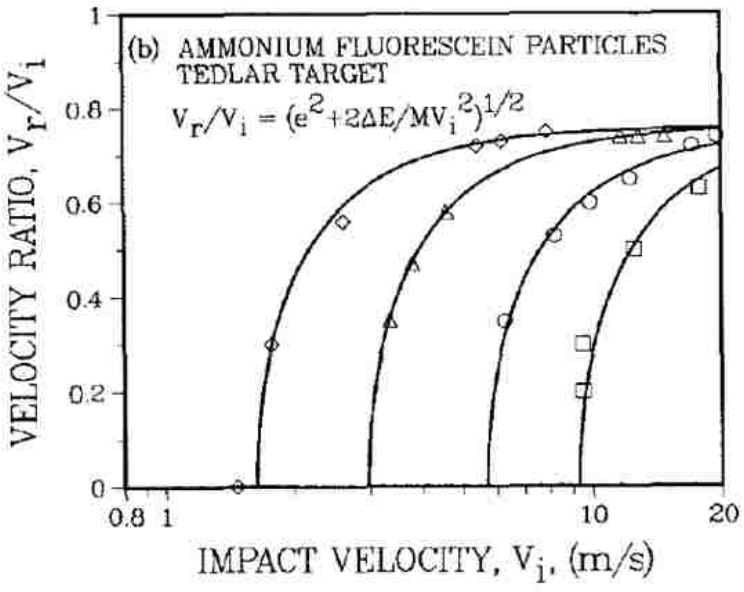

Figure 5.2 Dependence of restitution coefficient on impact velocity (Wall et al. 2007). The curves are for different particle sizes and the velocity ratio is the same concept as the restitution coefficient

In a case where particle accumulation is still in progress, the impact restitution coefficients should be expected to be low. This can be translated as particles are making wall impacts with large impact angles and small impact velocities. On the other hand, if the stationary bed reached equilibrium where all newly incoming particles are moving continuously, the opposite should be observed. The lifting capacity of the fluid flow also shows its ability to compensate the momentum loss of a particle after impact. If particles are lifted higher from the low side of the flow channel, it implies that flow has a good lifting capacity. It will also be shown that particles make less number of wall impacts for the same amount of horizontal distance covered, since the lifting capacity of the flow is higher, thus reducing the chance of momentum loss due to wall impact.

Obtaining the restitution coefficient is difficult due to the variety of particle materials, particle shapes and the irregularity of the impact surface encountered. Large numbers of experiments are needed for obtaining more comprehensive correlations, and a mathematical model is not available to our knowledge. For that reasons no attempt has been made to obtain restitution coefficients, so there will be no accumulation model incorporated to the computational setup. Instead, particle impact angles and impact velocities, together with lifting capacity of the flow will be compared at different flow rates in order to evaluate the likelihood of ongoing accumulation.

5.2 Analysis of Particle Tracks for Predicting the Stationary Cuttings Bed Height

The particles are set to make elastic collisions with wall surfaces in the present study, since the particle – wall impact restitution coefficients are not available. In a horizontal flow channel, particles will continue their forward motion regardless of the flow rate in the current simulation setup. In the proposed method for predicting the equilibrium stationary cuttings bed height, particle impact angles and impact velocities, together with lifting capacity of the flow are compared at different flow rates in order to evaluate the likelihood of ongoing accumulation. The particle impact angles and the impact velocities are extracted from continuous particle tracks obtained by the discrete phase model. A particle -wall collision will not be affected by the previous impact since the particle – wall collisions are set to be elastic and the velocity fluctuations are calculated as discrete piecewise linear functions. The lifting capacity of the flow is evaluated by comparing the distances covered at higher altitudes away from the low side surface.

A trial case is set up to capture if there is analogy between particle behavior in the simulations and the experimental findings. Flow field has been solved for the steady – state flow of water between horizontal parallel plates. A single particle that has a specific gravity of 2.6, sphericity value of 0.1 and in 4 mm size is released from the inlet surface and its track is calculated up to the outflow. This simulation is repeated for five different bulk velocities. Figure 5.3 shows the visualization of particle tracks together with the local fluid phase velocity magnitudes.

It can be intuitively said that the likelihood of particle accumulation decreases with increasing flow rate while keeping all other conditions the unchanged. Small particle impact angles and high impact velocities should be expected at higher flow rates. Also particles should be lifted higher. By only looking at the visualizations of particle tracks in figure 5.3, it can obviously be seen that particles are travelling at higher altitudes away from the low side, and travels more horizontal distances in suspension with increasing flow rate. The comparison of lifting capacity of the flow will be further quantified in this section.

The impact velocities for all particle – wall collisions form a single particle are averaged for each case. The comparison of the average impact velocities for each bulk velocity is shown in figure 5.4. The average impact velocity continuously increases with increasing bulk velocity, suggesting that the overall restitution coefficients will be higher at higher bulk velocities. Combining this with the notion that likelihood of particle accumulation decreases with increasing flow rates, the trend is in agreement with the experimental findings.

Bulk velocity: 1 ft/sec:

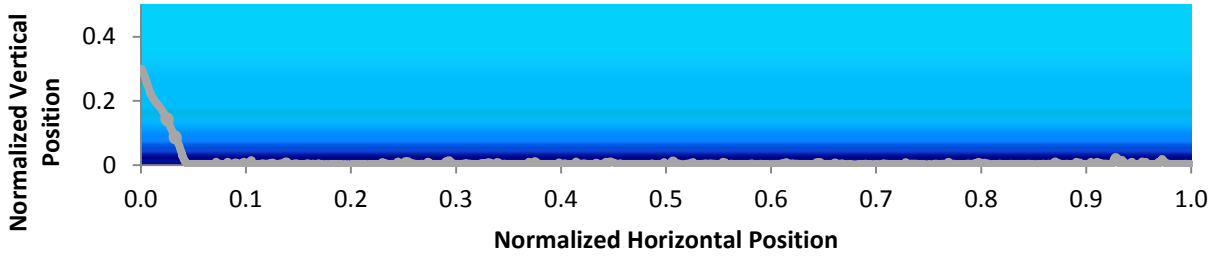

Bulk velocity: 2 ft/sec:

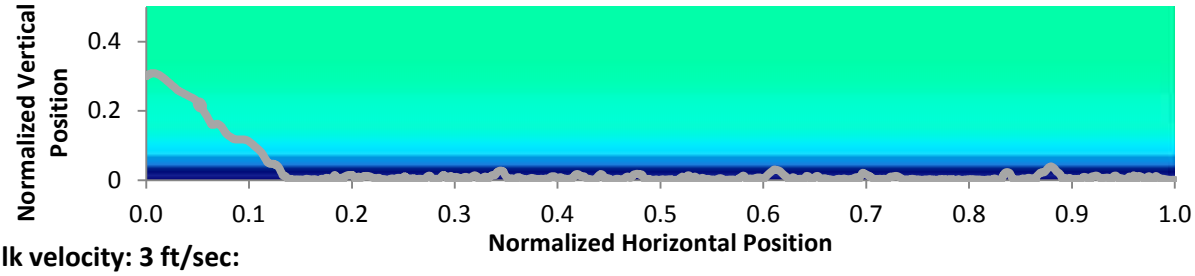

Bulk velocity: 3 ft/sec:

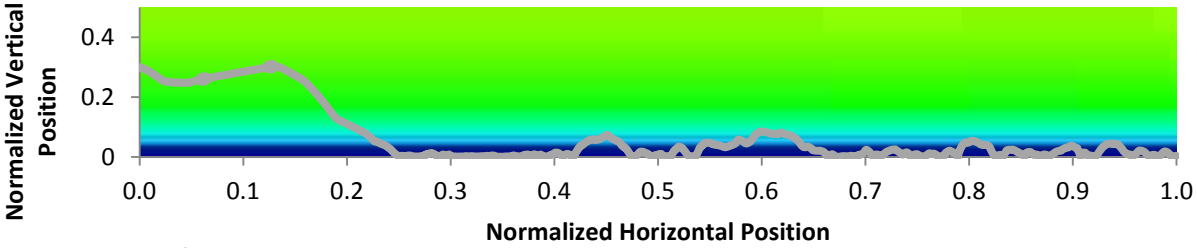

Bulk velocity: 4 ft/sec:

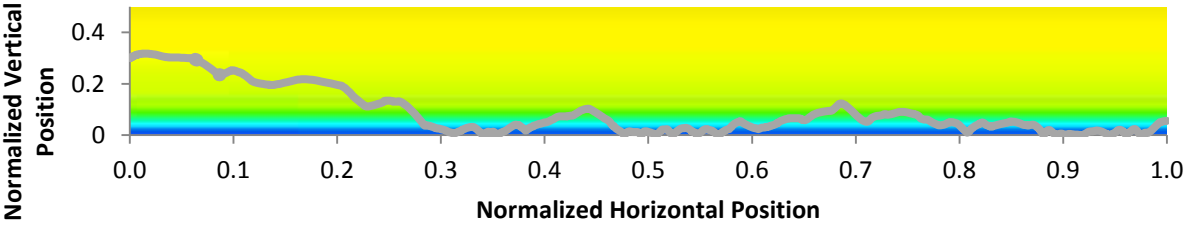

Bulk velocity: 5 ft/sec

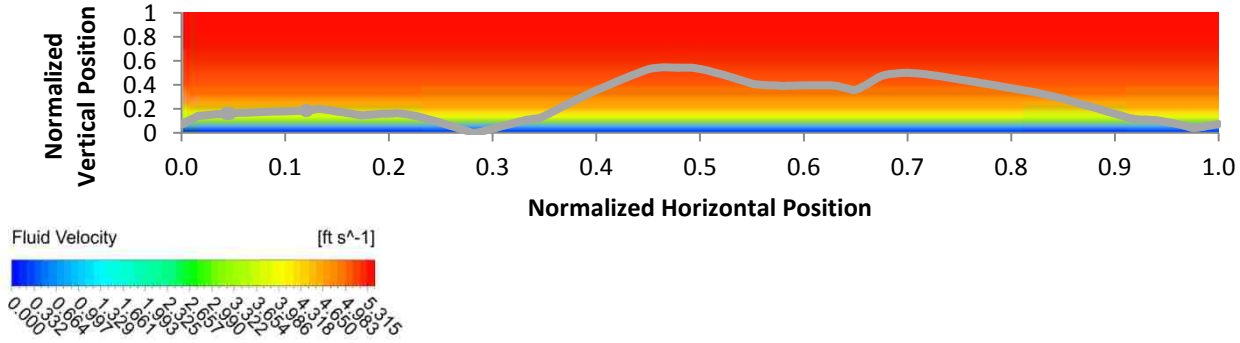

Figure 5.3 Particle tracks at different flow rates

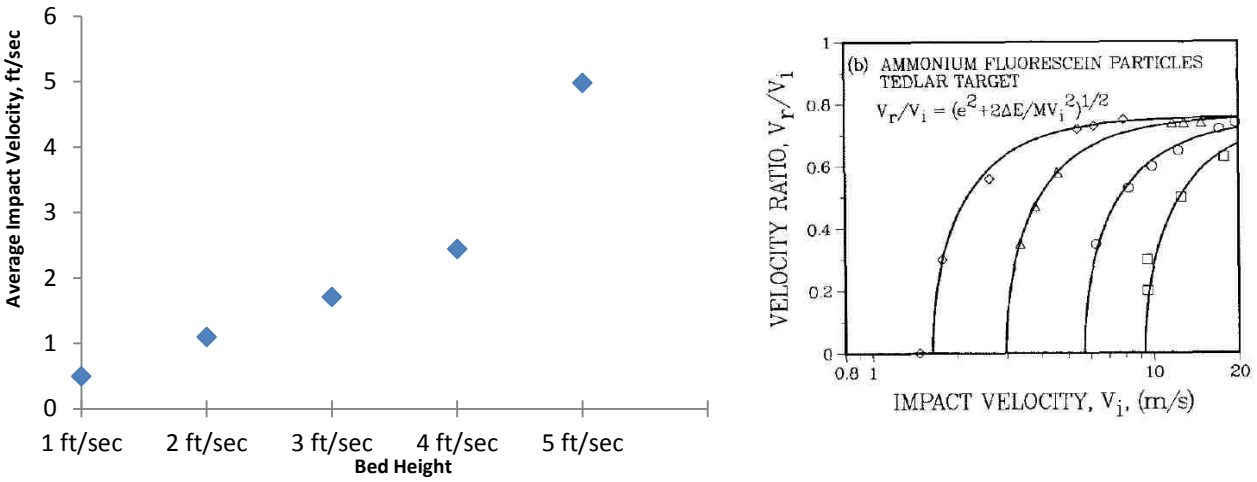

(a) (b)

Figure 5.4 a) Averaged impact velocities at different flow rates from simulations. b) Dependence of restitution coefficient on impact velocity

The number of particle – wall collisions having similar impact angles are placed into bins for each case. Figure 5.5 shows the particle – wall impact angle histograms for each case. It can be seen that the total number of wall collisions are decreasing as a result of increasing lifting capacity related to increasing bulk fluid velocity. It can also be said that the maximum impact angles encountered on each case decreases together with the number of collisions with larger impact angles. This shows that the overall restitution coefficients will be higher at higher bulk fluid velocities. This trend is also in agreement with the experimental results, considering that the likelihood of particle accumulation decreases with increasing flow rates.

Another parameter to look at is the lifting capacity of the flow which is to be evaluated in terms of distances travelled in higher altitudes away from the low side of the channel. The vertical cross section of the flow channel is divided into lanes having equal width, and the total distance covered in each lane is divided by the total horizontal distance. The fraction of distance covered in each lane is compared in the end. The lifting capacity is said to be low if particle has travelled in lanes closer to the low side for most of time. Figure 5.6 shows an example calculation. The particle track is from the demonstration case with 5 ft/sec bulk fluid velocity. The vertical cross section of the channel is divided into 10 lanes in this case and the borders of the lanes are referred as normalized vertical position. In this example, only the horizontal distance covered is calculated for the lane between the normalized vertical positions 0.4 and 0.5. Particle entered this lane three times during its travel.

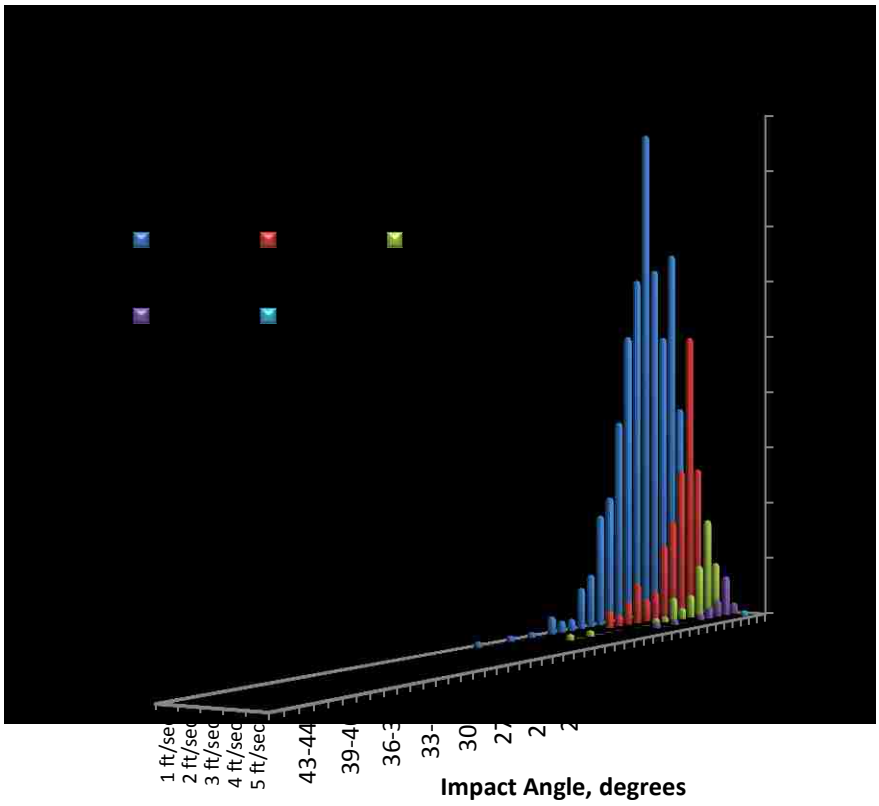

(a)

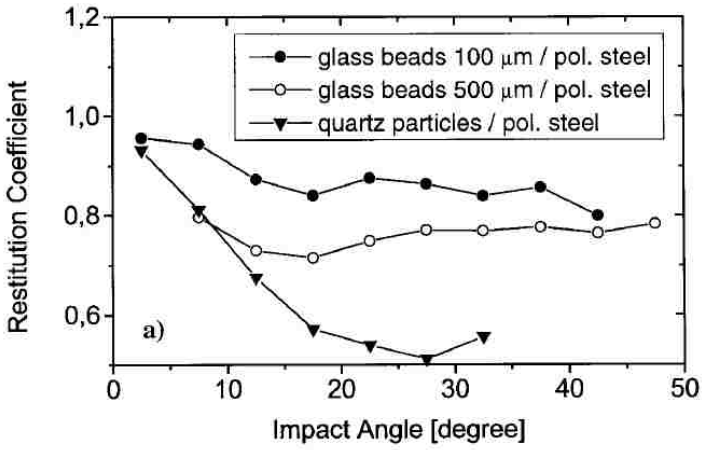

(b)

Figure 5.5 a) Number of collisions at different impact angles for various bulk fluid velocities b) Dependence of restitution coefficient on impact angle with particles having different size and sphericity. (Sommerfeld and Huber, 1999)

The fraction of distance covered in this lane is calculated as:

$[L_1 + L_2 + L_3]$ / Total Distance

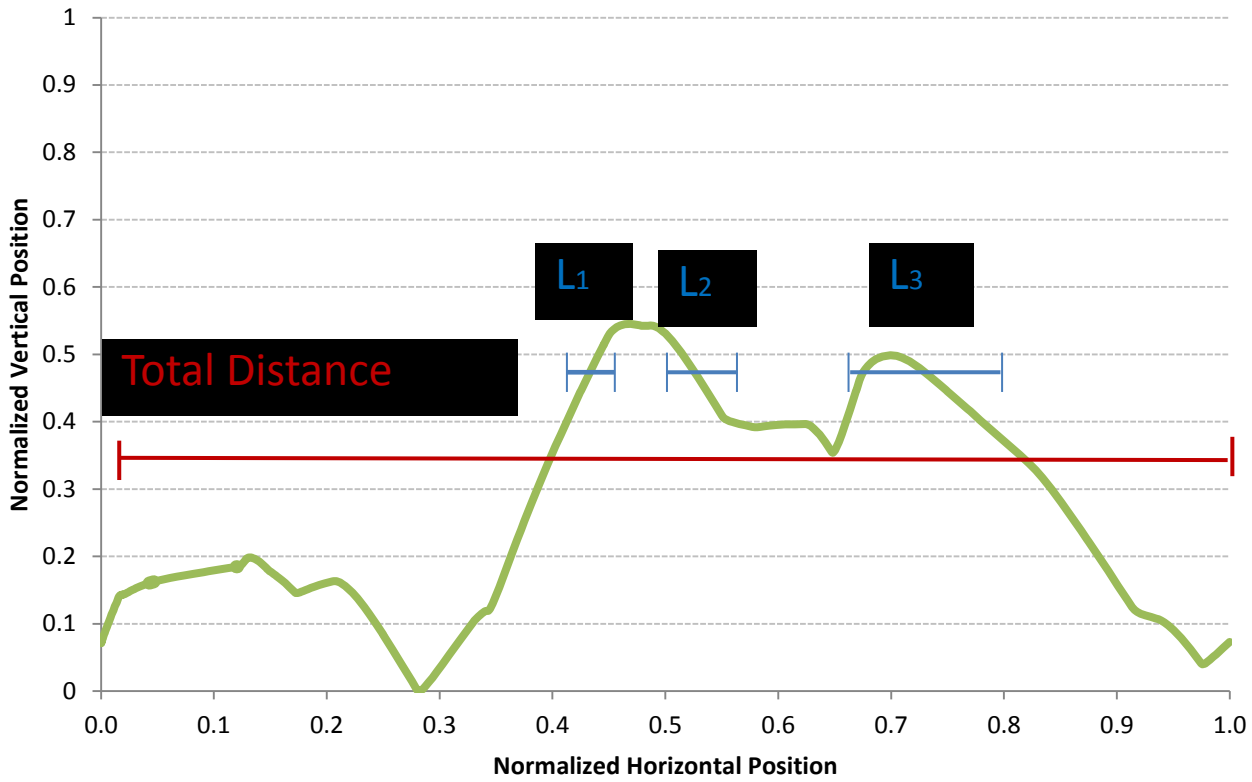

Figure 5.6 Example calculations for the fraction of distance covered in the lane between the normalized vertical positions 0.4 and 0.5

These calculations are repeated for each lane and the fraction of the total distance covered in different altitudes are compared for understanding the lifting capacity of the flow.

Figure 5.7 shows the fractions of horizontal distance covered in different altitudes for 5 different bulk velocities. The vertical cross section of the channel is divided into 0.5 mm increments in order to better understand the suspension capacity of the flow. The particle covered more than 90% of the total distance in the lane adjunct to the low side surface when the bulk fluid velocity was 1 ft/sec. The particle began to move in higher altitudes with increasing bulk fluid velocity. The fraction of distance covered in the lane adjunct to the low side surface is less than 10% and particle is moving in much higher altitudes compared to the cases with smaller bulk velocities for the case with 5 ft/sec bulk fluid velocity.

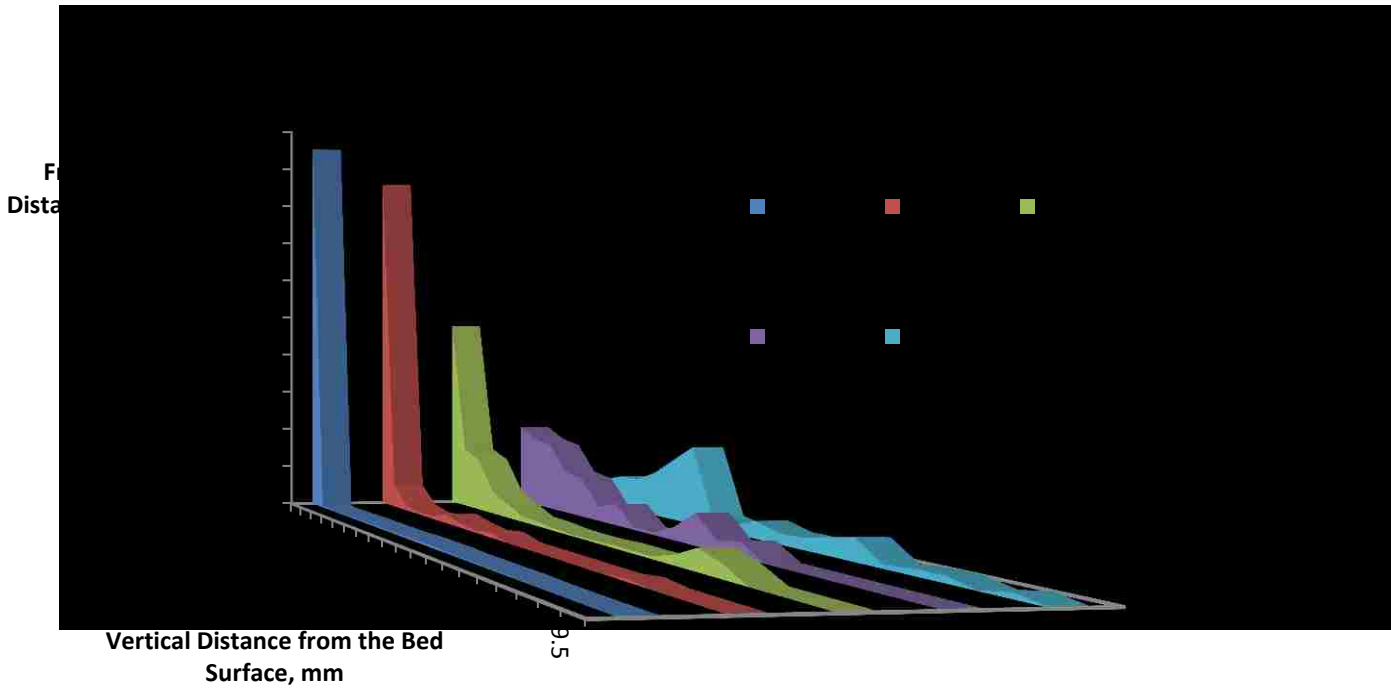

Figure 5.7 The fractions of horizontal distance covered in different altitudes for 5 different bulk velocities

The particle is travelling at higher altitudes with increasing bulk fluid velocity, in other words the lifting capacity of the flow increases with increasing volumetric flow rate. Comparing the lifting capacities at different bulk velocities, it can be suggested that the likelihood of accumulation is much higher for the cases with low bulk fluid since the flow will not be able to compensate for the momentum loss upon wall impact.

5.3 Analysis of Particle Motion

In the previous section, the sensitivity of particle motion to the flow rate and how to use this sensitivity to evaluate the likelihood of particle accumulation is presented. In this section, the physics behind the sensitivity of particle motion to the flow rate will be discussed.

First, the mechanism that lifts particles in a horizontal flow channel is to be investigated. The drag force and the gravitational force are perpendicular to each other in a horizontal flow channel, so gravitational settling has no compensation from the drag force. The other factor that can enable particle lifting is the Saffman's lift force. Figure 5.8 shows the number of particle – wall collisions having similar impact angles from the case with 1 ft/s bulk velocity, with and without the inclusion of Saffman's lift force. This type of analysis both covers the suspension capability of flow in terms of total number of collisions and the particle – wall interactions. As seen in figure 5.8, inclusion of Saffman's lift force made negligible impact on particle motion. The discrepancy is due to the random factors in calculation of turbulent

fluctuations in particle velocity. It may be suggested that Saffman's lift force is ineffective for this particle configuration. Since the particles are set in similar configuration for all other simulations, the Saffman's lift force is excluded from the computational setup for the sake of computational efficiency.

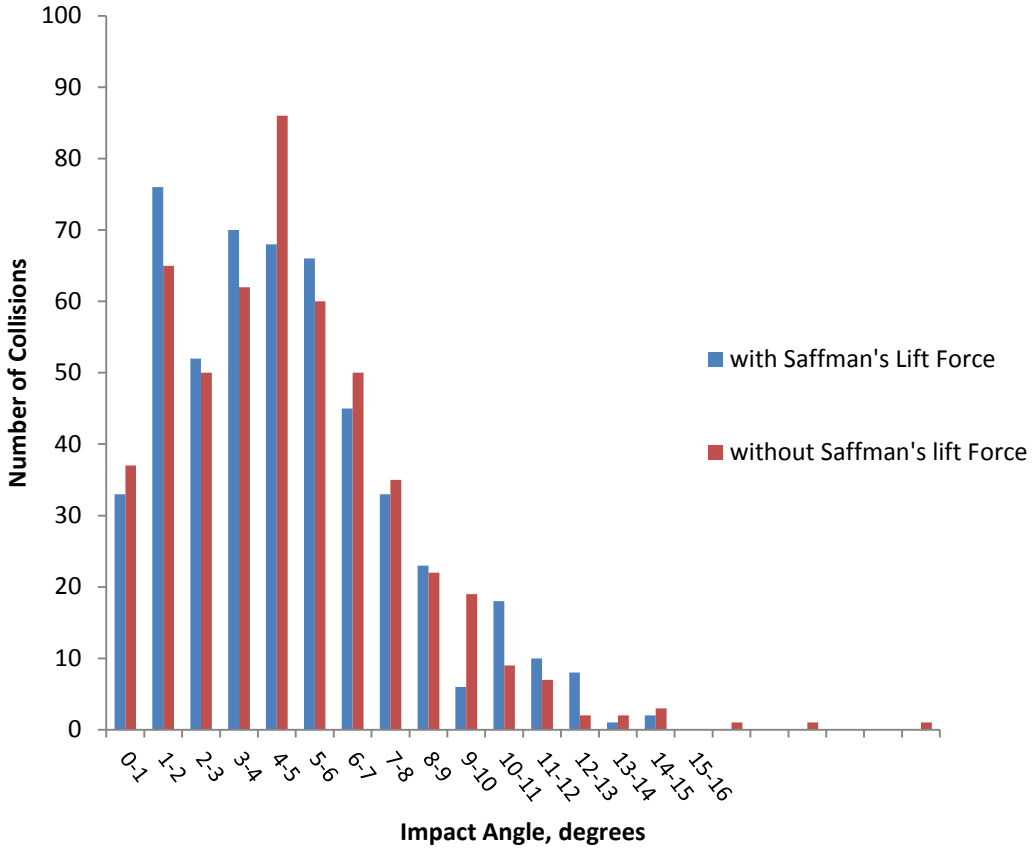

Figure 5.8 The number of particle – wall collisions having similar impact angles of the case with 1 ft/s bulk velocity, with and without Saffman's lift force

The other factor that can contribute to the particle lifting is the fluctuations in particle velocity due to turbulence eddies. A particle may be subjected to acceleration in any direction due to turbulence. When this acceleration is in the upward direction, it will result in the up lifting of the particle. As explained in the theory of the discrete phase model, instantaneous particle velocity has two components, in which the first component is calculated by the time integration of the instantaneous force balance on a particle. The forces acting on a particle are the drag force, buoyancy force, virtual mass force and the pressure gradient force for the present study. The second component is provided by the turbulence eddies where particle is accelerated when enters a turbulent eddy. The eddy lifetime, so the magnitude of acceleration is set by a random factor sampled from a normal distribution.

Figure 5.9 shows the effect of turbulence on instantaneous particle velocity. In the case where turbulence effects on particle motion is discarded, the particle immediately falls to the low side of the annulus and moves with constant velocity on the low side wall boundary, since there is no other effective force to provide lifting and the drag force is constant in the flow direction. For the case with turbulence effects, there are significant fluctuations in particle velocity during its motion along the flow channel.

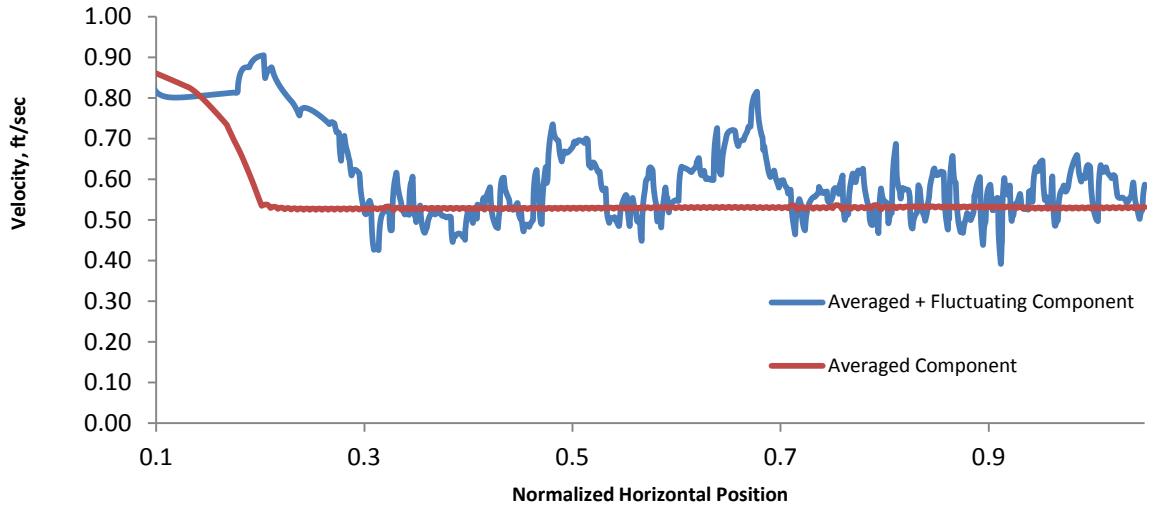

Figure 5.9 Only average and averaged + fluctuating components of instantaneous particle velocity. Bulk carrier phase velocity is 3 ft/sec

The effect of turbulence on the particle motion is going to be explained by comparing the instantaneous particle velocity components in the cases with 1 ft/sec bulk fluid velocity and 3 ft/sec bulk fluid velocity. As may be remembered from the previous section, the particle moved just above the low side of the channel, almost without suspension and made collisions with low impact velocities and high impact angles in the case with 1 ft/sec bulk fluid velocity. When the bulk fluid velocity is raised to 3 ft/sec, the particle started moving at higher altitudes away from the low side and made particle collisions with higher impact velocities and smaller impact velocities compared to the previous cases. The particle also travelled longer distances before hitting the low side surface. The likelihood of accumulation is said to be lower for the case with 3 ft/sec bulk fluid velocity.

The turbulence kinetic energy profiles for two cases are given in figure 5.10. As expected, the turbulence kinetic energy is higher in all regions, especially near the low side for the case with 3 ft/sec bulk fluid velocity. The fluctuations in particle velocity are expected to be higher for this case.

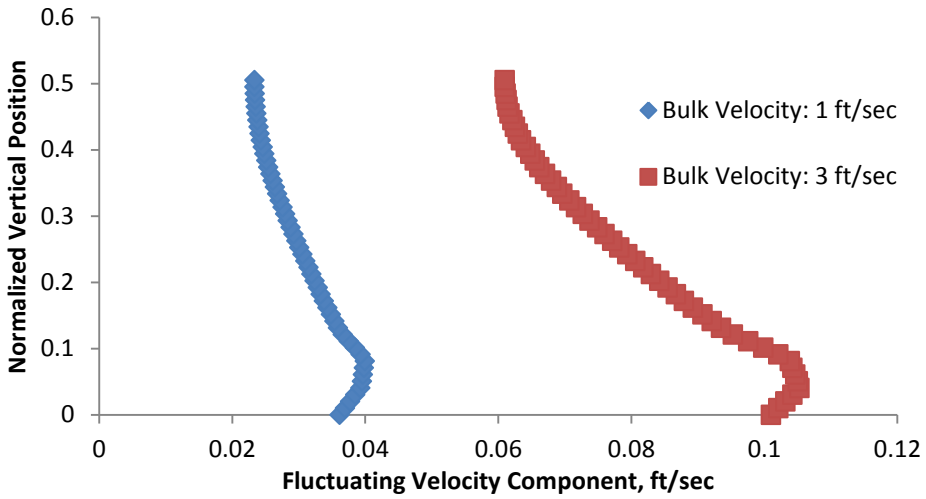

Figure 5.10 Fluctuating velocity components at two different bulk velocities

The fluctuations in particle velocity and the particle acceleration in the case with high bulk fluid velocity is much higher than the case with low bulk fluid velocity. This difference is more than expected from the contribution of turbulence eddies. When the particle is accelerated enough to take off from the low side of the channel, it moves to the plug region of flow which is in the middle part of the flow cross section, where the local fluid velocity is higher. The particle receives larger drag force in the plug region. For that reason, although the difference in local velocities and the turbulence kinetic energy for both cases over the low side are not that large, the particle acceleration is much higher in the case with higher bulk fluid velocity as seen in figure 5.11.

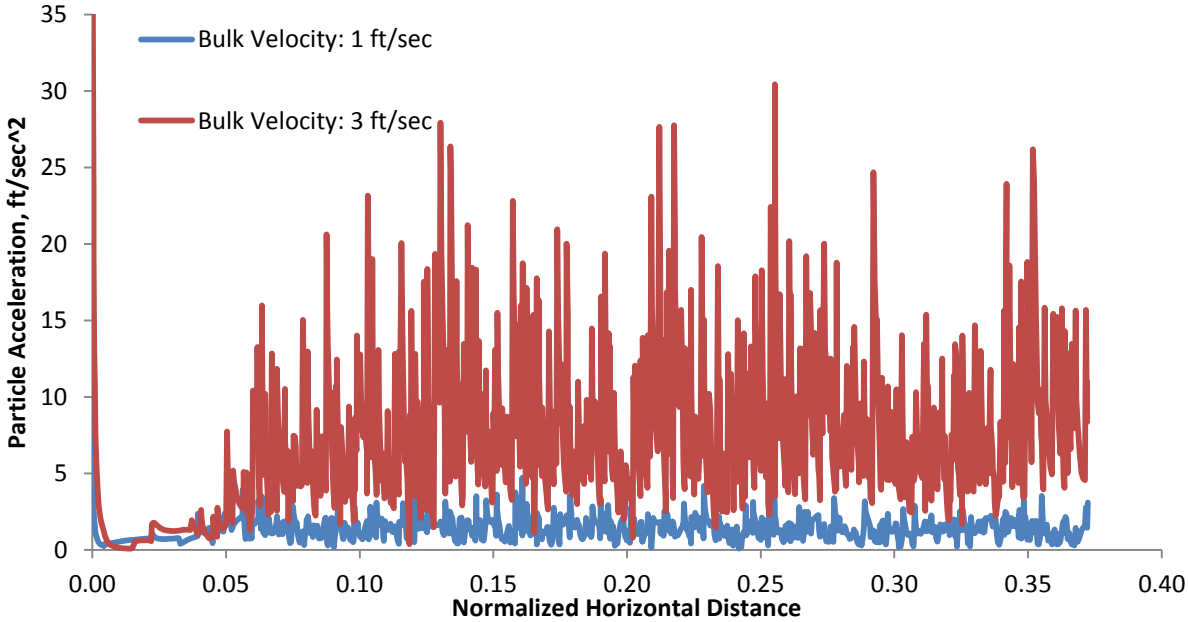

Figure 5.11 Particle acceleration at two different bulk fluid velocities

In order for a particle to continue motion, its particle – wall collisions should have small impact angles and high impact velocities. A particle would make a wall collision with a small impact angle if the particle velocity component parallel to the impact surface (Horizontal component) is much larger than the particle velocity component perpendicular to the impact surface (Vertical component) just before the impact. It will make a wall collision with a large impact angle if vice versa. Figure 5.12 shows the instantaneous ratio of horizontal to vertical components of the particle velocity for low and high bulk fluid velocity cases. It can be seen that the ratio of horizontal to vertical component of the particle velocity is much higher for the case with higher bulk fluid velocity, so, smaller impact angles are observed in that case.

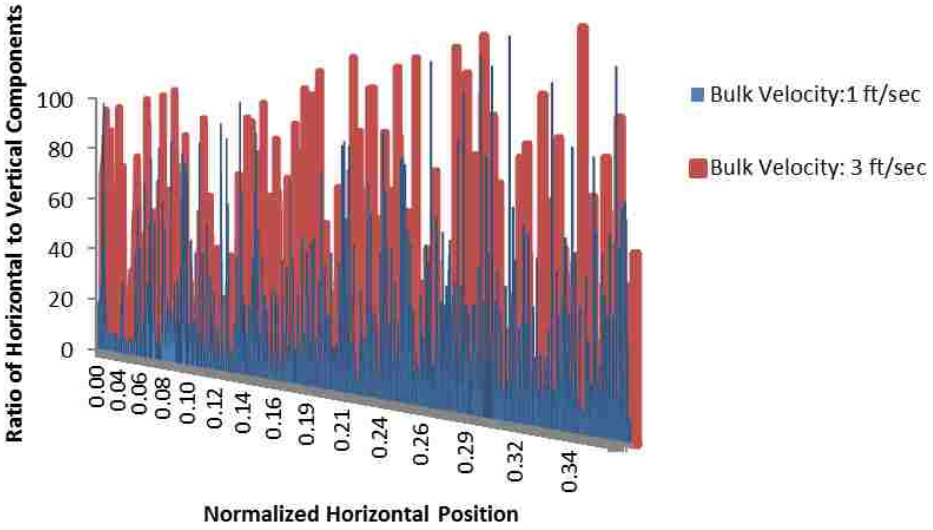

(a)

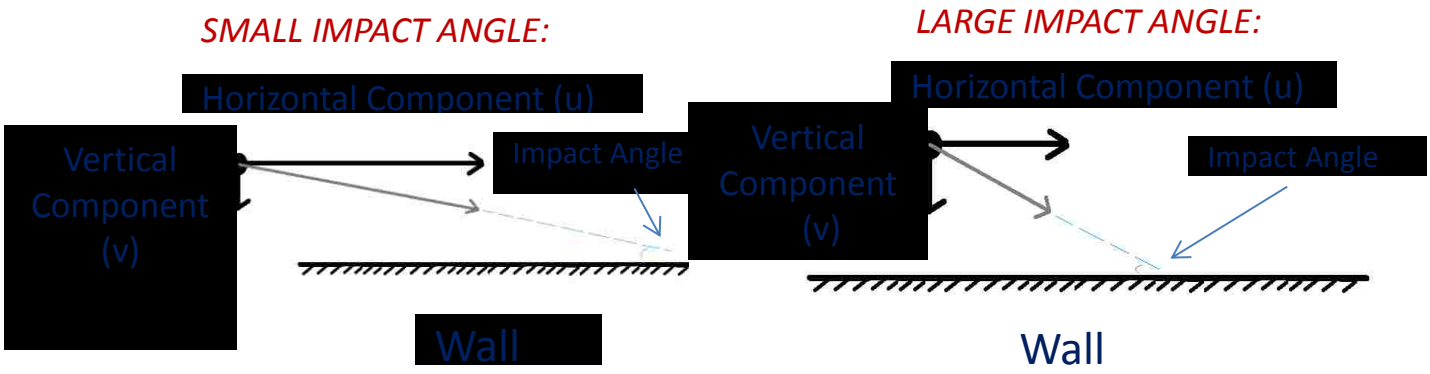

(b)

Figure 5.12 a) The comparison of the ratios of horizontal to vertical components of particle velocity at two different bulk fluid velocities b) Two dimensional velocity components of the particle prior to wall impact

The particle suspension with the aid of turbulence eddies also brings explanation to the experimental observations of Tomren et al. (1983) in their flow loop experiments at high angles of inclinations. They observed that the cuttings are transported in two distinct zones in which first zone is the closely grouped cuttings carried in a narrow layer just above the bed (Moving Bed) and the second group is the sparsely populated particles moving with very little slugging in the open channel above the stationary cuttings bed (Suspension layer). The logic dictates that particles should be moved into the suspension layer altogether if the lift force is high enough, however, turbulence eddies are dominantly responsible for the particle lifting instead of lifting force. If a particle successively enters eddies with longer eddy lifetimes, it will be lifted up to the plug region and will be subjected to higher drag. If it receives smaller acceleration, it will fall back to the stationary bed surface. Since, the probability of successively entering eddies with longer eddy lifetimes is low, the number of particles instantaneously seem to be moving in the suspension layer is smaller than the number of particles in the moving bed layer.

5.4 Application of the Computational Setup to the Cuttings Transport Problem

A method of evaluating the likelihood of particle accumulation based on the sensitivity of particle motion to the flow rate is presented earlier. In this section, how to adapt this method to determine the height of stationary cuttings bed will be explained. The computational domain consists of an annular section with a geometrically pre-defined stationary cuttings bed.

The flow geometry is designated as a three dimensional annular section with a pre – defined stationary cuttings bed. Simulation domain is cut in half and symmetry boundaries are defined on the cut surfaces. The aim in using symmetry boundaries is to reduce computational time. Inner face of the outer pipe and the outer face of the inner pipe are defined as no – slip wall boundaries and modified law of the wall is used on the surface of cuttings bed for incorporating wall roughness as described in section 3.2. The roughness only alters the carrier phase behavior and does not affect particle – wall interactions. In the first simulations, bulk velocity calculated from the mass flow rate is defined on the inlet boundary with the calculated turbulence boundary parameters; turbulence kinetic energy and specific dissipation rate. The outlet parameters from the converged simulation are used as the inlet parameters in the next simulation and successive simulations are performed until periodic conditions are reached. Figure 5.13 summarizes the boundary conditions for fluid flow.

Particles are injected from the inlet boundary along a line just above the bed surface. 70 particle injection points are placed on the line so that particle streams are covering all over the bed surface. Particles escape

(Deleted) from inlet, symmetry profile and outlet. Particles make fully elastic collisions on wall boundaries.

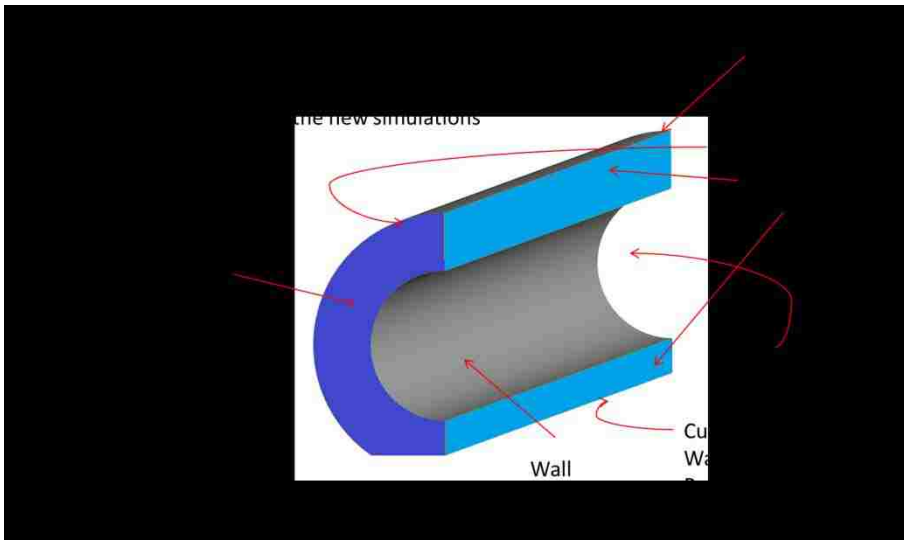

Figure 5.13 Boundary conditions for fluid flow

Two types of particle tracking methods are used. Steady particle tracking is used for collision analysis for bed height determination where particle paths are printed from the designated points on inlet to outlet surface. Unsteady particle is used for moving bed velocity estimation where particles are injected at designated time steps and their positions are printed. Figure 5.14 summarizes the boundary conditions for particle trajectories.

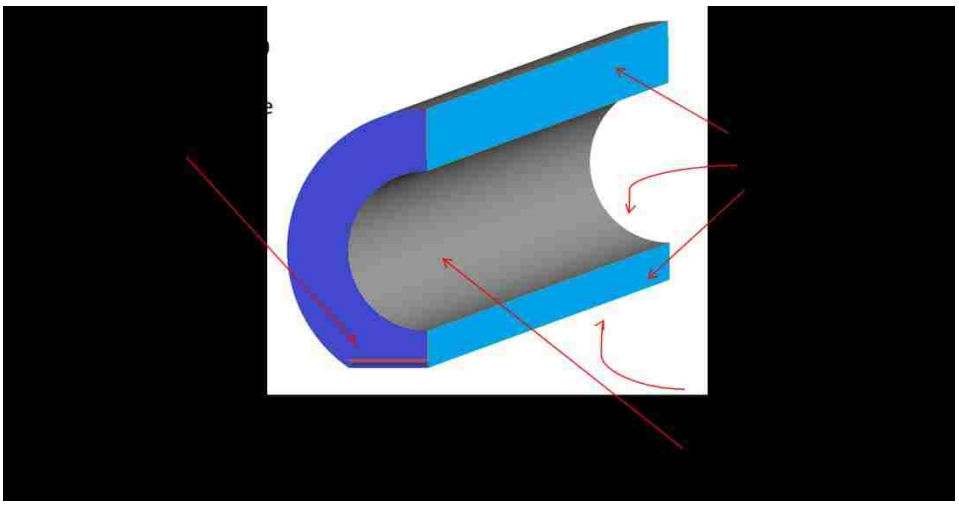

Figure 5.14 Boundary conditions for particle trajectories

Starting with a low bed height, successive simulations are performed by increasing the stationary bed height each time while keeping the mass flow rate constant. The particle paths obtained by steady-state particle tracking at each case with a different stationary cuttings bed are analyzed for evaluating the likelihood of ongoing cuttings accumulation. Impact velocities, impact angles and distance covered at different altitudes from simulations performed at different stationary cuttings bed heights are compared in the same way presented in section 5.2. The main purpose is to find large differences in those parameters after the actual bed height is exceeded. It is anticipated that the impact velocities should be low, the overall number of wall collisions should be high, there should be a large number of wall collisions with high impact angles and cuttings should travel close to the wall in general in simulation cases with assigned stationary bed heights lower than the equilibrium in reality. In this case the volumetric flow rate is not adequate to prevent cuttings accumulation. These trends should reverse in the cases where the assigned stationary bed heights are above the equilibrium. The visualization of particle tracks and the summary of simulation procedure is given in figure 5.15.

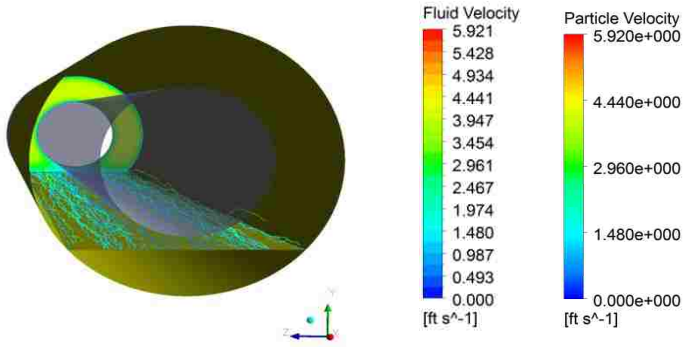

(a)

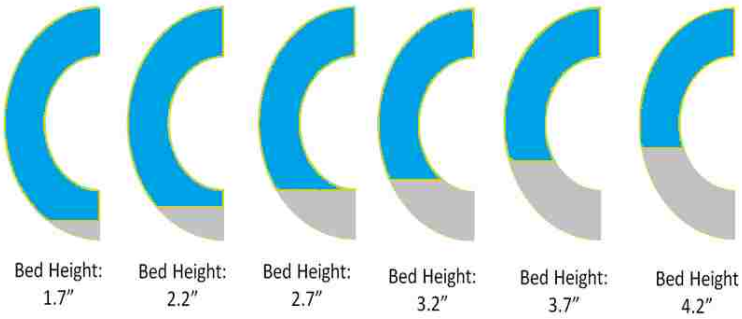

(b)

Figure 5.15 a) Visualization of particle tracks in the simulation domain. Particle tracks are colored according to their instantaneous velocity. Fluid velocity profile is also given. b) Change in flow cross section with increasing stationary cuttings bed height. A separate simulation is performed for each different cross section by keeping the mass flow rate constant.

5.5 Validation Results: Prediction of Stationary Cuttings Bed Height

In this section, the approach for predicting the stationary bed height described in the previous section is tested against the experimental data. The published experimental data from Garcia-Hernandez et al (2007) is used. In the experiments of Garcia-Hernandez et al (2007), they used a full scale flow loop with annular dimensions 8" x 4.5". Water is used as the carrier fluid and the flow loop was horizontal in the experiments in which results are used in this section. They used gravel particles in 3-5 mm size, and specific gravity of 2.6. In those experiments, once the periodic conditions in fluid flow are reached at a designated flow rate, particles are injected from one end of the flow loop and the accumulation of particles is waited. Once the stationary cuttings bed reached equilibrium and is stable, they took bed height measurements from the side of the transparent pipe. These measurements are averaged and the bulk liquid velocities are calculated by dividing the flow rate by the decreased annular cross section with cuttings bed.

All the experimental conditions described are replicated in the simulations. The cuttings are assumed to have a sphericity value of 0.1 since they are described as gravel. The first simulation is conducted with a stationary cuttings bed 1" lower than the actual (Measured) equilibrium. The stationary bed height is increased by 0.5" increments in the following simulations while keeping all other conditions constant. Five simulations are conducted for each flow rate where 2 simulations have stationary bed heights 1" and 0.5" lower than the actual equilibrium, one case have the actual equilibrium stationary bed height, and 2 cases have stationary bed heights 1" and 0.5" higher than the actual equilibrium. The main purpose is to see a significant decrease in likelihood of further accumulation for the cases with and higher than the actual (Measured) stationary cuttings bed height in terms of a substantial increase in the particle – wall impact velocities and altitudes cuttings travelling away from the bed surface and a significant decrease in the overall number of particle – wall collisions and the particle – wall collisions with higher impact angles.

The stationary cuttings bed height measurements from experiments with 200, 300 and 400 gpm flow rates are used for validation purpose. The aim is to validate the method at different flow rates for consistency, and also understand the effect of flow rate in stationary cuttings bed buildup process.

Visualization of particle tracks from cases with 1" lower and 1" higher stationary bed heights than the measured equilibrium with 300 gpm flow rate are given in figure 5.16. The velocity magnitude contours at the inlet are also shown and the particle tracks are colored by their instantaneous velocities. It can be noticed that more particles are moving at higher altitudes in the case with the higher stationary bed height.

The particle tracks are also smoother in the case with higher stationary bed which suggests that there are less wall collisions and wall collisions have smaller impact angles. Particle behavior at different bed heights with the same mass fluid flow rate will be compared quantitatively more in detail in further parts.

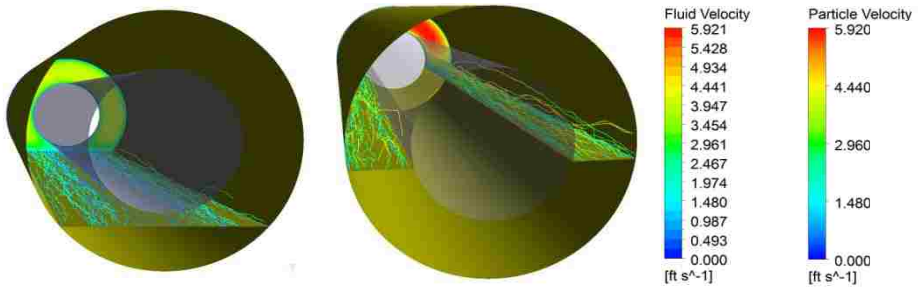

(a) (b)

Figure 5.16 Visualization of particle paths with fluid velocity contours at the background a) Bed Height is 1" lower than the actual bed height (1.4") b) Bed Height is 1" higher than the actual bed height (3.4")

The velocity magnitude contours of fluid phase at gradually increasing bed heights for three different flow rates are given in figure 5.17. The local fluid velocity immediately above the stationary cuttings bed surface remains slightly with increasing stationary cuttings bed height. However, plug region where the velocity is the highest becomes larger and widens towards the stationary cuttings bed surface. Although this increase does not directly aids particle lifting from the stationary bed surface, lifted particles enters the plug region more easily and travels longer horizontal distances in suspension since they are subjected to larger drag forces.

The cuttings accumulation rate should be expected to increase with increasing stationary bed height starting from a clean annulus, until the bed surface reaches the inner pipe. The local flow area between the low side of the outer pipe and the low side of the inner pipe shrinks with increasing bed height, so the local velocities drops in that region. It is certain that, if the cuttings accumulation starts in a clean annulus, the stationary cuttings bed will reach the low side of the inner pipe in short notice where the stationary bed height will be as high as the clearance between the outer and inner pipes.

Figure 5.18 shows the turbulence kinetic energy contours with increasing stationary bed heights at different flow rates. Pipe surfaces are smooth in simulations as in the experiments. The turbulence kinetic energy is produced at a higher rate above the stationary bed than other solid surfaces due to the roughness of the stationary bed surface. Turbulence kinetic energy production above the stationary increases as the

stationary bed height increases. The high turbulence kinetic energy is found to be the main factor in particle lifting in a horizontal channel as stated previously.

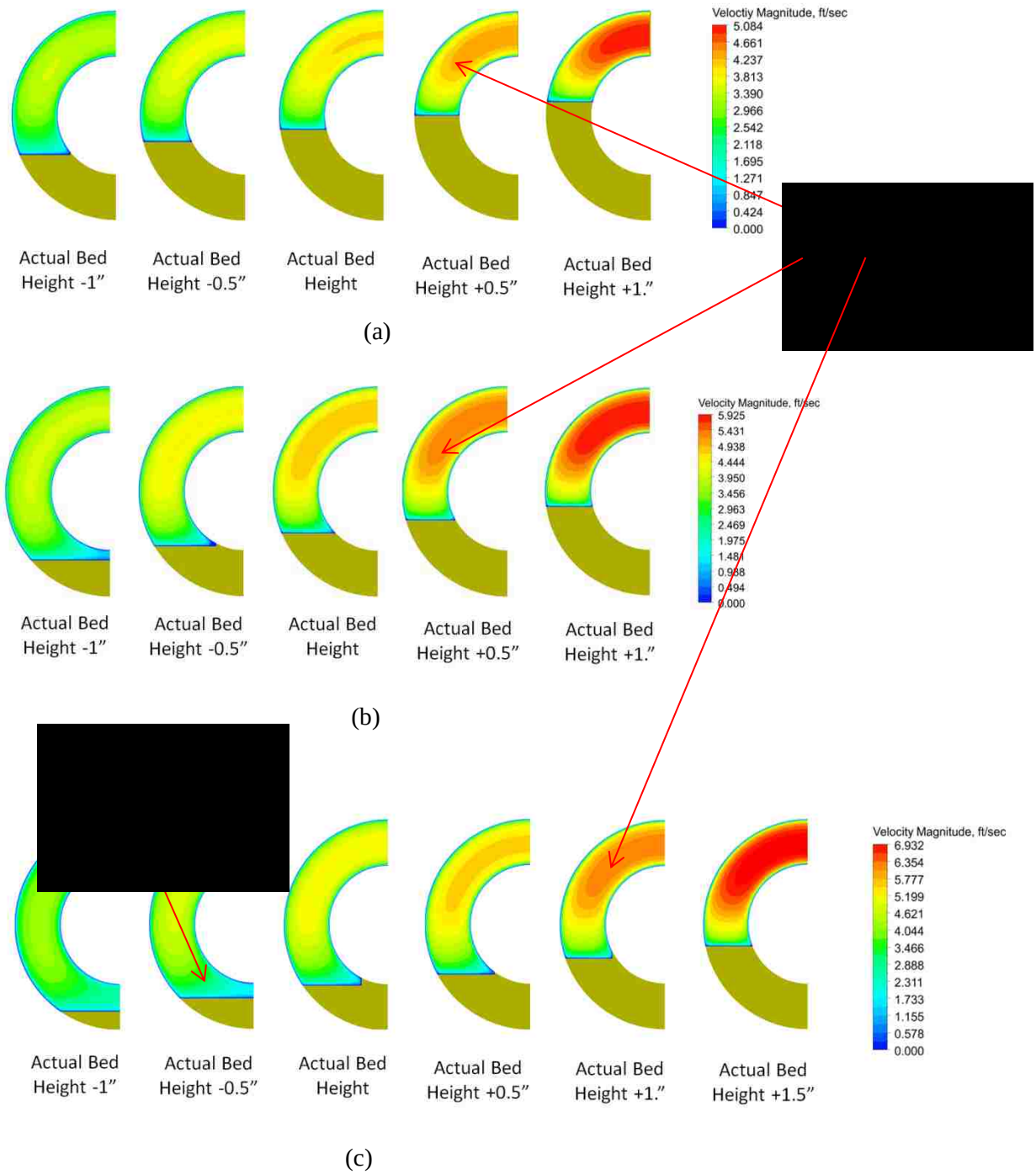

Figure 5.17 Velocity magnitude contours at different stationary bed heights a) 200 gpm flow rate with 3.5" actual bed height (Measured equilibrium) b) 300 gpm flow rate with 2.4" actual bed height. c) 400 gpm flow rate with 1.6" actual bed height

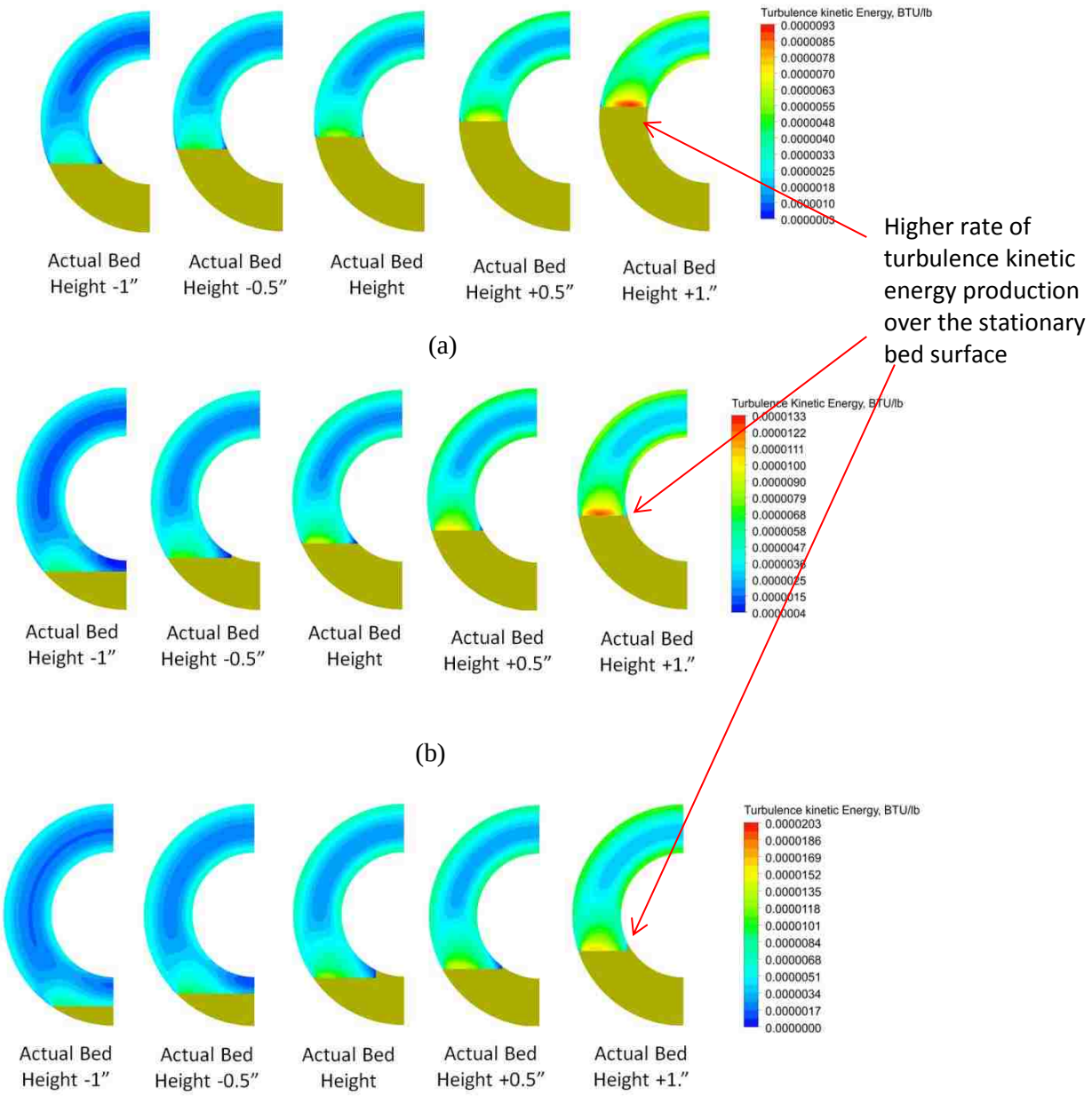

Figure 5.18 Turbulence kinetic energy contours at different stationary bed heights a) 200 gpm flow rate with 3.5” actual bed height (Measured equilibrium) b) 300 gpm flow rate with 2.4” actual bed height c) 400 gpm flow rate with 1.6” actual bed height

The particle tracks are analyzed same way as in the demonstration case. The likelihood of ongoing cuttings accumulation is assessed by looking for sharp changes in average impact velocities, total number of particle – wall collisions, number of particle – wall collisions with higher impact angles and the distance covered in higher altitudes with increasing stationary cuttings bed height.

The change in average impact velocity with increasing bed height can be seen in figure 5.19. There is a breakthrough in the trend after the actual bed height is exceeded. There is a large difference between the case with the actual bed height and the case with bed height 0.5" higher than the actual while differences between cases with lower bed heights than the actual are comparatively very small. The chance of ongoing accumulation in cases with stationary bed heights higher than the actual is much lower compared to cases with lower bed heights, due to much higher average impact velocities. The break in the increasing average impact velocity trend is seen between the cases with bed heights 0.5" and 1" higher than the actual for 400 gpm flow rate.

The number of particle – wall collisions with different impact angles are compared in different stationary bed heights in figure 5.20. For each flow rate, there is a significant decrease in the total number of collisions in the simulation domain after the actual bed height is exceeded. Also the number of collisions with higher impact angles is very low in the case with bed height 0.5" higher than the actual, when compared to the cases with lower bed heights for all flow rates. This also indicates that the likelihood of ongoing accumulation is very low when compared to the cases with lower bed heights. This differences signal the actual height of the stationary bed among the other cases.

Similar behavior is also seen in the fraction of distance covered in different altitudes. There is a substantial decrease in the distance covered close to the bed surface between the cases with higher and lower bed heights than the actual. Particles are also seen to travel in higher altitudes once the actual bed height is exceeded. This behavior shows that the suspension capability of the flow is significantly enhanced in the case with bed heights higher than the actual.

The significant jump in the average impact velocities, considerable reduction in total number of particle – wall collisions and particle – wall collisions with higher impact angles, together with the enhancement in the suspension capability of flow indicates the actual height of the stationary cuttings bed among the other trial cases. Similar breakthroughs in trends are observed in all three cases with different mass flow rates.

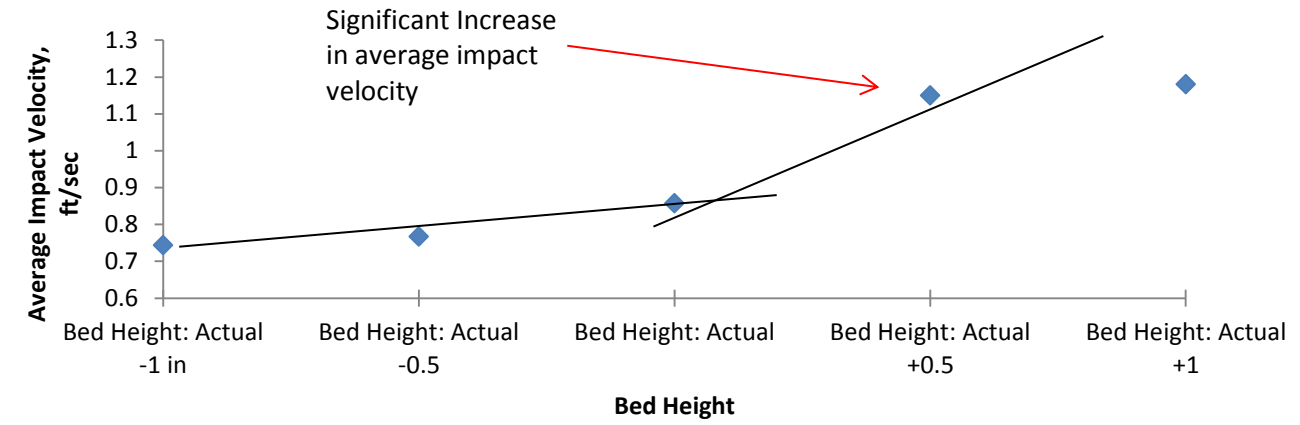

(a)

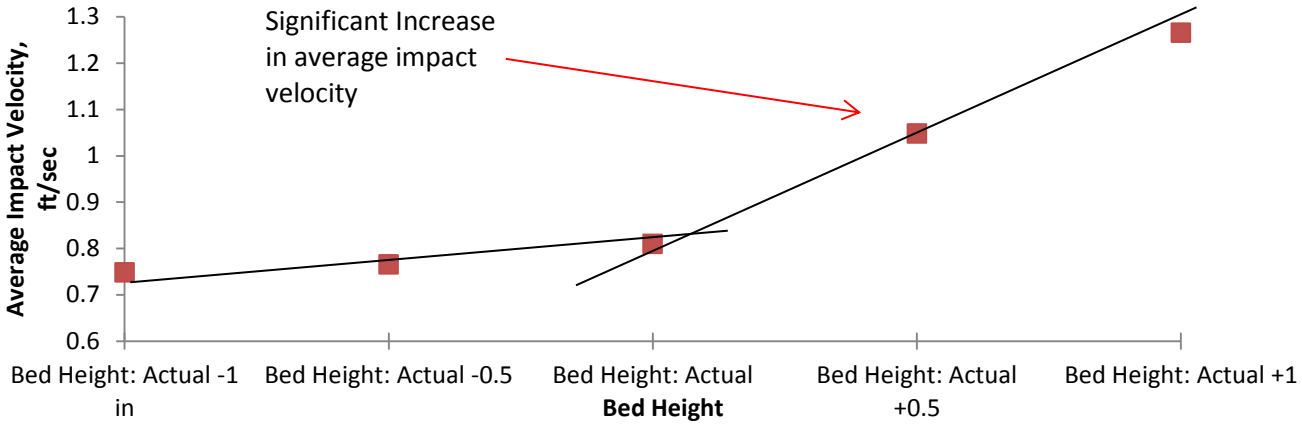

(b)

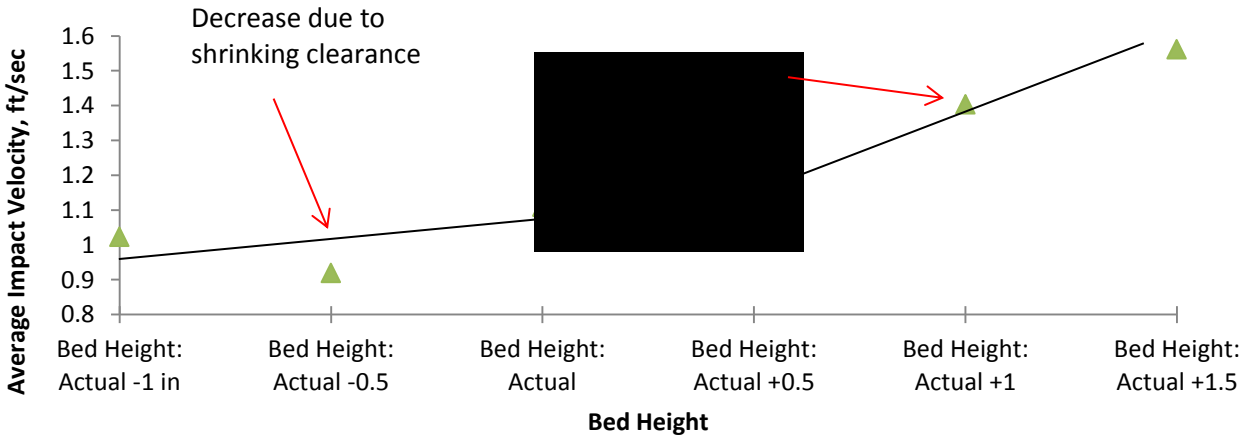

(c)

Figure 5.19 Average impact velocities at different stationary bed heights a) 200 gpm flow rate with 3.5" actual bed height (Measured equilibrium) b) 300 gpm flow rate with 2.4" actual bed height c) 400 gpm flow rate with 1.6" actual bed height

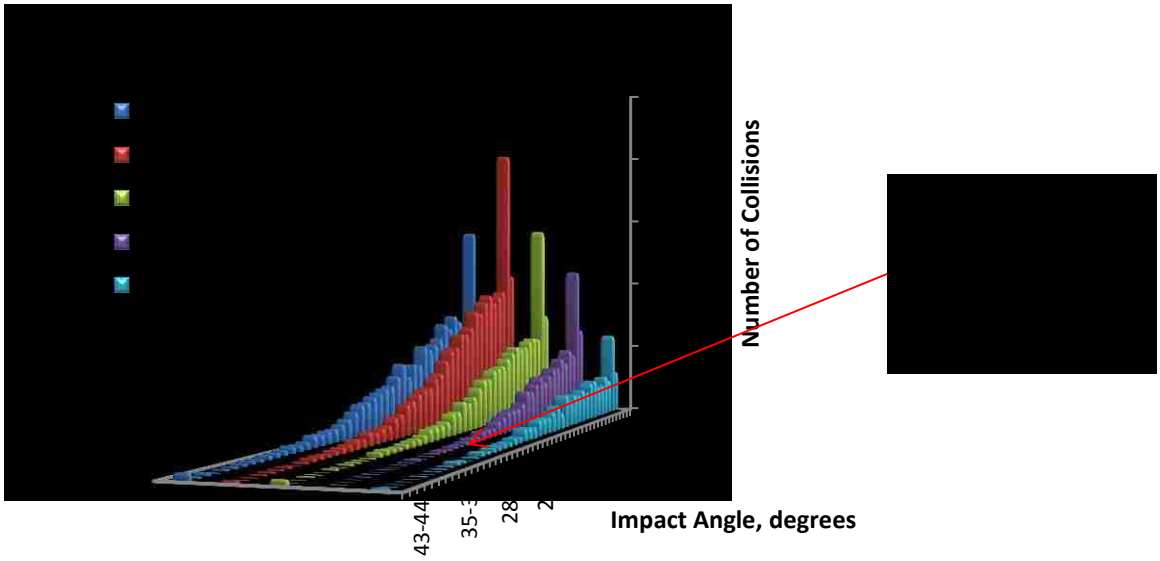

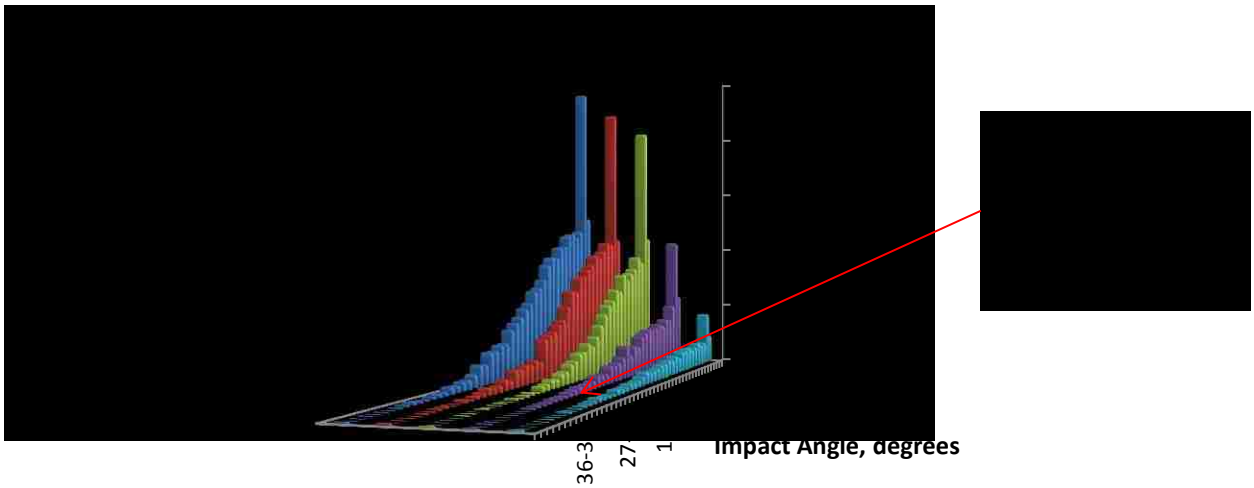

(b)

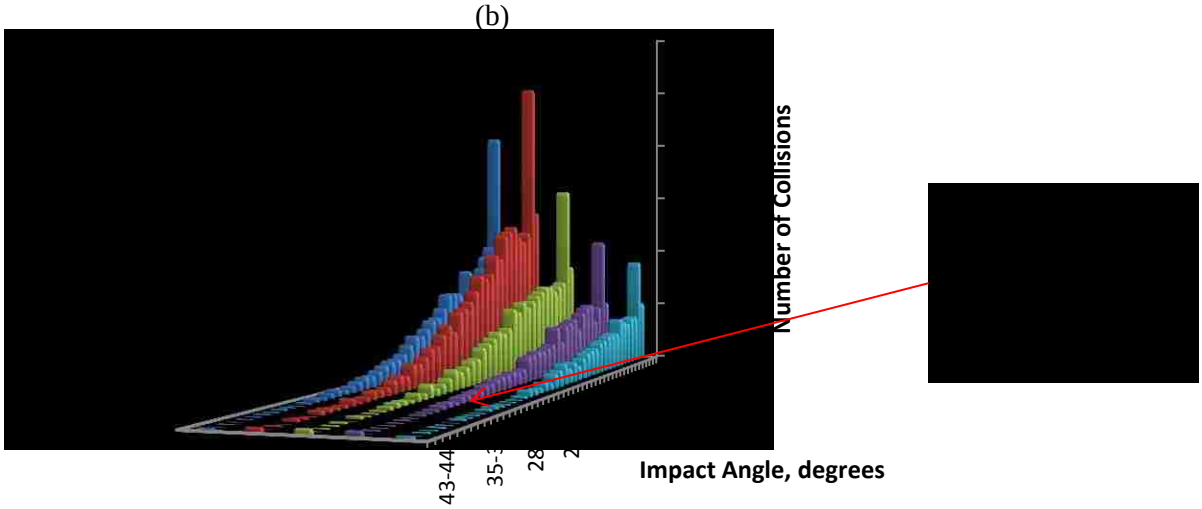

(c)

Figure 5.20 Number of collisions with different impact angles at different stationary bed heights a) 200 gpm flow rate with 3.5" actual bed height (Measured equilibrium) b) 300 gpm flow rate with 2.4" actual bed height c) 400 gpm flow rate with 1.6" actual bed height

(a)

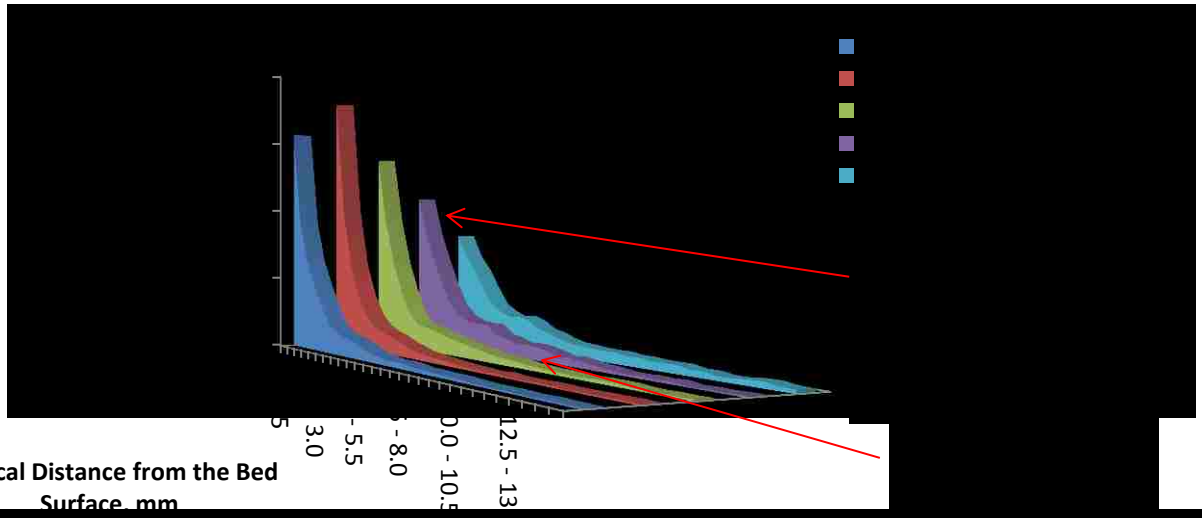

(b)

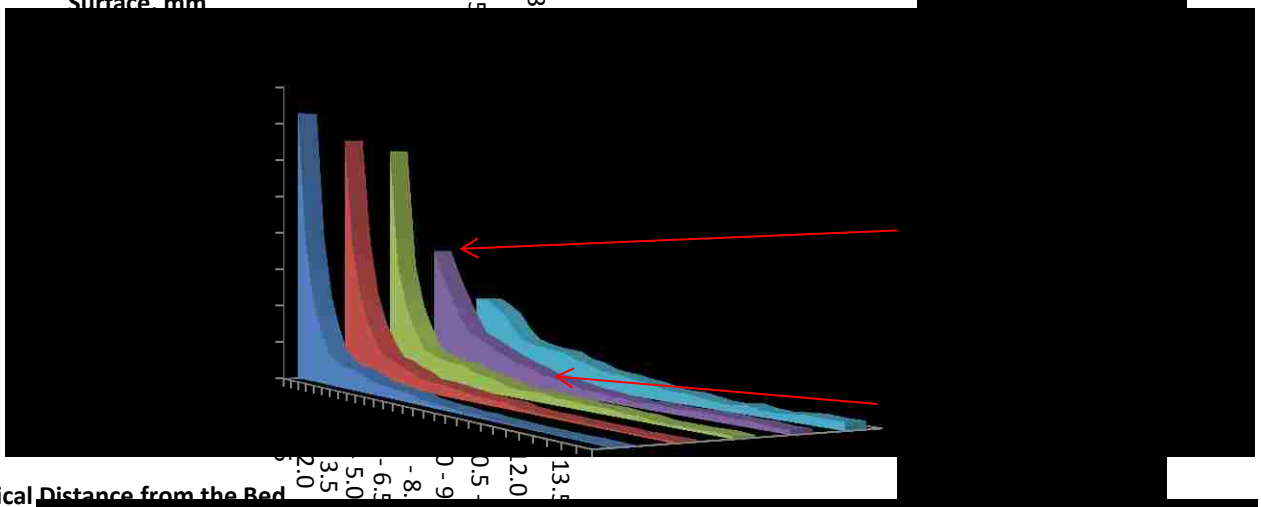

(c)

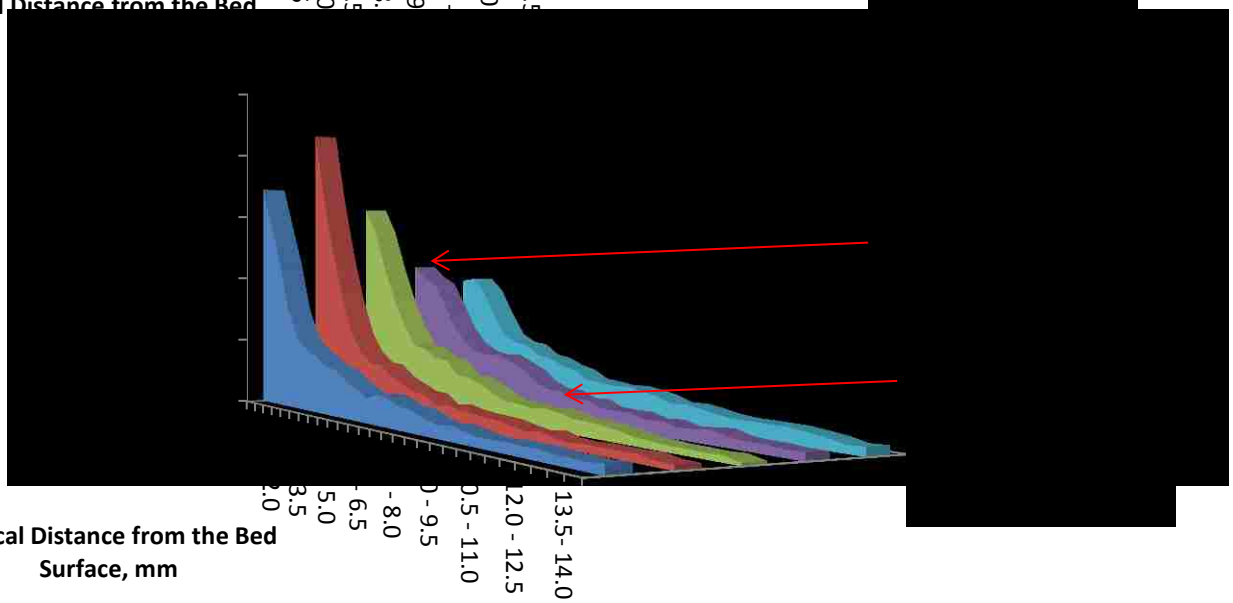

Figure 5.21 Fraction of distance covered in different altitutes at different stationary bed heights a) 200 gpm flow rate with 3.5" actual bed height (Measured equilibrium) b) 300 gpm flow rate with 2.4" actual bed height c) 400 gpm flow rate with 1.6" actual bed height

6. VALIDATION RESULTS: PREDICTION OF THE AVERAGE TRANSPORT VELOCITY

After predicting the equilibrium stationary bed height, the second step is to estimate the average velocity of particles for calculating the circulation time necessary for carrying all moving particles to the surface. Unsteady particle tracking is used in determination of the average particle velocity in the flow direction. 70 particles are injected at every time step until the number of particles escaped from the outflow is stabilized and the instantaneous velocities of particles are averaged. The average moving layer velocities are measured by image velocimetry method in the same study of Garcia – Hernandez et al (2007). Marked particles are tracked by a moving camera and their velocities are measured by image analysis. Numerous particles are tracked until the change average moving layer velocity is in reasonable limits. Same data set is used as in section 5 where the stationary bed heights and moving bed velocities are measured at 200, 300 and 400 gpm flow rates and water is used as the carrier fluid in a horizontal annulus.

Same experimental parameters are applied to the simulation as in section 5 and the measured bed heights are also incorporated as geometrical cut surfaces. Particle size is taken as the average of the size range given in the experimental paper which is 4 mm, and is applied to all particles. The particles are assumed to have a very low sphericity. A sphericity value of 0.1 is assigned to all particles. The simulation results are reasonably in agreement with the experimental results as shown in figure 6.1. At this stage, it is assumed that there is no more accumulation in progress once the stationary cuttings bed reached equilibrium and flow is capable enough to adequately recover the momentum loss of particles upon impact.

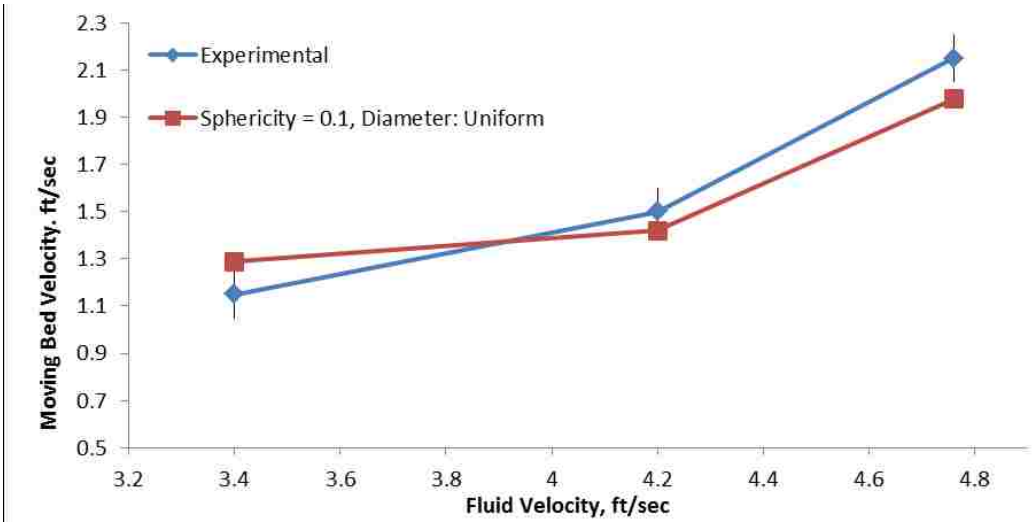

Figure 6.1 Comparison of average particle velocities obtained computationally to the experimental measurements

The particle velocities are averaged in order to mimic the measurement process in the experimental process. However, lateral particle velocity profile can also be obtained from computational data for optimizing drilling parameters for more efficient cleaning. Figure 6.2 shows the lateral particle profiles at different flow rates where the cross section of the annulus is divided into 12 section and the particle velocities falling into each section are averaged. Increments with very few particles are excluded from the graph, since few particles in suspension can have extreme values.

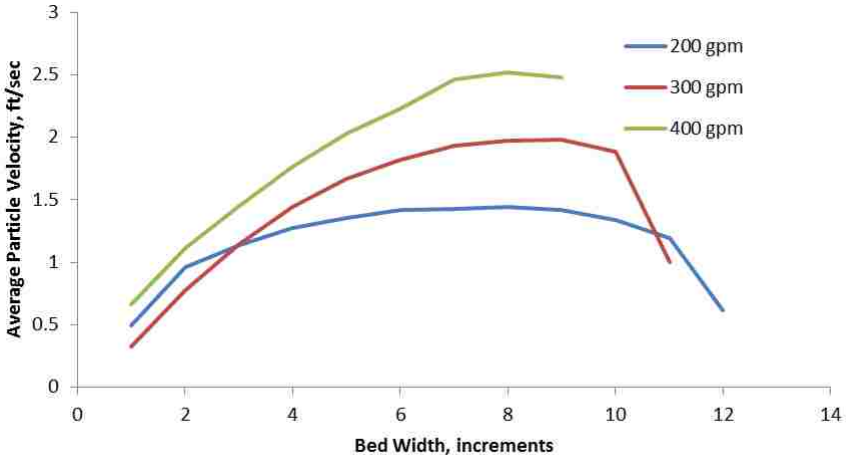

Figure 6.2 Particle velocity profiles in the lateral direction

Figure 6.3 shows the particle velocity profiles in spanwise direction. Particle velocities falling into each 0.5 mm vertical increment are averaged. Particle velocities found to be increasing exponentially starting from the bed surface.

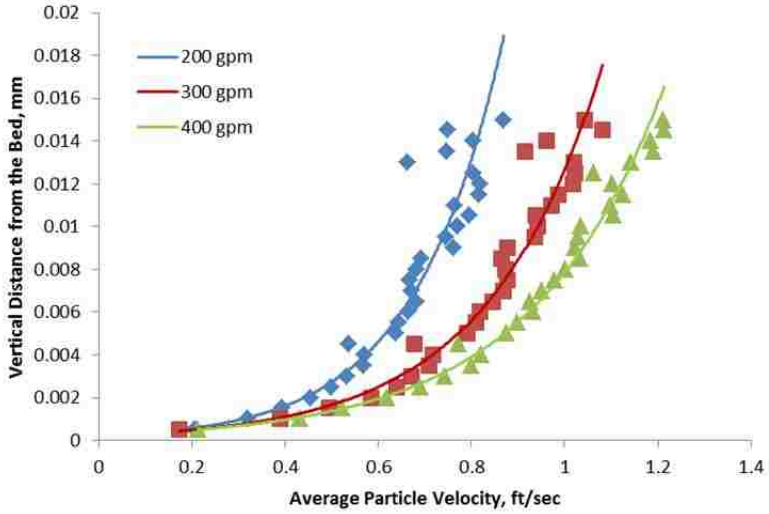

Figure 6.3 Particle velocity profiles in the vertical direction

7. PARAMETRIC STUDY: EFFECTS OF VARIOUS DRILLING PARAMETERS ON CUTTINGS TRANSPORT PROCESS

The effects of inner pipe rotation, inner pipe rotation speed, wellbore inclination, fluid density, rheology, particle shape and particle size distribution, are going to be investigated in this part. The same simulation and analysis procedures are used as in the validation section. A single parameter is changed from the base case to see how local flow field and the particle behavior are influenced.

The effect of flow rate is in accordance with the experimental data as shown in the numerical setup validation section where the equilibrium bed height reduces with increasing flow rate. The effects of inner pipe rotation and wellbore inclination will be checked through validation with the experimental data. The height of the equilibrium bed height is reported to be reducing with the initiation of inner pipe rotation, while all other parameters are held constant in the experimental study of Garcia – Hernandez et al. (2007). Similarly, the equilibrium bed height is also reported as lower in smaller borehole inclinations with regard to the larger borehole inclinations while all other conditions are kept as the same.

The effects of inner pipe rotation speed, fluid density and rheology will be investigated qualitatively by case studies. The investigated parameter is changed while all other parameters are held constant, in order to see the influence of that parameter on the flow characteristics and particle behavior. The effects of particle size, shape and particle size distribution on the average particle transport velocity is assessed by altering these parameters in the validation case simulations conducted for predicting the average transport velocity. The influence of inner pipe rotation speed is investigated through comparing the fluid velocity magnitude and turbulence kinetic energy contours at different inner pipe rotation speeds.

7.1 The Effect of Borehole Inclination

Garcia-Hernandez et al. (2007) reported a lower equilibrium bed height in the case with 300 gpm flow rate and 20 degrees of borehole inclination compared to the same case with horizontal inclination. The numerical setup is going to be validated with similar experimental data from the same study as used in section 5, which only the borehole inclination is changed this time. The sensitivity of the equilibrium stationary cuttings bed height is to be said to overlap with the experimental data if the numerical setup is validated for the case with borehole inclination. The inclination is defined simply by changing the direction of gravity.

The velocity and turbulence kinetic energy profiles are shown in figure 7.1. Similar to the 300 gpm and 400 gpm horizontal cases, local velocities just over the bed height is increasing constantly with increasing

bed height, and there is a steady buildup of turbulence kinetic energy concentrated close to the bed surface.

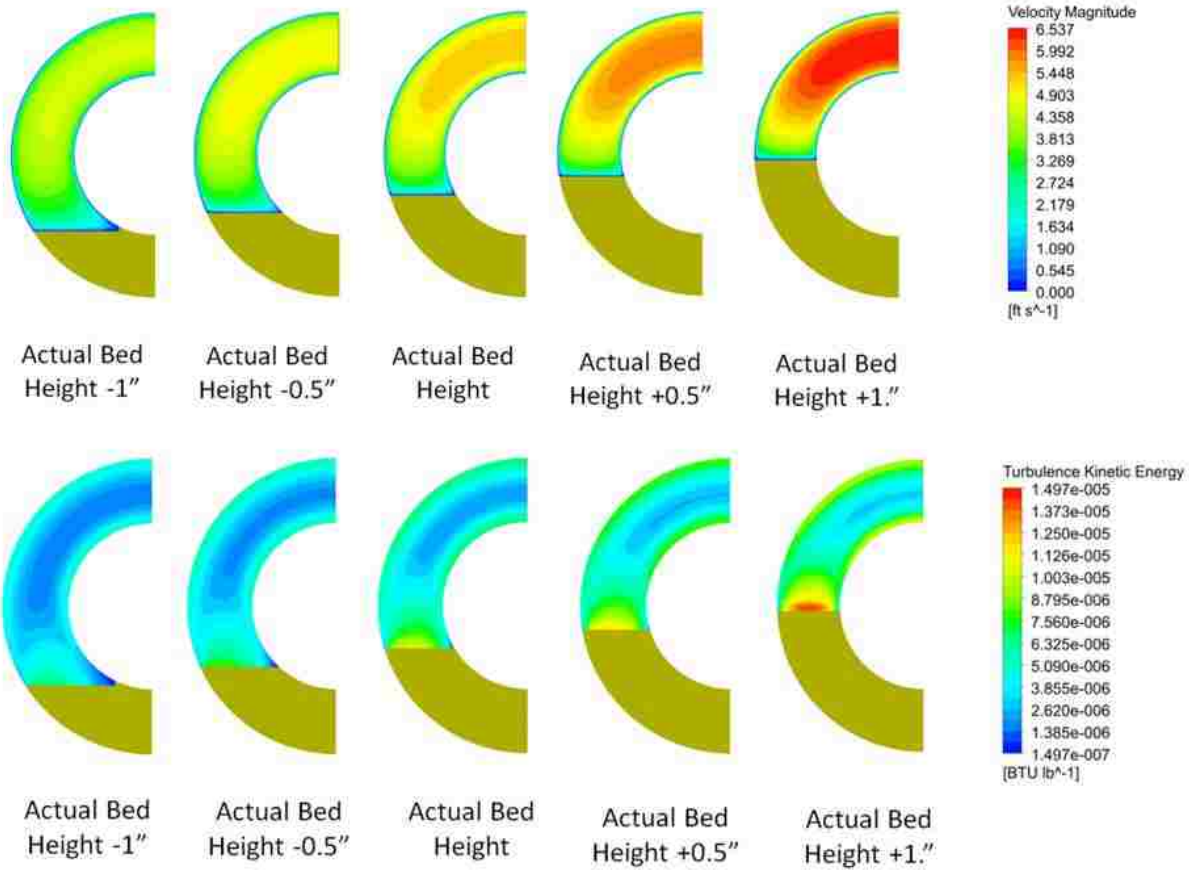

Figure 7.1 Velocity magnitude and turbulence kinetic energy contours at different bed heights for 300 gpm in a wellbore with 20 degree inclination

The impact velocities increased tremendously once the actual bed height is reached as seen in figure 7.2. The 30 percent increase in the impact velocity from ABH -0.5" to ABH clearly marks the actual height of the stationary bed.

The sharp decrease in the total number of collisions at actual bed height also agrees with the impact velocity and the distance covered in suspension comparisons. The collisions with high impact angles are also nearly vanished at the actual bed height. The impact angle histograms are given in figure 7.3.

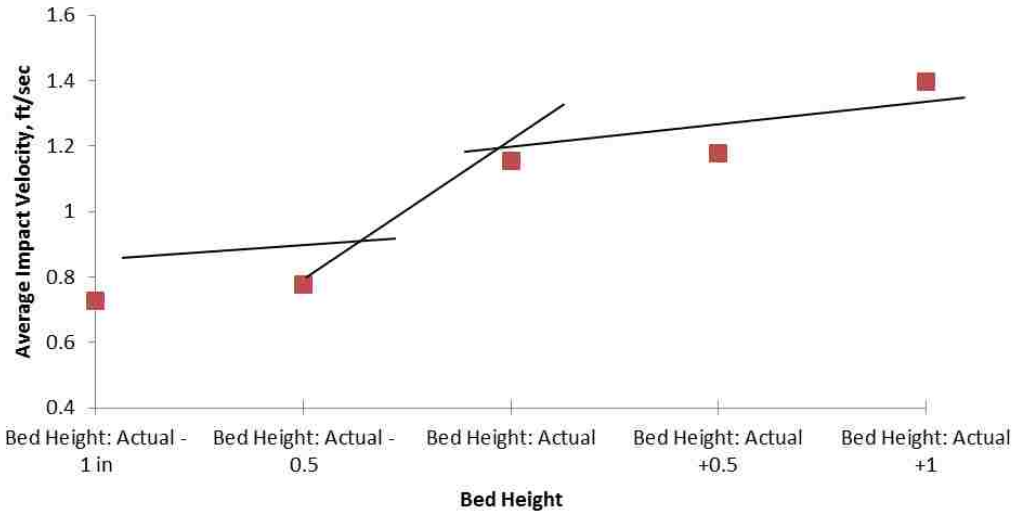

Figure 7.2 Averaged impact velocities at different bed heights for 300 gpm flow rate in a wellbore with 20 degree inclination

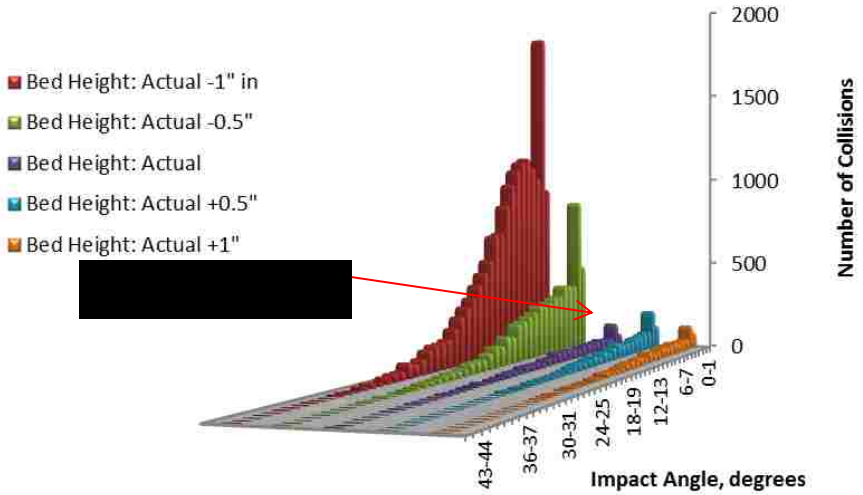

Figure 7.3 Total number of collisions at different impact angles for 400 gpm in a wellbore with 20 degree inclination

The particle distances covered in different altitudes is also a quite visible indicator of the actual bed height. The particles moving close to the bed surface dramatically decreased, and the distances covered higher altitudes increased significantly once the actual bed height is reached. The particle loaded section

of the flow is much larger in the case with the actual bed height, so it will look like a thick moving bed while looking at the annulus from the side, which fits the description given by Garcia-Hernandez et al (2007) in their experimental study. The particle distances covered in different altitudes are shown in

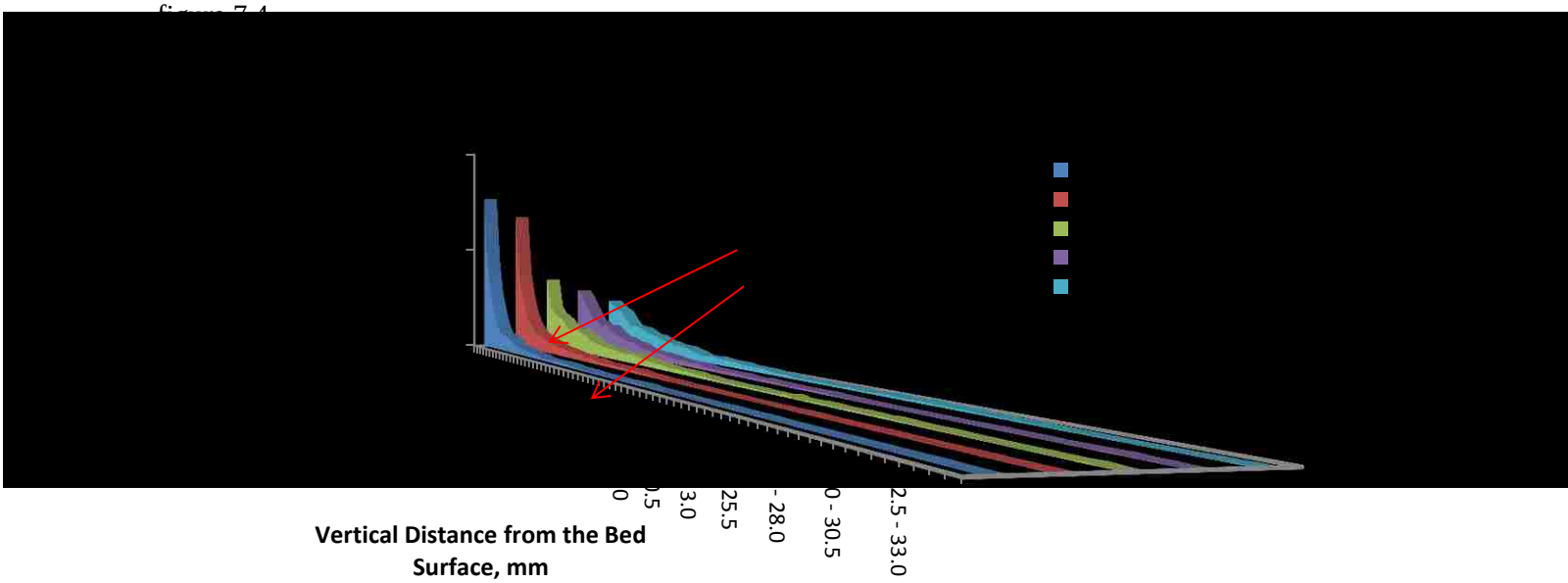

Figure 7.4 Percentages of distance covered in the flow direction at different vertical intervals for 300 gpm in a wellbore with 20 degree inclination

The indicators of the actual bed height are much stronger in this case compared to previous ones. The stationary bed height is lower in the inclined case as given in the experimental study, and the suspension pattern is much more visible. The reason for that is because the drag force has a substantial component in the opposite direction of the gravitational force in this case where the borehole is inclined 20 degrees.

7.2 The Effect of Inner Pipe Rotation

The effect of inner pipe rotation will be investigated in the same fashion as done for the effect of borehole inclination. The capability of the numerical setup in predicting the equilibrium stationary bed height in a case with inner pipe rotation will be validated with experimental data form Garcia-Hernandez et al. (2007). The equilibrium stationary bed heights are reported as lower after the inner pipe rotation is initiated while all other conditions are the same. The aim is to capture the same effect by predicting the measured stationary bed height in the experiment with 40 rpm inner pipe rotation and horizontal inclination.

The effect of rotation is realized by defining the inner pipe surface as a moving wall, rotating around its own axis in the clockwise direction (fig. 7.5). This time only three levels of hypothetical bed heights is simulated with 300 gpm flow rate and horizontal wellbore, since the bed height exceeds the lower end of the inner pipe if the bed height is increased further. Simulations are conducted for hypothetical stationary bed heights 0.5" lower and higher than the measured equilibrium, together with the measured equilibrium bed height. Since the flow field is not symmetric in the cross section, full scale annular geometry is used instead of cut-in half annular geometry with symmetry boundaries. The particle behavior in different locations of the simulation domain is also found to be highly non-uniform unlike the cases with no inner pipe rotation, where the impact velocities, particle – wall collisions and lifting capacity of the flow are mostly homogenous for the bulk of the flow domain. A different analysis strategy is used in the cases with inner pipe rotation. Bed surface is divided into 12 increments spanwise and particle behavior and the lifting capacity of the flow in each increment are analyzed separately.

The fluid local velocity magnitude and the turbulence kinetic energy contours are shown in figure 7.5. The local fluid velocity just above the stationary bed on the sides increases with increasing stationary bed

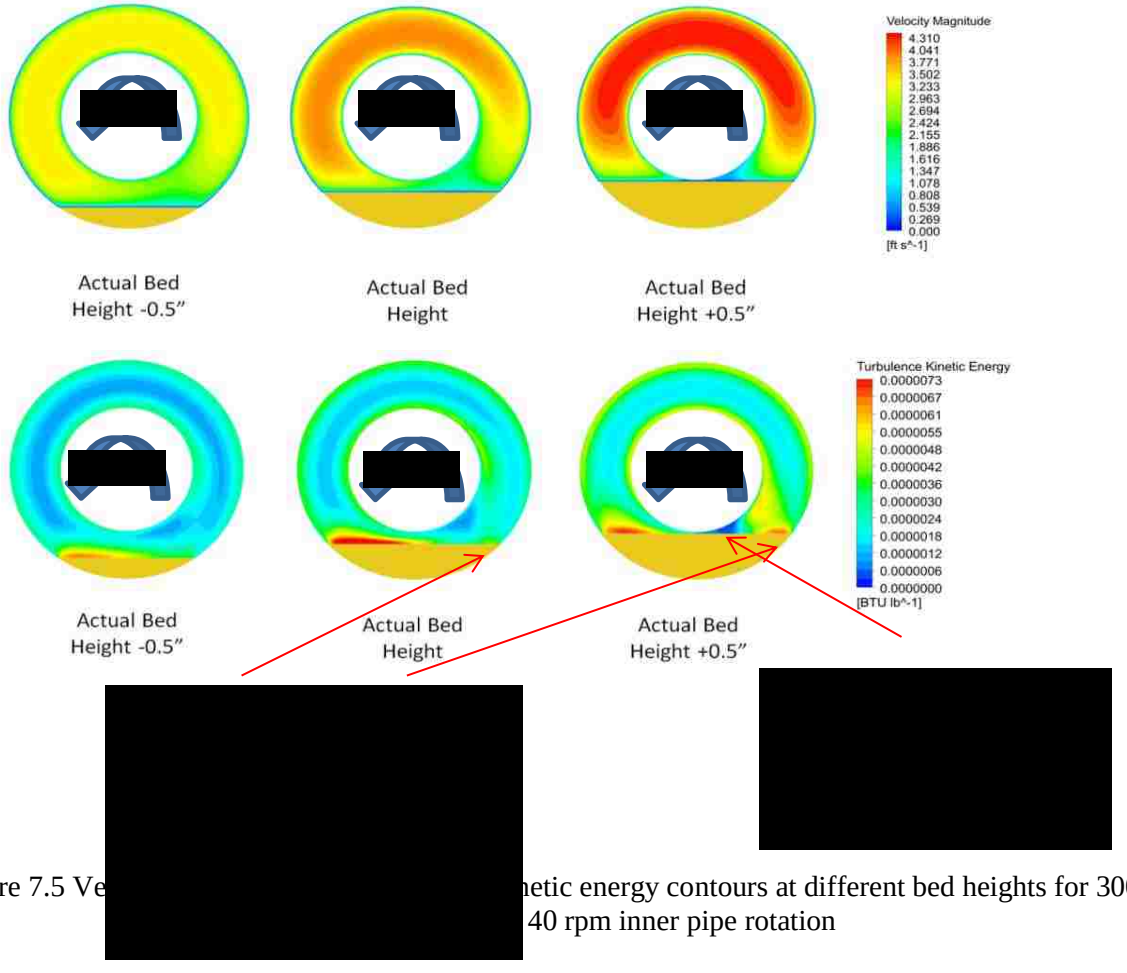

Figure 7.5 Ve netic energy contours at different bed heights for 300 40 rpm inner pipe rotation

height, while the local fluid velocity just under the inner pipe decreases. There is significant amount of turbulence kinetic energy production on the left hand side of the stationary bed surface from the beginning. Although the turbulence kinetic energy production on the right hand side of the bed surface is very low in the first case, it matches the right hand side when the measured equilibrium bed height is exceeded by 0.5". There is a narrow zone where the turbulence kinetic energy just under the inner pipe. The turbulence kinetic energy further decreases in this zone with increasing bed height and it will be shown that all moving particles are swept into this zone when the measured equilibrium bed height is exceeded. For that reason, this region will be called the "Particle convergence zone".

Figure 7.6 shows the average impact velocity in each spanwise increment at different stationary cuttings bed heights. The increase in stationary cuttings bed heights have more complicated effects on average impact velocities throughout the domain. The average impact velocities are decreasing on the left hand side with the increasing stationary bed height since the clearance is reducing in that region. The same reducing clearance effect is much more pronounced in the area just under the inner pipe, especially in the particle convergence zone where the turbulence kinetic energy is very low. The average impact velocities are slightly increasing on the far right hand side of the domain.

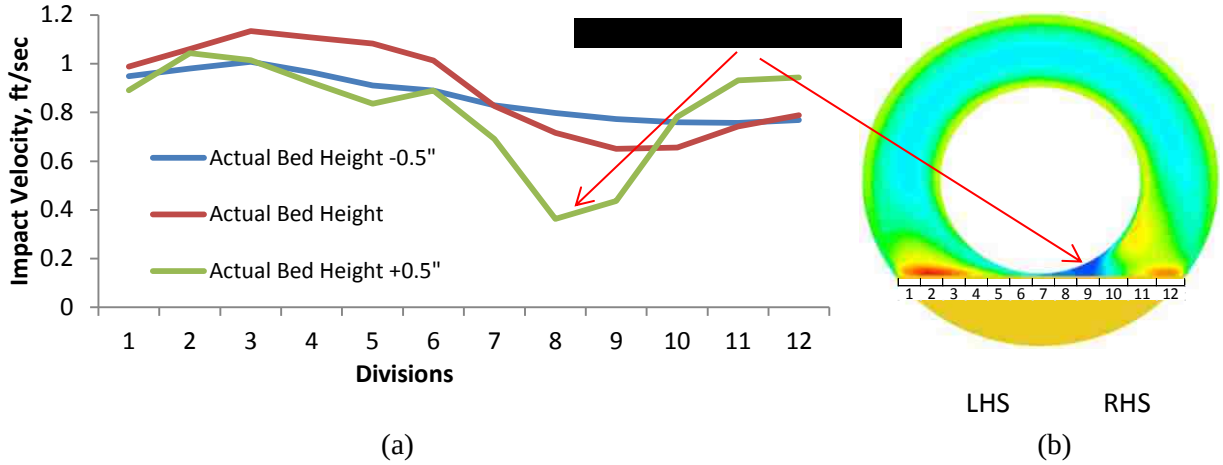

Figure 7.6 a) Averaged impact velocities in each spanwise increment for three different bed heights with 300 gpm flow rate and 40 rpm inner pipe rotation b) Increments on the simulation domain

Similar trends are also observed in particle – wall collisions as in the average impact velocities. Total number of particle-wall collisions and the maximum impact angles observed was very low on the left hand side in the case with stationary bed height 0.5" lower than the measured equilibrium. Majority of particles on the left hand side are swept to right hand side in the case with measured equilibrium stationary bed height. In the case with stationary bed height 0.5" higher than the measured equilibrium, all particles are swept into the particle convergence zone. The increasing fluid velocity and the turbulence

kinetic energy, together with the tangential sweep due to inner pipe rotation forced all particles into the convergence zone. Particle – wall collision histograms can be seen in figure 7.7.

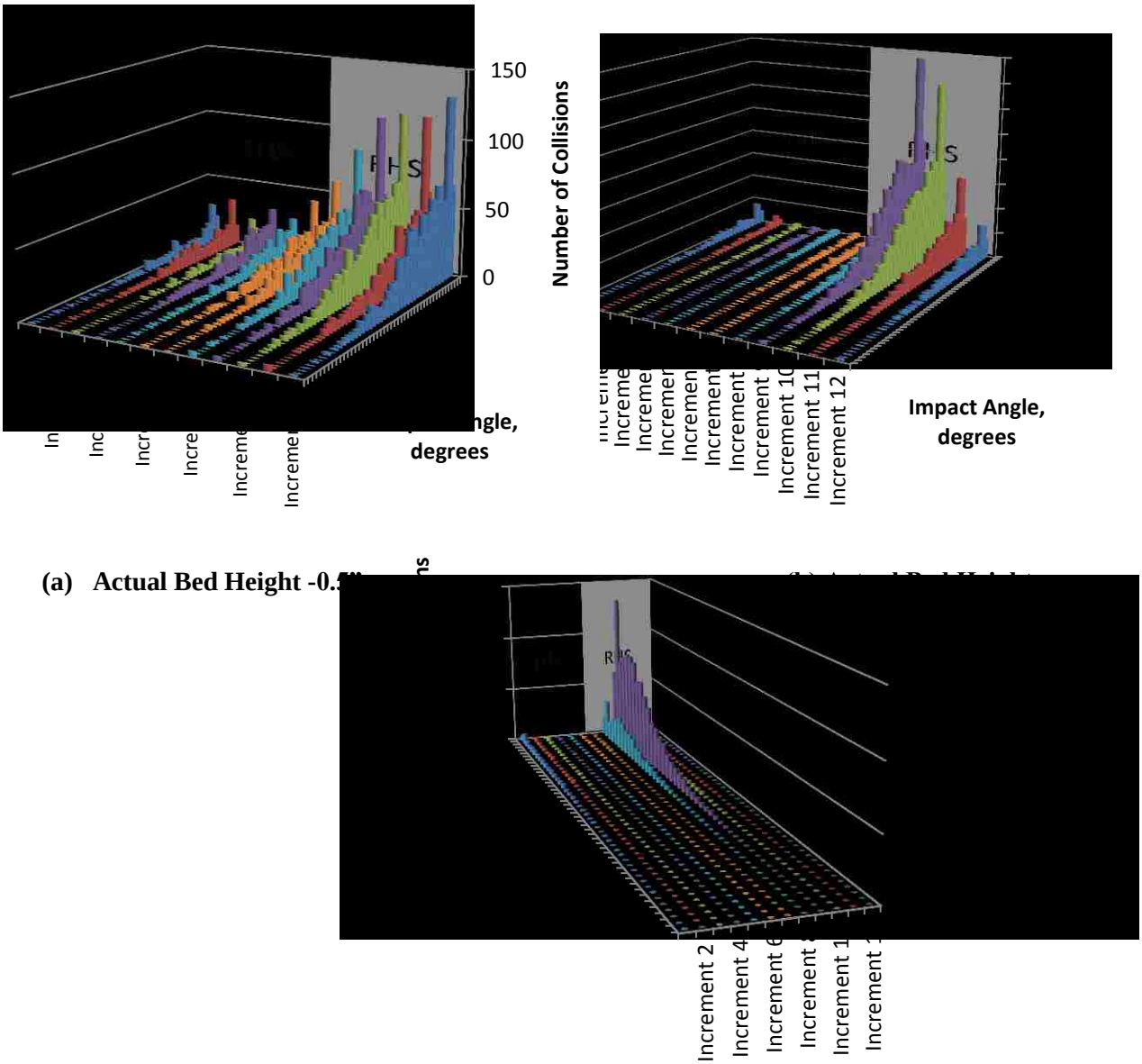

(a) Actual Bed Height -0.5”

(c) Actual Bed Height +0.5”

Figure 7.7 Number of collisions with different impact angles in each increment at different bed heights

Particle suspension levels also follow the same trend as seen in figure 7.8. Suspension levels were reasonably low on the left hand side for all stationary bed heights. The suspension levels steadily

improved on the right hand side with increasing stationary bed height. However, particles moved almost without taking off from the surface in the particle convergence zone.

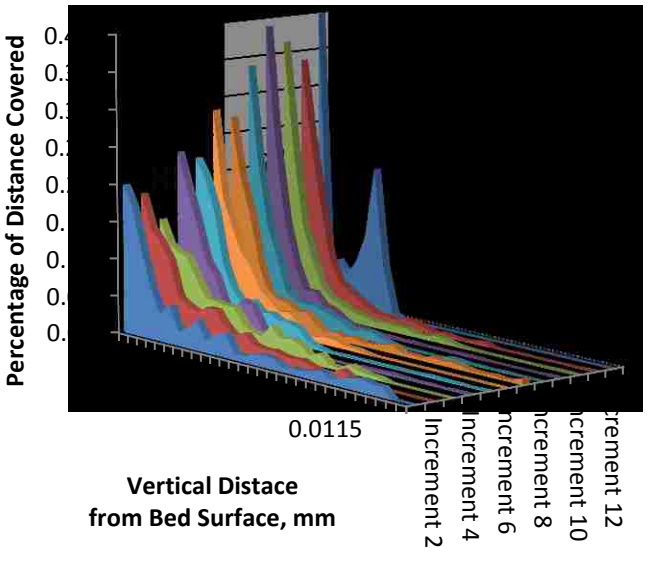

(a) Actual Bed Height -0.5”

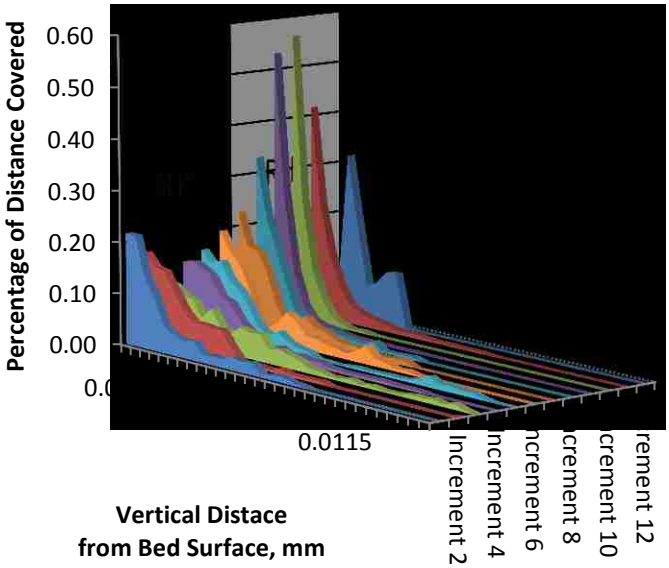

(b) Actual Bed Height

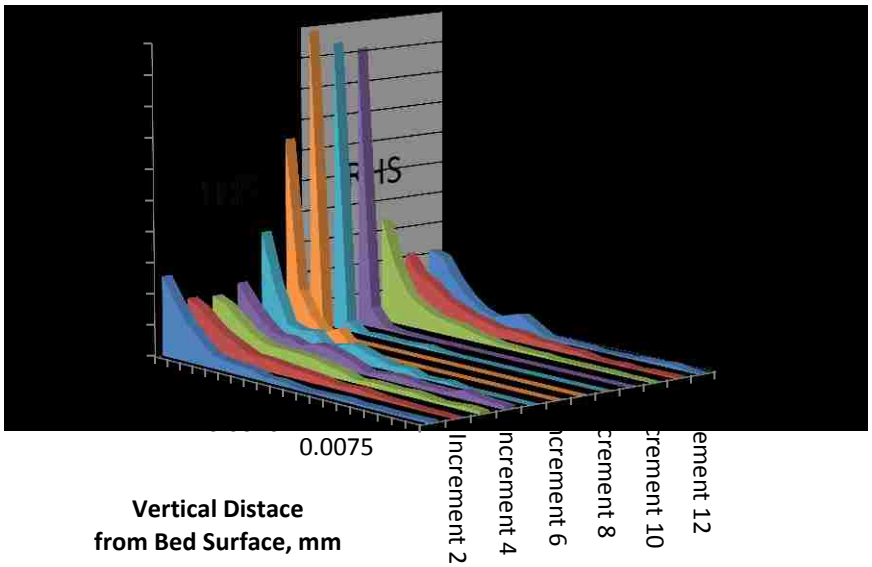

(c) Actual Bed Height +0.5”

Figure 7.8 Distance covered in suspension at each increment of simulations with different bed heights

Tomren et al. (1983) observed that particles are swayed tangentially with inner pipe rotation, resulting in a higher buildup of cuttings on one side. Similar conclusions can also be drawn from the simulations. Particle – wall collisions and the lifting capacity of flow was favorable on the left hand side for all hypothetical stationary bed heights. The particle – wall collisions and the lifting capacity of flow on the right hand side reached the same levels only in the case with stationary bed height 0.5" higher than the measured equilibrium. This shows that the stationary bed height should be higher on the right hand side in the equilibrium phase. The visualization of particle tracks clearly shows the swaying of particles from left to the right of the flow domain in figure 7.9.

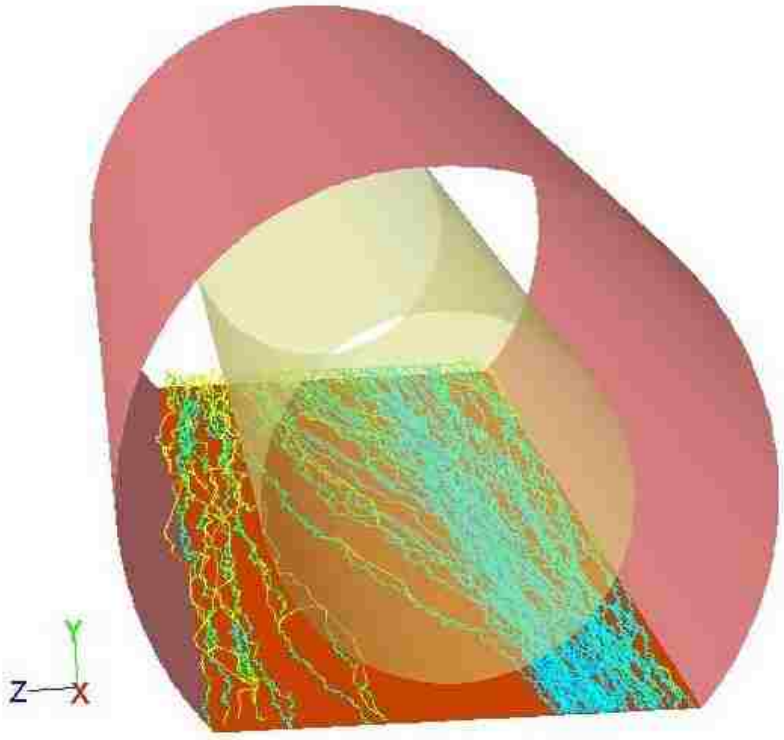

Figure 7.9 Visualization of particle tracks at different stationary bed heights from the simulations with inner pipe rotation

The degree of particles suspension was not large in the simulations as described by the study of Garcia – Hernandez et al. (2007). The effect of pipe rotation should be expected to be larger, since there is an energy contribution in the form of vibrations of the inner pipe, accompanying rotation. A slight bend or eccentricity will result in orbital movement of the inner pipe, creating much greater shear.

7.3 The Effect of Inner Pipe Rotation Speed

The effect of inner pipe rotation speed is assessed qualitatively by comparing the fluid velocity magnitude and turbulence kinetic energy contours at different rotation speeds and keeping all other parameters constant. The simulation setup used in section 7.2 is taken as the base case and the rotation speed is altered. Since the particle motion is largely understood in flows with inner pipe rotation, only the velocity magnitude and turbulence kinetic energy contours are examined in this section.

Local velocity distribution becomes more asymmetric with increasing inner pipe rotation as seen in figure 7.10. The local velocities just above the bed surface are very high on the left hand side and very low on the right hand side for the 40 rpm case. The overall local velocities over the stationary bed surface become higher as the inner pipe rotation speed increases, although distribution is becoming more asymmetric.

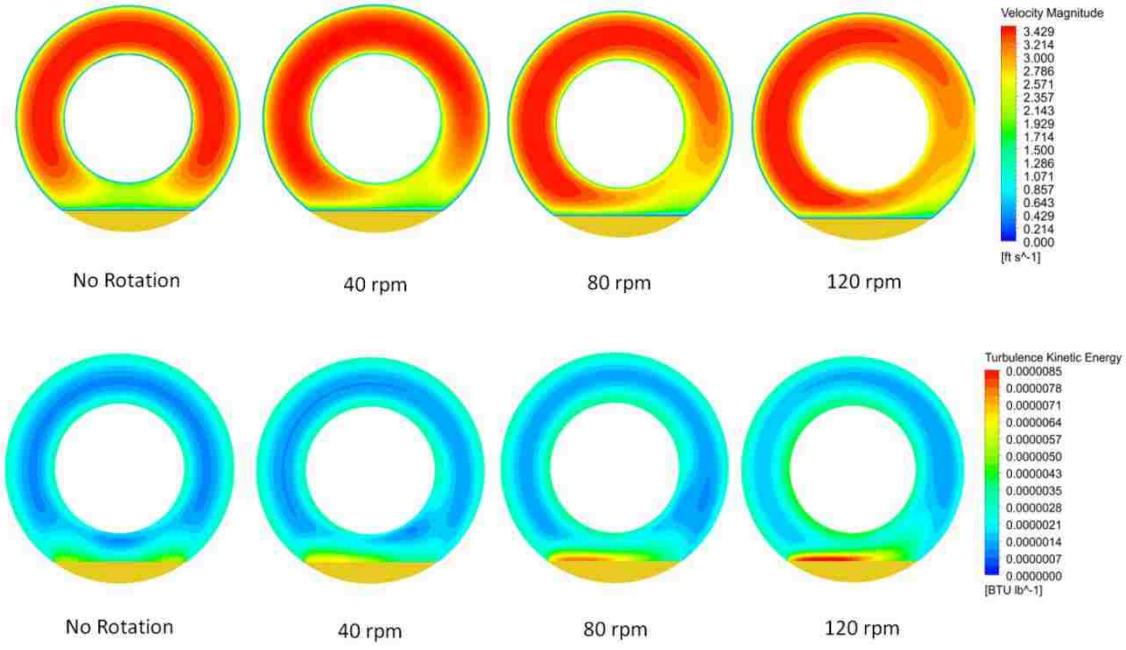

Figure 7.10 Velocity magnitude and turbulence kinetic energy contours at different inner pipe rotation speeds

A particle convergence zone is noticeable just under the inner pipe for the case with no rotation. Intense particle accumulation can occur in these spots especially at high stationary beds as encountered in section 7.2. This spot vanishes as the rotation speed increases. Turbulence kinetic energy is low just under the inner pipe and higher in the sides in the case with no rotation. Turbulence kinetic energy production rate increases in the left hand side of the stationary bed surface and in the middle at 40 rpm rotation speed. As

the rotation speed increases, turbulence kinetic energy production rate over the stationary bed surface starts to increase on the left hand side and high turbulence kinetic energy concentration spreads the right side. As a result of these, a more flat stationary cuttings bed should be expected at higher inner pipe rotation speeds.

7.4 The Effect of Fluid Density

The effects of the fluid density are investigated qualitatively by changing the density of the water from 8.33 ppg to 10 ppg and 11 ppg respectively in separate simulations. The base case is taken from the model validation part with 300 gpm flow rate, 20 degrees of borehole inclination and a stationary bed height 0.5" lower than the measured equilibrium. Only the density of the carrier fluid is altered while keeping all other parameters constant. There was no significant change in average impact velocities with increasing carrier fluid density as seen in figure 7.11.

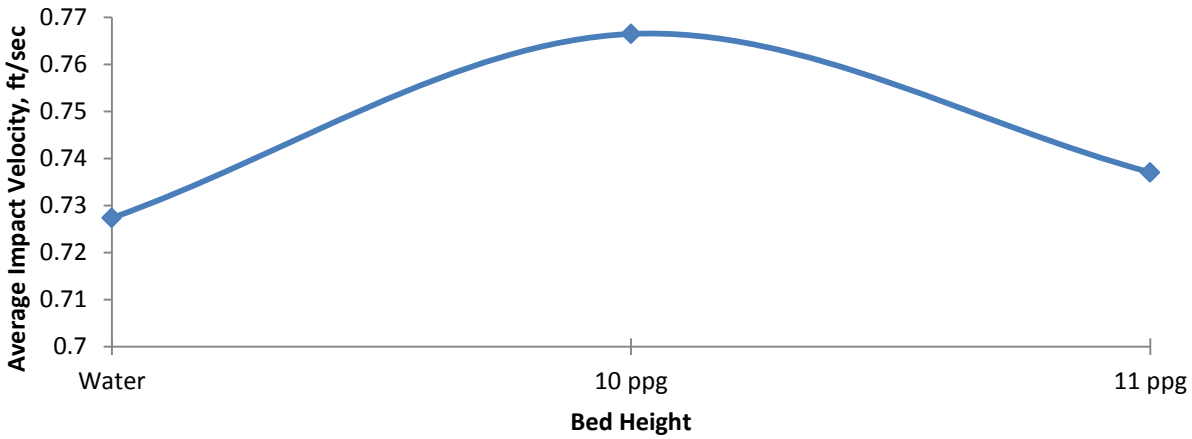

Figure 7.11 Averaged impact velocities at flows with different fluid densities

The distances covered in different altitudes away from the bed surface are given in figure 7.12. There is substantial improvement the lifting capacity of the flow while changing the density from 8.33 ppg (Water) to 10 ppg. However there is only slight improvement from 10 ppg to 11 ppg. Similar trend is also observed in impact angle histograms given in figure 7.13. This shows that the turbulence effects are much more dominant than the buoyancy effects after a critical point in density is exceeded.

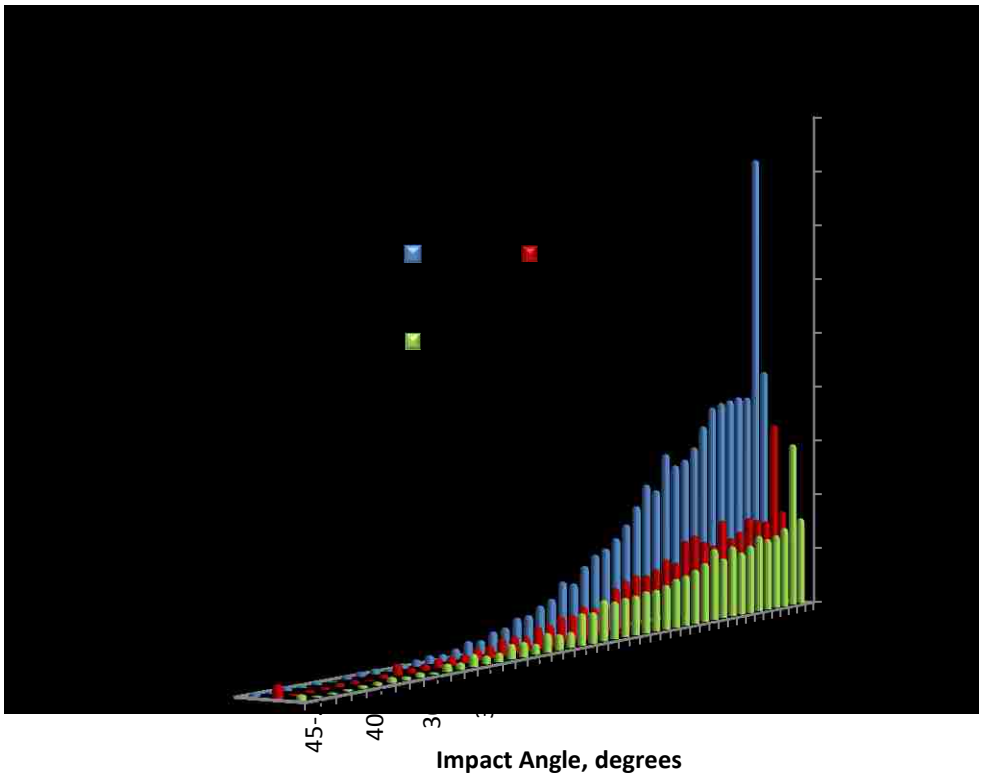

Figure 7.12 Percent s

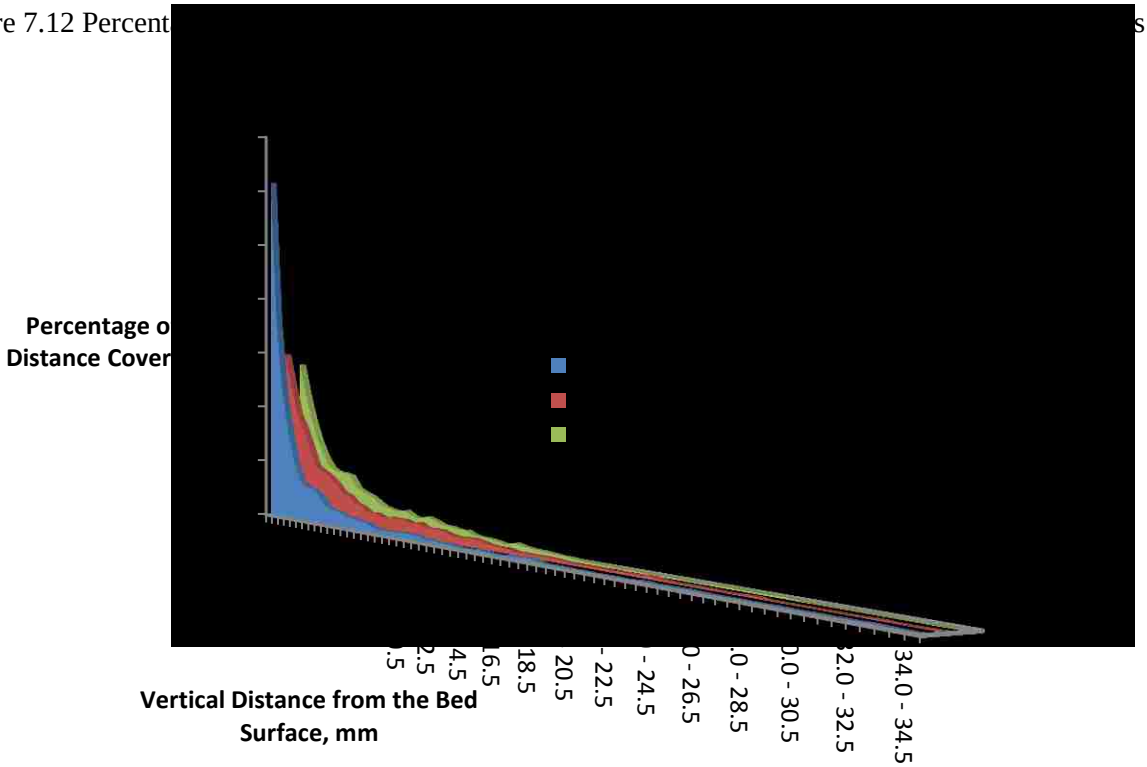

Figure 7.13 Total number of collisions at different impact angles at flows with different fluid densities

There were no visible changes in local velocities as shown in figure 7.14; however, there is an increase in the turbulence kinetic energy production rate just over the bed height as the density is increased. The difference between 8.33 ppg (Water) and 10 ppg cases is significant; however, the turbulence kinetic energy production rate slightly increases from 10 ppg to 11 ppg cases.

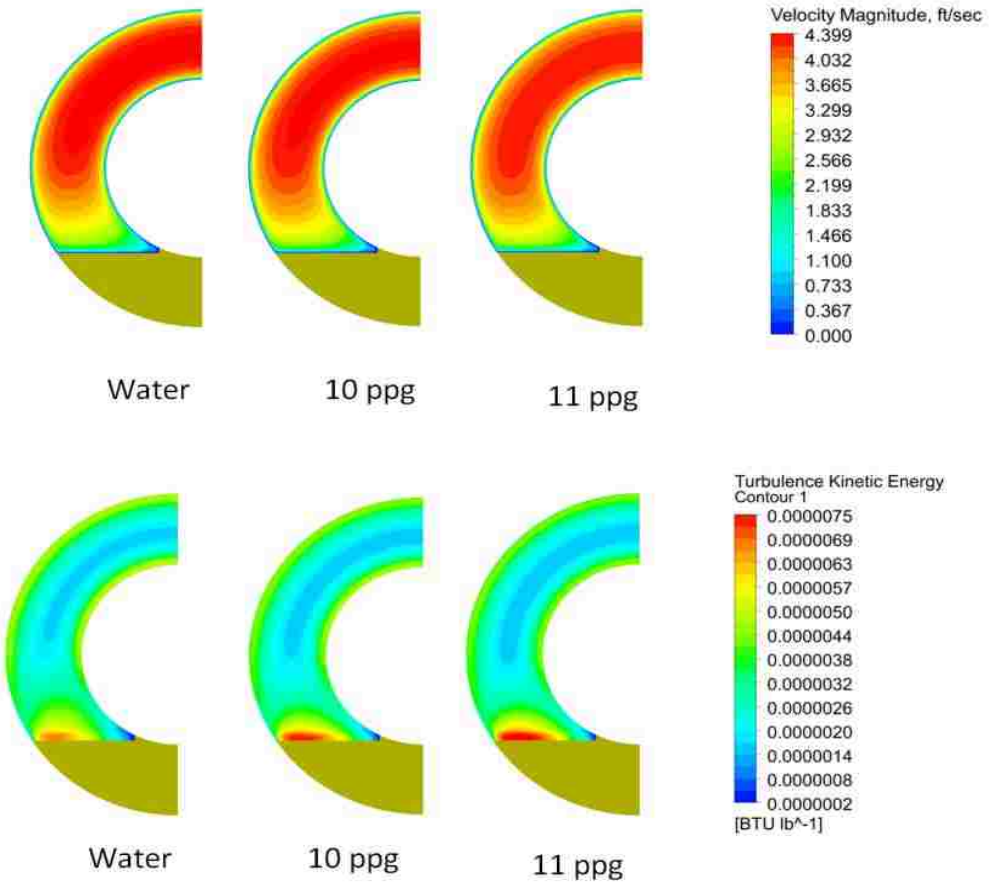

Figure 7.14 Velocity magnitude and turbulence kinetic energy contours at flows with different fluid densities

7.5 The Effect of Fluid Rheology

The effect of fluid rheology is assessed qualitatively by comparing the effects of carrier fluids having different rheological properties in cuttings bed buildup process. The same horizontal annular section is used as in the model validation cases with a constant stationary bed height. Different hypothetical Herschel-Bulkley fluids categorized into groups and their performance is compared together with water as a sample with Newtonian rheology. The first group of yield power law fluids has the same low yield point value and different fluid consistency (k) and fluid behavior (n) indexes. The fluids in the second group

has a higher shared yield point value and also has different fluid consistency (k) and fluid behavior (n) indexes. The rheological parameters of each carrier fluid are given in table 7.1 and their rheological behavior can be seen in figure 7.15.

Table 7.1 The yield power law parameters of four different hypothetical fluids tested

		n	k, cp	Yp, lb/100 ft2
First Group (Medium Effective Viscosity)	**Low Yp, Low k, Low n**	0.7	50	5
	Low Yp, High k, High n	0.9	70	5
Second Group (High Effective Viscosity)	**High Yp, Low n**	0.7	150	15
	High Yp, High n	0.9	150	15

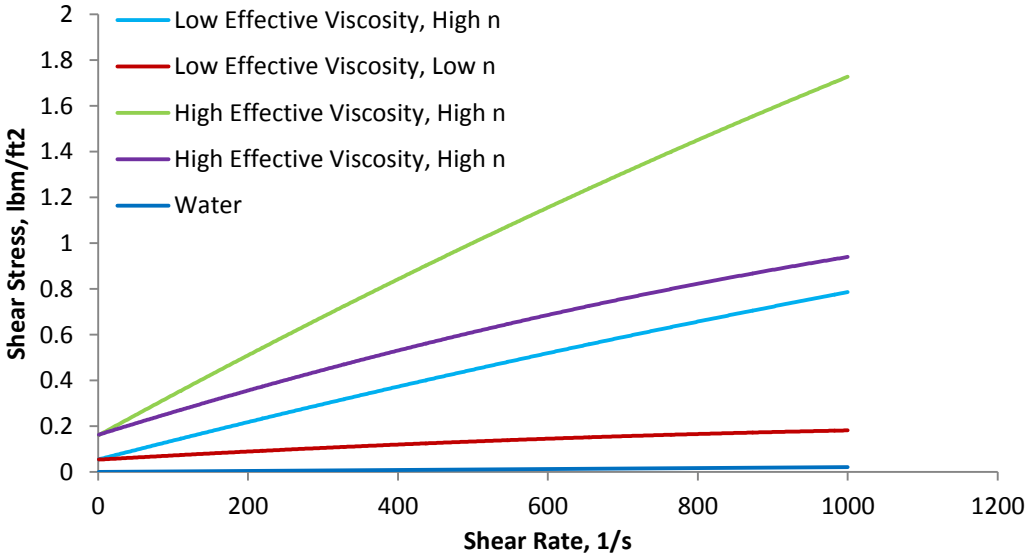

Figure 7.15 Rheological behaviors of hypothetical Yield Power Law Fluids

Figure 7.16 shows the fluid phase velocity magnitude and the turbulence kinetic energy contours. The yield point is found to be the most influential parameter in flow regime and the local velocity distribution. The change in fluid consistency index and the fluid behavior index had negligible impact on flow characteristics for the fluids with the same low yield point value. The fluid consistency index and the fluid behavior were effective in altering the flow characteristics for the fluids with the same high yield point value where the flow is almost laminarized.

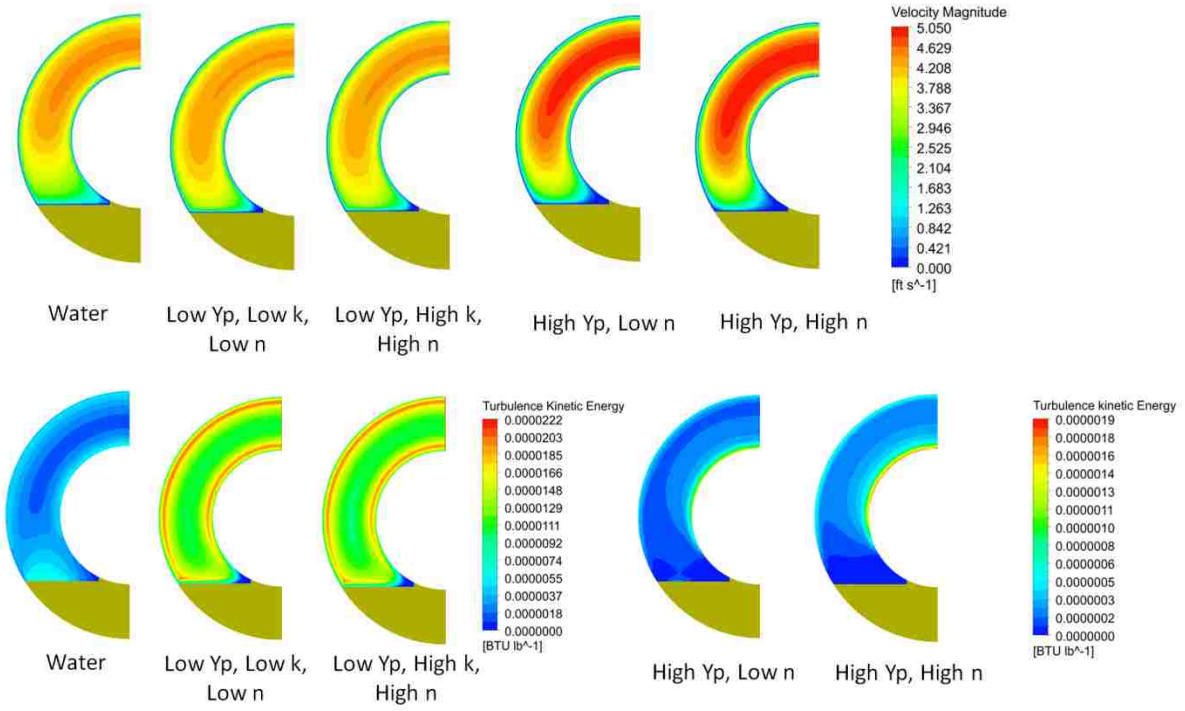

Figure 7.16 Velocity magnitude and turbulence kinetic energy contours with fluids having different rheological properties

The turbulence kinetic energy production is increased substantially from water to medium effective non-Newtonian viscosity cases. There is negligible turbulence kinetic production energy near the narrow wedge between inner pipe and bed surface, where particle accumulation should be expected. The fluid behavior index had no impact in the medium effective viscosity group, since eddy viscosities are much larger than effective molecular viscosities. The effective molecular viscosities on the velocity profile along a line perpendicular to the flow direction are shown with eddy viscosities in figure 7.17. The number of collisions at different impact angles was quite similar for medium viscosity cases as in figure 7.19, although the suspension profiles were much different. Although the carrying capacity of both flows is very similar, particle paths in suspension can be different since the random component of the particle velocity becomes more dominant at high turbulence kinetic energy regions.

Further increase in the effective viscosities completely dissipated the turbulence. The flow is laminarized in high effective viscosities. Turbulence kinetic energy with high effective viscosities are shown with a different legend with a much lower scale in order to show that fluid behavior index affects turbulence in high effective viscosities. However, since the flow became almost laminar, it has no prospect of carrying particles, rendering the effect of fluid behavior index meaningless. The eddy viscosities and molecular viscosities can be equally important in transient flows. However, two equation models, k-epsilon and k-omega are not capable of capturing transient regimes. Similar observations are reported in separate

studies by Becker et al. (1991) and Okrajni and Azar (1985). They stated that change in fluid rheology has negligible effect in cuttings transport performance in turbulent regime and they also recommended that the turbulent regime is more effective for highly deviated wellbores.

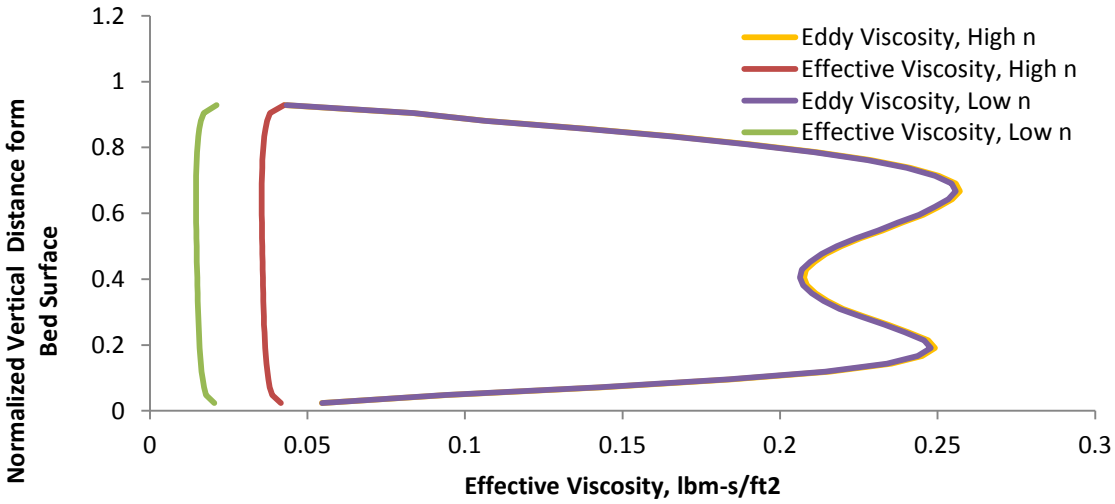

Figure 7.17 Molecular viscosities versus eddy viscosities

Particle suspension considerably increased in fluids with medium effective viscosities compared to water as carrier fluid as shown in figure 7.18. Most suspension is seen in the case with medium effective viscosity and low n case. Significant increase can also be seen in impact angle histograms. Total number of collisions and collisions with high impact angles dropped significantly in medium effective viscosity cases. However there is only slight difference in medium effective viscosities with different flow behavior indexes. Impact angle

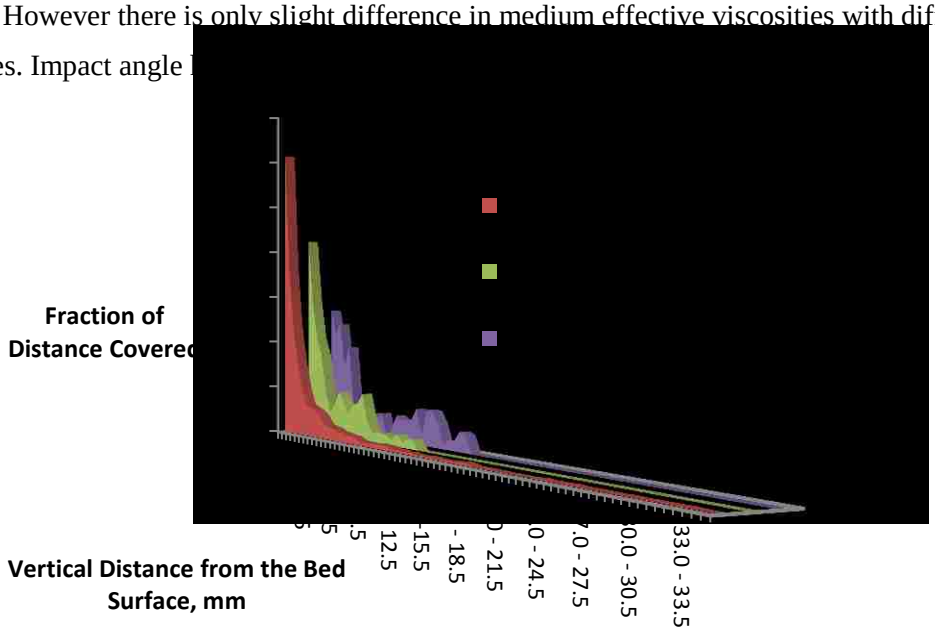

Figure 7.18 Percentages of distance covered in the flow direction with fluids that have different rheological properties

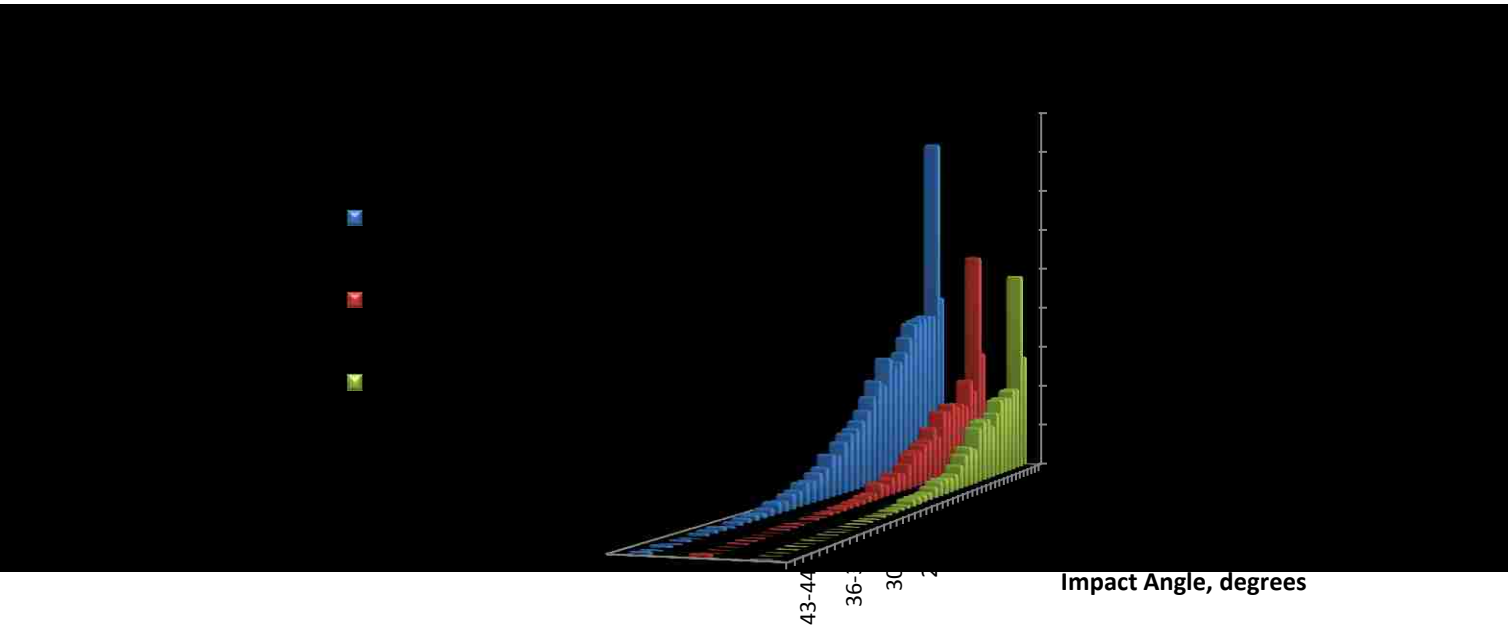

Figure 7.19 Total number of collisions at different impact angles with fluids that have different rheological properties

All particle paths were incomplete in the cases with high effective viscosities. In other words particle paths could not reach outflow at a designated number of time steps, showing that flow is incapable of carrying particles by all means. The total number of collisions was so high, and no suspension is seen, so the particle data of high effective viscosity cases were excluded from the analysis charts previously shown.

7.6 The Effects of Particle Size Distribution and Particle Sphericity

The effects of particle size distribution and particle sphericity is qualitatively investigated. The simulation setups used for validating the average transport velocities predictions in three different flow rates (Chapter 6) are selected as the base cases. The changes in average transport velocity are compared between the simulations where different uniform sphericities and size distributions are used. The base cases were simulated by using a uniform particle size of 4 mm and a sphericity value of 0.1. For the effect of particle size distribution the bases cases are simulated by using Rosin-Rammler size distribution which has the range of 3 to 5 mm as in the experimental study, and a random mean is assigned as 4 mm whole all other parameters are the same as in the base case. For the effect of particle sphericity, the base cases are simulated by using fully spherical particles this time. The average transport velocities obtained from

the simulations performed by altering the particle properties are compared to the base cases and the results from experiments of Garcia-Hernandez et al. (2007) as seen in figure 7.20.

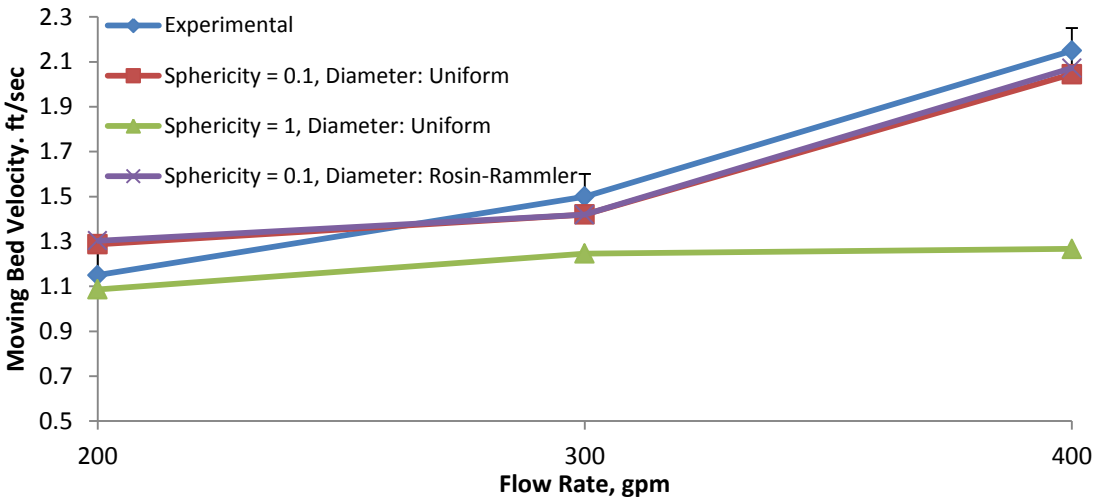

Figure 7.20 Comparison of moving bed velocities with different sphericity values and size distributions. Error margin of experimental data is ±0.5 ft/sec for all data points.

Using a size distribution or a uniform size yielded similar values with negligible difference. Sphericity however, predicted the average moving bed velocity fairly low at high flow rates. A rigorous estimation of sphericity remains difficult; however, at the least a visual description of particle shapes could still be very useful in making better assumptions. At the same time, it can be concluded that non-spherical particles are easier to transport as their average transport velocity is found to be higher with spherical particles. The reason for this is that the non-spherical particles have larger surface areas and thus larger drag force.

8. RESULTS AND DISCUSSIONS

A method of estimating the stationary bed height is presented. Particle tracks are obtained by the discrete phase model which follows the Eulerian–Lagrangian approach. The method is based on the analysis of particle tracks in terms of impact angles and velocities together with the suspending capability of the flow in form of distance covered in different altitudes away from the bed surface. The particles are set to make elastic collisions with the bed surface since the particle -wall impact restitution coefficients are difficult to obtain. The likelihood of particle accumulation is evaluated by comparing the particle – wall impact angles and velocities with suspending capability of the flow at different stationary bed heights, since the prediction of particle motion after the impact is not possible within the current method.

Since drilled cuttings are much heavier than the carrier fluid, they tend to settle down on the low side of the annulus. Saffman's lift force is found to have a negligible contribution for suspending particles, so the particle acceleration due to turbulence eddies is understood to be the most important factor that leads to particle suspension. In the simulations conducted as a part of the present study, acceleration due to turbulence eddies is calculated with the local turbulence kinetic energy around the particle and multiplied by a random number, which represents eddy lifetime. Probability of a particle to obtain higher momentum vertical to the stationary bed surface increases with increasing turbulence kinetic energy. Once the particle moved away from the surface, it will move to the plug region of the flow where fluid velocity is much higher than in the vicinity of the stationary bed surface. Therefore, particle will also be subjected to significantly larger drag force, resulting in larger distances covered in higher altitudes. It can be seen that distance covered in higher altitudes away from the bed surface increases with increasing local turbulence kinetic energy in all simulated cases.

Tomren et al. (1986) observed that closely grouped particles are transported in a thin layer just above the surface (Moving bed) and just above this layer, particles are travelling sparsely in their experiments.. This phenomenon is also observed in the visualization of simulations. If a particle successively enters strong eddies, it will obtain a larger velocity component vertical to the bed surface, thus, traveling in higher altitudes. Since the probability of entering strong eddies successively is low, the number of particles traveling at higher altitudes is also small. If a more stable lifting force was in effect, particles should have altogether move into suspension pattern.

Particle momentum loss due to wall impact would affect the general motion of the particle. Turbulence is found to be the major contributor to particle lifting. At low volumetric flow rates, where the turbulence effect is limited, restitution coefficients are expected to be lower. Low restitution coefficients, with

limited compensation of momentum from drag and turbulence will lead to the termination of particle motion in actual conditions. At higher flow rates, the degree of momentum loss due to impact will be lower as the impact velocities would increase and overall number of particle - wall collisions with higher impact angle would decrease. Besides that, increasingly dominant instantaneous turbulent fluctuating vertical velocity component will minimize the effect of momentum loss due to wall impact. The effect of momentum loss due to impact on the rest of the motion is considered to be diminishing with increasing instantaneous turbulent velocity fluctuations.

Particle–wall impact restitution coefficient is a function of impact velocity and impact angle, as well as impact surface roughness and particle shape (Sommerfeld and Huber, 1999). Since a convenient universal method for obtaining the restitution coefficient is not available to our knowledge, particle track analysis is performed for all parameters mentioned before. A single parameter may not provide enough evidence for whether the accumulation is still in progress or not for the given flow conditions, since the combined effects of those parameters determine the termination of particle motion. Incorporation of functions defining restitution coefficients into the current setup will remove the requirement for comparative particle track analysis.

The forces calculated on a single particle are the drag force, gravitational force, pressure gradient force and the virtual mass force. Turbulence effects are also incorporated by the random walk model. This scheme was adequate to detect significant differences in particle behavior (Particle – wall impact angles, particle – wall impact velocities, and distance covered in different altitudes) between the cases where particle accumulation is still in progress and the cases where further accumulation is not possible. Better accuracy in predicting the particle motion can be made possible by adding more forces to the equation describing the force balance on the particle. These forces can be especially important when the functions for momentum loss due to wall impact are available.

The Eulerian (Fluid flow) and Lagrangian (Solids flow) phases are coupled in one – way fashion, where the fluid flow stimulates the particle motion, however, fluid flow is not affected by the presence of the solid phase. The assumption was that the effect of solids motion in the fluid can be neglected for low solids concentrations. However, one –way coupling renders the capability of model to respond to solids flow rate, in other words, the rate penetration. Using a two – way coupling scheme, where particle streams destroy local turbulence kinetic energy proportional to the solids flow rate can provide better estimations of the flow field and the particle motion, especially for higher rate of penetration. However, two – way coupling is computationally more demanding.

A uniform size of 4 mm is assigned to all particles, which is the mean of given particle size range, 3 to 5 millimeters in the experimental study. The simulations performed for validating the computational setup with experimental data where unsteady particle tracking is used for determining average particle velocity is also performed by using a size distribution for the same given size range. Using a size distribution was only slightly different than the results obtained with a uniform size. However, this change can be more pronounced for different size ranges. A more detailed investigation for the effect of particle size distribution may be necessary for drawing more solid conclusions.

Particle shape is found to be effective on the particle motion in the parametric study. All particles are assumed to have a sphericity value of 0.1. This assumption is made according to the statement that gravel is used for representing cuttings in the experimental study. Although the simulation results are in very good agreement with the experimental data, the sphericity assumption may be overshadowing other factors such as the lack of models for particle – particle collisions and the other forces acting on a particle other than the ones used in this study such as Saffman's lift force, Basset force, Magnus force, and cohesive force between particles in the presented computational setup. A more complete set of forces in the governing equation of DPM and incorporation of the particle – particle collisions would provide better supported estimations of particle velocities. Also more detailed description of the particle shape would help assigning a more accurate sphericity value.

The inner pipe rotation swayed the particles tangentially and when looking at the particle impact and suspension parameters, it can be concluded that bed height should be higher on the side of the annulus opposite to the direction of rotation. This result exactly matches the experimental observations of Tomren et al. (2007). However, although the bed height estimations are in close agreement with the experimental data from Garcia-Hernandez et al. (2007), much higher levels of suspension is described in the experimental study. In the simulations, the inner pipe strictly rotates around its own axis. In reality, mechanical vibrations of the inner pipe would also contribute energy to the flow, resulting in greater turbulence. Also the downwards pipe bending due to gravity would cause orbital movement, creating much larger shear even if the pipe bending is slight. In real drilling conditions where the drilling pipe is under compression, it will make sinusoidal movement which will provide enormous mechanical blending action, destroying and mixing the stationary bed.

9. CONCLUDING REMARKS AND FUTURE DIRECTIONS

Capability of the Navier–Stokes equations (mass and momentum conservation) along with SST k- ω turbulence closure model to predict the velocity profiles of non-Newtonian fluids flowing in turbulent regime for pipe flow is presented with satisfactory match against the experimental data of Pinho and Whitelaw (1990) and Pereira and Pinho (1994).

A method for predicting stationary bed height based on comparative analysis of particle tracks obtained by the discrete phase model is presented. Parameters such as the particle - wall impact velocity, particle – wall impact angles, and distance covered in higher altitudes away from the stationary bed surface is examined at pipe flows with different stationary bed heights. Particle behavior at pipe flows with different stationary bed heights is compared in order to capture significant changes. The actual height of the bed is determined based on the change in particle behavior between pipe flows with different bed heights. The accuracy of predictions is shown by comparing model results to the experimental data.

Capability of discrete phase model in unsteady particle tracking mode in predicting the average particle velocities at different flow rates are shown through validation with the experimental data of Garcia-Hernandez et al. (2005).

The sensitivity of the equilibrium stationary bed height to flow rate, wellbore inclination, and inner pipe rotation are shown through validation with experimental data of Garcia-Hernandez et al. (2005). The effects seen in the simulations are in agreement with the experimental observations.

The sensitivity of the equilibrium stationary bed height to carrier phase density and rheology, particle shape and particle size distribution and the inner pipe rotation speed are studied qualitatively. Insights obtained through this parametric study were useful in understanding the underlying fluid dynamics of cuttings transport in highly deviated wellbores.

To this end, it is recommended to simulate the cuttings transport with two-way fluids-solids coupling to make sure that the approximations of one-way coupling are indeed representative. Lack of particle-wall interactions in DPM led to a tedious analysis procedure. In the future simulations using Discrete Element Method (DEM), some of the deficiencies of DPM can be overcome and could lead way to model the cohesive forces accounting for accumulation of cuttings on the bed.

REFERENCES

1. Adari,R.B., Miska S. Z, Kuru E., Bern P., and Saasen A., "*Selecting Drilling Fluid Properties and Flow Rates For Effective Hole Cleaning in High-Angle and Horizontal Wells*", Annual Technical Conference and Exhibition held in Dallas, Texas, October 2000.

2. Becker T. E., Azar J.J, "*Mud-Weight and Hole-Geometry Effects on Cuttings Transport While Drilling Directionally*", Society of Petroleum Engineers, Paper No: 14711, August 1985

3. Becker T. E., Azar J.J, Okrajni S. S., "Correlations of Mud Rheological Properties with Cuttings-Transport Performance in Directional Drilling", SPE Drilling Engineering, March 1991

4. Bilgesu H. I., Ali M. W., Aminan K., Ameri S., "*Computational Fluid Dynamics (CFD) as a Tool to Study Cutting Transport*", SPE Eastern Regional Meeting Held in Lexington, Kentucky, October 2002

5. Brown N.P., Bern P.A., Weaver A., "*Cleaning Deviated Holes: New Experimental and Theoretical Studies*", SPE/IADC Drilling Conference held in New Orleans, Louisiana, March-February 1989

6. Cho H., Shah S.N., Osisanya O. S., "*A Three-Segment Hydraulic Model for Cuttings Transport in Horizontal and Deviated Wells*", 2000 SPE/Petroleum Society of CIM International Conference on Horizontal Well Technology held in Calgary, Alberta, Canada, 6-8, November 2000

7. Clark, R.K., and Bickham K.L., *"A Mechanistic Model for Cuttings Transport"*, SPE 69th Annual Technical Conference and Exhibition, New Orleans, September 1994.

8. Duan M., Miska S., Yu M., Takach N., Ramadan A., Zettner C., "*Transport of Small Cuttings in Extended Reach Drilling*" SPE International Oil and Gas Conference and Exhibition, Bejing, China, December, 2006

9. Eesa M. , Barigou M.,"*CFD Investigation of the Pipe Transport of Coarse Solids in Laminar Power Law Fluids*", Chemical Engineering Science 64, October 2008

10. Fluent Release 12.0 Theory Guide, ANSYS Inc. , January 2009

11. Fluent Release 12.0 User Manual, ANSYS Inc. , January 2009

12. Ford J.T., Peden J.M., Oyeneyin M.B., Gao E., and Zarrough R., Heriot-Watt U., "*Experimental Investigation of Drilled Cuttings Transport in Inclined Boreholes*", 65th Annual Technical Conference and Exhibition of the Society of Petroleum Engineers held in New Orleans, Louisiana, September 1990

13. Ford, J.T., Goo E., Oyeneyin M.B., Peden, J. M., Larrucia M.B., Parker D., "*A New MTV Computer Package for Hole Cleaning Design and Analysis*", SPE Drilling & Completion, September 1996

14. Gao E., and Young A.C., "*Hole Cleaning in Extended Reach Wells: Field Experience and Theoretical Analysis Using a Pseudo-Oil (Acetal) Based Mud*", SPE/IADC Drilling Conference held in Amsterdam, February 1995

15. Garcia-Hernandez A. J., "*Determination of Cuttings Lag in Horizontal and Deviated Wells*", Report for TUDRP Advisory Board Meeting, Tulsa-Oklahoma, November 2005

16. Joseph G. G., Hunt M. L., "Oblique Particle –Wall Collisions in a Liquid", Journal of Fluid Mechanics, Volume 510, February 2004

17. Kelessidis V. C., Mpandelis G. E., "*Hydraulic Parameters Affecting Cuttings Transport for Horizontal Coiled Tubing Drilling*", 7th National Congress on Mechanics, Chania, Greece, June, 2004.

18. King, I., and Trenty, L., "*How the 3D Modeling Could Help Hole-Cleaning Optimization*",SPE Annual Technical Conference and Exhibition, Dallas, Texas, October 2000

19. Klessidis V.C., Bandelis G.E., "*Flow Patterns and Minimum Suspension Velocity for Efficient Cuttings Transport in Horizontal and Deviated Wells in Coiled Tubing Drilling*", SPE Drilling & Completion, December 2004

20. Luo Y., Bern P. A., Chambers B. D., "*Flow Rate Predictions for Cleaning Deviated Wells*", IADC/SPE Drilling Conference, New Orleanns, LA, February 1992

21. Martins A. L., Sa C. H. M., Lourenco A. M. F., Campos W., "*Optimizing Cutting Circulation in Horizontal Well Drilling*" International Petroleum Conference & Exhibition of Mexico, Villahermosa, Mexico, March, 1996

22. Martins A. L., Santana C. C., "*Evaluation of Cuttings Transport in Highly Deviated Wells – A Dimensionless Approach*", SPE Second Latin American Petroleum Engineering Conference, Caracas, Venezuela, March 1992

23. Mendoza R.S., Gutierrez A. G., "*A Two-Region Hydraulic Averaging Model for Cuttings Transport During Horizontal Well Drilling*", Journal of Canadian Petroleum Technology, Volume 47, Number 3, March 2008

24. Nazari T., Hareland G., Azar J.J., "*Review of Cuttings Transport in Directional Well Drilling: A Systematic Approach*", SPE Western Regional Meeting, Anaheim, California, May 2010

25. Nguyen D., Rahman S.S., "*A Three-Layer Hydraulic Program for Effective Cuttings Transport and Hole Cleaning in Highly Deviated and Horizontal Wells*" IADC/SPE Asia Pacific Drilling Technology Conference, September 1996

26. Okrajni S., Azar J.J., "*The Effects of Mud Rheology on Annular Hole Cleaning in Directional Wells*", SPE Annual Technical Conference and Exhibition held in Las Vegas, September, 1985

27. Ozbayoglu M. E., Miska S. Z., Reed T., Takach N., "*Analysis of the Effect of Major Drilling Parameters on Cuttings Transport Efficiency for High-Angle Wells in Coiled Tubing Drilling Operations*", SPE/IcoTA Coiled Tubing Conference and Exhibibit held in Houston, Texas, March 2004

28. Paredes G. E., Mendoza S.R., Candia O. C., "*Averaging Model for Cuttings Transport in Horizontal Wellbores*", Journal of Petroleum Science and Engineering 55 (2007) 301 - 316

29. Peden J.M., Ford J.T., and Oyeneyin M.B., "*Comprehensive Experimental Investigation of Drilled Cuttings Transport In Inclined Wells Including the Effects of Rotation and Eccentricity*", Europec 90, The Hague, Netherlands, October 1990

30. Pereira A. S., Pinho F. T., " Turbulent Pipe Flow Characteristics of Low Molecular Weight Polymer Solutions" , Journal of Non-Newtonian Fluid Mechanics, Vol. 55, February 1994

31. Pinho F.T., Whitelaw J.H., "*Flow of Non-Newtonian Fluids in Pipe*", Journal of Non-Newtonian Fluid Mechanics Vol. 34, Elsevier Science Publishers B.V., Amsterdam, Netherlands, 1990

32. Ramadan A., Skalle P., S.T. Johansen S. T., Svein J., Saasen A.,"*Mechanistic Model for Cuttings Removal from Solid Bed in Inclined Channels*", Journal of Petroleum Science and Technology 30 (2001) 129–141, April 2001

33. Rubiandini, R., "*Equation for Estimating Mud Minimum Rate for Cuttings Transport in an Inclined-Until-Horizontal Well*", Middle East Drilling Technology Conference, Abu – Dhabi, November 1999

34. Sample K.J., Bourgoyne A.T., "*Development of Improved Laboratory and Field Procedures for Determining the Carrying Capacity of Drilling Fluids*", 53rd Annual Technical conference and Exhibition of Society of Petroleum Engineers of AIME held in Houston, Texas, October 1978

35. Sanchez A.R., Azar J.J., Bassal A.A., Martins A.L., "*Effect of Drillpipe Rotation on Hole Cleaning During Directional-Well Drilling*", SPE/IADC Drilling Conference , Amsterdam, The Netherlands, March 1997

36. Sifferman T.R., Becker T.E., "*Hole Cleaning in Full Scale Inclined Wellbores*", SPE Annual Technical Conference and Exhibition held in New Orleans, Louisiana, September 1990

37. Sommerfeld M, Huber N, "*Experimental Analysis and modeling of Particle – Wall Collisions*", International Journal of Multiphase Flow 25 (1999) 1457-1489

38. Tomren P.H, Iyoho A.W., Azar J.J., "*Experimental Study of Cuttings Transport in Deviated Wells*", SPE Annual Technical Conference and Exhibition held in San Francisco, October 1983

39. Vieira Neto J.L., , Martins A. L., Silveira Neto A., Ataida C.H., Barrozo M. A. S., "*CFD Applied to Turbulent Flows in Concentric and Eccentric Annuli with Inner Shaft Rotation*", The Canadian Journal of Chemical Engineering, Volume 89, August, 2011

40. Wall S. , John W., Wang H.C., Goren S. L., "*Measurements of Kinetic Energy Loss for Particles Impacting Surfaces*", Measurements of Kinetic Energy Loss for Particles Impacting Surfaces, Aerosol Science and Technology, 12:4, 926-946, June 2007

APPENDIX – I OVERVIEW OF DISCRETE PHASE MODEL

Discrete Phase Model (DPM) is a mathematical tool that navigates a large number of particles in the flow field by including body forces and defining particle – wall interactions. The effect of particle shape on particle motion can also be incorporated to this model by a non-spherical drag law correlation. Discrete Phase Model uses Euler – Lagrange approach and assumes relatively dilute suspensions. The continuous phase- and discrete phase- equations are solved in a partially coupled fashion where the continuous phase calculations are performed in an Eulerian reference frame and the discrete phase calculations are performed in a Lagrangian reference frame. Trajectory of a particle can be obtained by twice integrating the acceleration (from force balance) of the particle. The effect of turbulence as the particle velocity perturbations due to turbulence eddies is also included here by the "Random Walk Model".

A general governing equation defining the force balance on a single particle at a given time instant is as follows:

$$\frac{\partial u_p}{\partial t} = F_D(u - u_p) + \frac{g_x(\rho_p - \rho)}{\rho_p} + F_x$$

In the equation above, $F_D(u - u_p)$ is the drag force per unit particle mass, where u and u_p denotes the fluid, and particle velocities; and F_D, the drag force. $\frac{g_x(\rho_p - \rho)}{\rho_p}$ is the gravitational force, where , ρ_p and ρ are the fluid and particle densities; and g_x the gravitational acceleration. F_x denotes any other relevant force term that can be included. The drag force is given by:

$$F_D = \frac{18\mu}{\rho_p d_p^2}\frac{C_D Re}{24}$$

Here, C_D is the drag coefficient μ is the molecular viscosity, d_p is the particle diameter and Re is the relative Reynolds number which is defined as:

$$\mathrm{Re} \equiv \frac{\rho \mathrm{d_p} \left|\mathrm{u_p} - \mathrm{u}\right|}{\mu}$$

The drag coefficient for spherical particles:

$$\mathrm{C_D} = \mathrm{a_1} + \frac{\mathrm{a_2}}{\mathrm{Re}} + \frac{\mathrm{a_3}}{\mathrm{Re}^2}$$

Here, the constants $\mathrm{a_1}, \mathrm{a_2}$ and $\mathrm{a_1}$given by Morsi and Alexander can be used for a wide range of Reynolds numbers. For non-spherical particles, Haider and Levenspiel correlation is used to calculate the drag coefficient:

$$C_D = \frac{24}{Re_{sph}}\left(1 + b_1 Re_{sph}^{b_2}\right) + \frac{b_3 Re_{sph}}{b_4 + Re_{sph}}$$

The constants are calculated by the shape factor, which is the ratio of the surface area of a sphere having the same volume as the particle, to the actual surface area of that particle:

$$\Phi = \frac{s}{S}$$

The model constant for the non-spherical drag coefficient:

$$b_1 = \exp(2.3288 - 6.4581\Phi + 2.4486\Phi^2$$

$$b_2 = 0.0964 + 0.5565\Phi$$

$$b_3 = \exp(4.905 - 13.8944\Phi + 18.4222\Phi^2 - 10.2599\Phi^3$$

$$b_4 = \exp(1.4681 + 12.2584\Phi - 20.7322\Phi^2 + 15.8855\Phi^3$$

Among other important forces added to the right hand side of the general governing equation in this study are the forces due to external pressure gradient and force arising due to the rotation of reference frame. The additional force due to pressure gradient is defined as:

$$F_x = \left(\frac{\rho}{\rho_p}\right) u_{pi} \frac{\partial u}{\partial x_i}$$

Virtual mass force is the force required for accelerating the surrounding fluid. It is the equivalent of adding a mass to a particle.

$$F_x = \frac{1}{2}\frac{\rho}{\rho_p}\frac{d}{dt}(u - u_p)$$

Moving reference frame is used to incorporate the inner pipe rotation in the annulus for some of the parametric studies. The reference frame is rotated about the X-axis, so the additional force on the particle in the Y-direction is:

$$F_x = \left(1 - \frac{\rho}{\rho_p}\right)\Omega^2 y + 2\Omega\left(u_{z,p} - \frac{\rho}{\rho_p}u_z\right)$$

APPENDIX – II DATA ANALYSIS PROCEDURE

The averaged flow parameters along the flow direction are nearly constant, since the flow reaches fully developed conditions during each simulation. However, local velocities may vary on the cross sections of various stations. These variations are examined further by dividing the transverse bed surface into 12 lanes along the flow direction. The particle trajectories statistics for each lane are compared to each other in order to quantify the degree of variation. It was found that the total number of particle-wall collisions was much higher and the impact velocities were lower in the two lanes representing the junctions (or corners) of wellbore and drillpipe surfaces with cuttings bed. However, the particle trajectory statistics in the remaining 10 lanes located away from these corner flows are found to be closer to each other in all simulations. Thus, the data on the two side lanes were filtered out during the analysis and the averaged value for these10 lanes is reported. It can also be concluded that there will always be more accumulation in the areas close to the walls. This data analysis procedure is explained using the data from a simulation with 200 gpm flow rate and 2.4" stationary bed height in the following paragraphs.

Fig. A-1 shows the total number of particle-wall collisions at each transversal increment (referred to as lane in earlier section). Much larger numbers of particle-wall collisions are noted in the lanes 1 and 12 (corners of wellbore surface, and drillpipe surface with cuttings bed respectively) as compared to the "interior" lanes.

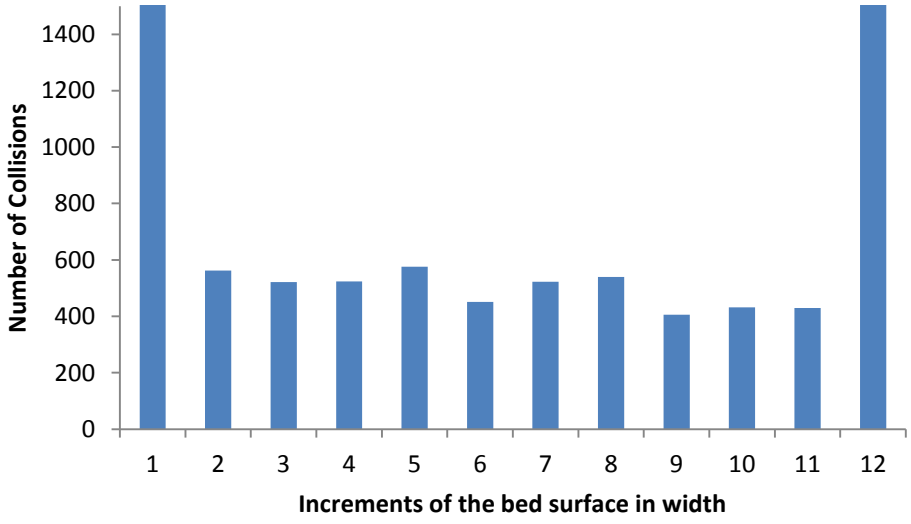

Fig. A-1 Total number of particle-wall collisions in each transverse increment

Fig. A-2 shows the distribution of average particle impact velocities at each transverse section. The low values of impact velocities in the corners are expected due to low flow velocity in the corresponding regions. The standard deviation of the impact velocities in the remaining lanes is 0.08 ft/sec, and therefore, the average value of these "interior" transverse sections is taken as the average impact velocity near the cuttings bed.

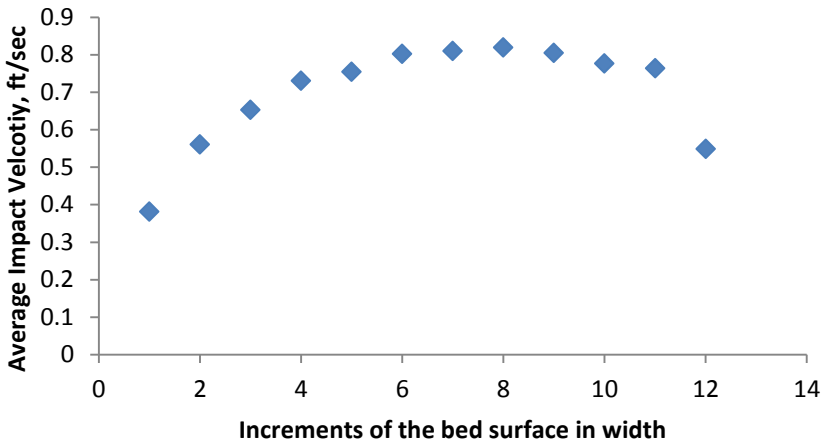

Fig. A-2 Impact particle velocities at each transverse increment

Fig. A-3 shows that both the velocity magnitude and the turbulence kinetic energy are low in the corners. Similar behavior was observed in all simulations, so the data close to the corners were "filtered out" from the analysis by dividing the surface into lanes for all data analysis.

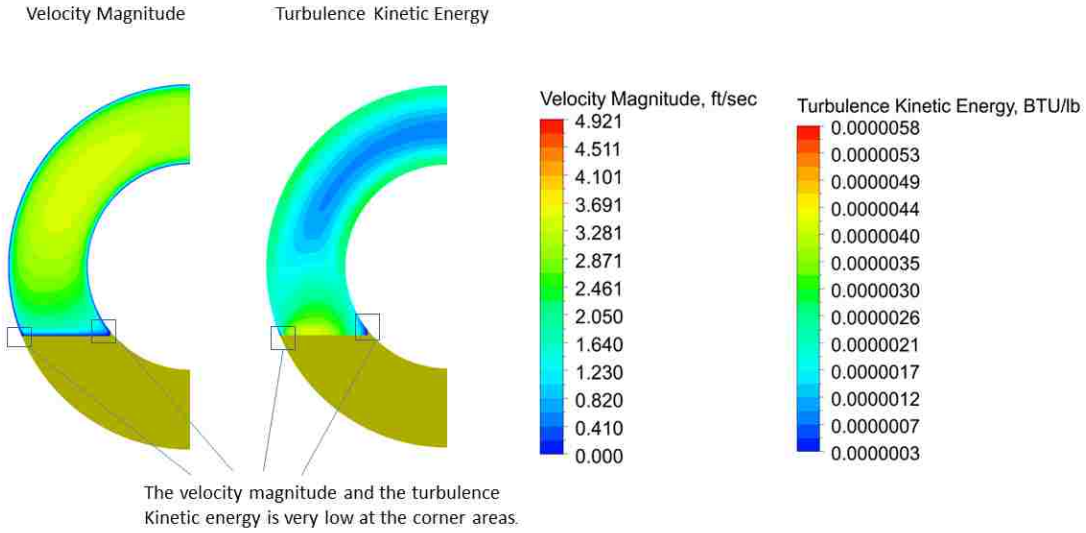

Fig. A-3 Carrier phase velocity magnitude and turbulence kinetic energy contours. Low values are observed near the corners (shown in insets)

VITA

Doguhan Yilmaz was born in Izmir, Turkey.

He obtained his Bachelor degree in Petroleum Engineering from Istanbul Technical University in 2007.

He worked in Binagadi Oil Company, Azerbaijan from 2007 to 2009 and in Turkish Petroleum International Company, Turkey in the first half of 2010.

He enrolled in the Craft & Hawkins Department of Petroleum Engineering at Louisiana State University in the Fall 2010 to work towards a Masters degree in petroleum engineering in May 2013.